Antibody mediated autoimmunity – characterizing the pathomechanism of autoantibodies derived from myasthenia gravis patients and healthy donors

Inauguraldissertation
zur
Erlangung der Würde eines Doktors der Philosophie
vorgelegt der
Philosophisch-Naturwissenschaftlichen Fakultät
der Universität Basel

von

Sebastian Holdermann

2024

Genehmigt von der Philosophisch-Naturwissenschaftlichen Fakultät

auf Antrag von

Erstbetreuer: Prof. Dr. Tobias Derfuss

Zweitbetreuer: Prof. Dr. Markus Rüegg

Externer Experte: PD Dr. med. Bettina Schreiner

Basel, den 28.05.2024

Prof. Dr. Marcel Mayor
Dekan

Table of Contents

Abbreviations

α-BTX	alpha-Bungarotoxin
ACh	acetylcholine
AChR	acetylcholine receptor
ADCC	antibody-dependent cellular cytotoxicity
AICD	activation-induced cell death
AID	activation-induced cytidine deaminase
AQP4	aquaporin-4
BAFF	B-cell activating factor
BCR	B cell receptor
BSA	bovine serum albumin
CDR	complementary-determining region
CD	cluster of differentiation
CR	complement receptor
CXCL	chemokine C-X-C motif ligand
Fab	fragment antigen binding
FACS	fluorescence activated cell sorting
FcR	fragment crystallizable receptor
FO	follicular
GC	germinal center
GMFI	geometric mean fluorescence intensity
IL	interleukin
ITAM	immunoreceptor tyrosine-based activating motif
LIC	ligation independent cloning
LRP4	lipoprotein receptor protein 4
mAb	monoclonal antibody
MAC	membrane-attack complex
MACACS	membrane-antigen capture activated cell sorting
MHC	major histocompatibility complex
MIR	main immunogenic region
MG	myasthenia gravis
MOG	myelin oligodendrocyte glycoprotein
MuSK	muscle-specific kinase
MZ	marginal zone
NMJ	neuromuscular junction
OAP	orthogonal array of particles
PBMC	peripheral blood mononuclear cells
PTMG	passive transfer myasthenia gravis
RA	rheumatoid arthritis
RAG	recombination-activating genes
SHIgMA	somatically hypermutated IgM AChR-specific
SLE	systemic lupus erythematosus
VDJ	variable, diversity, joining

Summary

Background and rationale: Myasthenia gravis (MG) represents a prototypic autoimmune disease in which hypermutated, autoreactive B cells produce antibodies against proteins located at the post-synaptic membrane of the neuromuscular junction. Despite decades of prolific research that determined the acetylcholine receptor (AChR) as most prevalent autoantibody target and described several processes that mediate the clinical symptoms, little is known about the fundamental pathomechanisms of AChR-specific autoantibodies and the B cells producing them. We established a method to isolate B cells from the peripheral blood of patients and healthy donors that recognize a specific membrane-antigen, which provided the exceptional opportunity to characterize AChR-specific, monoclonal antibodies and B cells.

Results: We produced six monoclonal MG patient-derived IgG antibodies that bound specifically to the human AChR, of which none exhibited pathogenic properties when tested in vitro and in vivo. However, combinations of autoantibodies with distinct AChR-subunit specificities generated an increased complement activation even if the individual antibodies were incapable of activating complement. Similarly, an antibody combination with synergistic subunit-specificities proved pathogenic when tested in live rats. With a subsequent animal study, which included the pathogenic antibody combination and additionally a C5 complement inhibitor we demonstrated the causal relationship between increased complement activation and myasthenic symptoms. To explain the observation of enhanced activation by antibody combinations we constructed three different hypotheses: the density model, the antigen array model, and the hexamer model. All three competing hypotheses postulated distinct structural patterns for the antigen-antibody interaction. The opposing predictions for complement activation depending on specified antibody characteristics allowed us to experimentally test the three models. We used anti-AChR IgG antibodies with different properties and even included somatically hypermutated, AChR-specific IgM isolated from MG patients and healthy donors. At present, the results of the antibodies tested individually and in combination suggest that the antigen array hypothesis is the most accurate. Further evaluation of the AChR-targeting IgM antibodies revealed that neither the relative binding strength nor the number of hypermutations had a positive impact on complement activation and a class switch to IgG caused a loss of binding capacity.

Conclusion: The antibody repertoire is a determining factor for the pathology in MG, as single, seemingly non-pathogenic antibodies can induce disease symptoms if included in a combination with synergistic AChR-subunit specificities. Even antibodies incapable of

complement activation due to an inept IgG subclass can participate in complement-driven pathogenicity by cross-linking receptors and stabilizing an advantageous antigen arrangement. A hexameric arrangement according to the prevalent model might not be necessary nor sufficient to activate the complement cascade, as indicated by IgM antibodies with strong specific binding to the AChR but without the ability to activate the complement system. These hypermutated IgM B cells that lose their binding when switched to IgG do not constitute a pathogenic precursor of the autoimmune disease. Finally, the population of somatically hypermutated, AChR-specific IgM B cells encountered in MG patients and healthy donors alike, probably reflect a regulatory B cell phenotype.

1. Introduction

1.1 The immune system – adaptive immunity

The physiological purpose of the immune system is to defend the host against pathogenic infections and foreign substances. Agents such as bacteria, viruses and parasites but also singular components like proteins, toxins and lipopolysaccharides elicit an immune response. In certain conditions these protective mechanisms can be damaging to the host, especially if a self-molecule activates the immune system, also known as an autoimmune response (1, 2). In general, the immune system can be divided into two subsystems responsible for the early and the late response. The innate immunity provides a first line of defence based on invariant pattern recognition receptors to detect common pathogens and foreign structures as well as damage associated with it (1). Furthermore, the innate immune system acts as physical and chemical barrier with several major functions including the recruitment of immune cells to the site of infection or injury, pathogen clearance either by cellular components or soluble effector molecules and the activation of the adaptive immune system through antigen presentation (3). The adaptive immunity is characterized by an outstanding specificity for distinct antigens while retaining a high diversity. It generates a delayed response to a primary infection, but due to the capacity to form an immunological memory the adaptive immune system provides a lasting immunity and enhanced protection against repeated exposure to the same pathogen (1, 2, 6). Thus, adaptive immunity constitutes the late response of the immune system.

Similar to innate immunity, the adaptive immune response comprises cell-mediated effector mechanisms which are mostly facilitated by different T lymphocytes with specialized functions and a humoral response produced by antibody-secreting B lymphocytes (1, 3, 4). Antibodies

are soluble molecules with a characteristic Y-shape composed of two, usually identical binding sites for antigens and a single constant region (5). The structure of the constant domain imparts different functional properties and serves as the basis for the definition of five distinct classes of antibodies (7). Antibodies provide three major effector mechanisms in the context of the humoral immune response: first, neutralization of viruses and bacterial toxins; second, opsonization of pathogens and foreign particles for phagocytosis; and third, the activation of the complement system which enhances opsonization, propagates inflammation and cell lysis (1, 2, 5). B lymphocytes and antibody-mediated effector mechanism are of special importance in the scope of this doctoral thesis and will be discussed in greater detail in the following sections.

1.2 B cell Biology

B lymphocytes in conjunction with T lymphocytes represent the adaptive arm of the immune system. They are produced throughout the entire life of an individual and originate from multipotent hematopoietic stem cells that give rise to all blood cells (8, 9). The differentiation of a common lymphoid progenitor into a certain cell lineage is accompanied by expression of interleukin 7 (IL-7) receptors and interaction with early determining factors such as the cytokine stem-cell factor (SCF) and chemokine stromal cell-derived factor 1 (SDF-1) that drive differentiation towards the B cell-lineage in the bone marrow (1, 10). B lymphocyte development can be divided into two phases, depending on the specialized lymphoid tissue in which maturation takes place. First the lymphocyte progenitor resides in the bone marrow, the central lymphoid tissue, where the progression through the different developmental stages is dependent on the assembly of a functional, not self-recognizing B cell receptor (BCR) (1, 2, 9, 11). This BCR represents the membrane-tethered antigen receptor, which will be secreted as antibody by the activated, fully matured B cell (12). After several stages of differentiation, the immature B cell expresses a number of surface proteins that facilitate the migration from the bone marrow into peripheral lymphoid organs, such as the lymph nodes and the spleen, where the second phase of the development commences. At this point the B cell fate is mostly antigen dependent, as BCR activation and supporting signalling pathways, for example from B cell activating factor (BAFF) receptors, provide the necessary stimulus for B cell survival and differentiation into the final effector cell types (1 8, 9). The following sections will provide a detailed insight into B cell development and illustrate the fundamental processes that precede antibody production.

1.2.1 B cell development in the bone marrow

The earliest B-cell stage found in the bone marrow is called pro-B cell and defined by activity of the transcription factor E2A and the early B-cell factor (EBF) which induce expression of central proteins for the rearrangement of the variable (V), the diversity (D) and the joining (J) gene segments of the BCR (1, 13, 14). As mentioned above, the BCR represents the antibody as transmembrane receptor, consisting of two identical heavy and light chains with an additional transmembrane and cytoplasmic domain (5). The heavy chain is composed of one variable and three constant domains whereas the light chain only includes one constant domain in addition to a single variable domain (1, 5). These variable domains are encoded by VDJ and VJ gene segments for the heavy and light chain respectively. Multiple copies of each gene segment are clustered at three genetic loci distributed on three separate chromosomes, two encoding the light and one the heavy chain genes. Sequencing of the human genome revealed more than 40 functional V gene, 23 D gene and 6 J gene segments as part of the heavy chain locus (1, 15). Only one of the V, D and J segments is selected in the process of somatic recombination which is initiated in the pro-B cell stage.

The recombination-activating genes RAG1 and RAG2 produce indispensable components of the V(D)J recombinase and create a tremendous combinatorial diversity (16). However, the process of gene rearrangement leads to double-strand breaks that are repaired by imprecise non-homologous end joining, resulting in uncontrolled loss or addition of nucleotides. Insertions and deletions pose a threat to B-cell development and indeed about 45% of B cells are lost due to negative selection at this stage. However, the introduced junctional diversity is one of the principal mechanisms for the generation of a comprehensive BCR and immunoglobulin repertoire (1, 17). Another essential transcription factor of the pro-B cell maturation stage is Pax5, which mediates the expression of the CD19 receptor and whose absence prevents further development. With the expression of CD19 and an intact constant domain of the heavy chain which signifies successful rearrangement, the cell advances to the next developmental stage called the pre-B cell (18, 19).

Several processes are initiated in a pre-B cell, including the generation of a surrogate receptor, which consists of the newly assembled heavy chain and an invariant light chain that promotes cross-linking of multiple surrogate receptors (20). Clustering of linked pre-B receptors mediate the down-regulation of the VDJ recombinase to ensure the expression of a single heavy chain per B cell and enforces allelic exclusion (21, 22, 25). Additionally, proliferation is stimulated before the RAG protein-guided gene rearrangement of the light chain continues. Similar to

allelic exclusion, the light chains display isotypic exclusion, resulting in the expression of either a lambda or a kappa light chain (23). The occurrence of one isotype over the other is used for diagnostic purposes, as the distribution proved to be stable throughout the population and a divergence from this ratio indicates a lymphoproliferative disorder (1). Once the combined heavy and light chain are expressed as surface IgM, the pre-B cell becomes an immature B cell and reaches the final stage of development in the bone marrow (1, 9, 12).
Formation of a membrane complex with the transmembrane proteins Igα and Igβ that carry cytoplasmic phosphorylation sites, so called immunoreceptor tyrosine-based activation motifs (ITAMs), enable signal transduction and the first test of the antigen receptor for reactivity to self-antigens (12, 27). Central tolerance refers to regulatory mechanisms that eliminate such autoreactive immature B cells from the emerging B cell pool (12). However, autoreactive B cells can be rescued from clonal deletion by the mechanism of receptor editing (26, 27). In this process, the prolonged expression of RAG permits ongoing light chain gene rearrangement to modify the specificity of the B cell. If the efforts are unsuccessful, the autoreactive B cell is subjected to cell death by apoptosis. In contrast, the encounter with a low valency self-antigen does not necessarily result in clonal deletion, but triggers a stage of anergy in which the autoreactive B cell becomes functionally inactive (1, 28). Immature B cells that endured the surveillance mechanisms of the central tolerance or were positive selected by continuous, subliminal signalling of unligated BCR emigrate from the bone marrow into the blood (1, 2, 12).

1.2.2 B cell development in the peripheral lymphoid tissue

Immediately after B cells emerge from the bone marrow, they are subjected to the peripheral tolerance that further reduces autoreactive B cells. Emigrant B cells are still functionally immature, therefore the encounter and activation by sufficient quantities of antigen renders the B cell anergic, mediates antigen receptor desensitization or induces apoptosis (11, 29, 30). Under normal circumstances, B cells migrate to the spleen where they differentiate into naïve mature B cells and start to express additional surface receptors such as membrane-anchored IgD that functions as secondary BCR (1, 11). Mature naïve B cells recirculate the blood and enter the lymph node through high endothelial venules located in the interfollicular region. Inside this specialized lymphoid tissue, naïve B cells aggregate in follicles and reside for about 24 hours to probe for their cognate antigen (8, 31). Follicular dendritic cells and other resident cell types of the follicle express the chemokine C-X-C motif ligand 13 (CXCL13), producing

a gradient that guides naïve B cell towards secondary lymphoid structures (32). On the contrary, the antagonistic molecule gradient of sphingosine 1-phosphate promotes the egress from the lymphatic system into the blood and drives B cells to repeat this journey (33).

B cells at this stage are called transitional immature (TI) and develop either into follicular B cells or marginal zone B cells depending on the lymphoid tissue they are located in and the interplay of three signals: BAFF, NOTCH2 and BCR (1, 2, 9, 34, 35). BAFF is an essential survival factor produced by follicular cells, most importantly follicular dendritic cells, that bind to different receptors expressed by B cells including the BAFF receptor (BAFF-R). Signals from the BAFF-R activates the NF-kB pathway which provides survival while also upregulating the expression of NOTCH receptor 2 (NOTCH2) (9, 36, 37). This receptor binds the delta-like protein 1 (DLL1), expressed by a variety of cells in the spleen, upon which, it is cleaved and the intracellular domain transported to the nucleus where NOTCH2 functions as transcription factor for genes involved in the development of marginal zone (MZ) B cells (9, 35). All of these processes take place in the context of a weak BCR signalling. Intense clustering of the BCR due to antigen recognition activates the Bruton's tyrosine kinase (BTK) which inhibits the NOTCH2 signalling pathway and facilitates gene expression for the commitment to the follicular (FO) B cell fate (38). In summary, weak BCR signalling in addition to NOTCH2 activity drives the development of MZ B cells, while strong BCR signals and a lack of NOTCH2 promotes the differentiation into follicular B cell. BAFF-R signalling acts as mediator between the two pathways by skewing the development towards a MZ B cell fate for high BAFF concentrations, however the complete absence of BAFF prevents the maturation of any peripheral B cell lineage (39).

The major differences between MZ and FO B cells are the quality of the antibody response and the memory formed after antigen encounter. MZ B cells feature several pattern recognition receptors (PRR), such as the toll-like receptor (TLR) and are defined by upregulated complement receptor CD21 as well as surface IgM expression which allow for a T-cell independent activation (9). The antibodies produced are predominantly low-affinity IgM, even though class-switch recombination to IgG or IgA has been reported (40, 41). Nevertheless, T-cell independent antigens can generate long-lived plasma cells and memory B cells with a phenotypically distinct profile compared to B cells that responded by means of T-cell help (42). FO B cells encounter antigen through BCR binding, rapidly internalize and degrade the antigen into a linear epitope that can be loaded onto a major histocompatibility complex (MHC) class II molecule (43, 44). The MHC class II antigen - peptide complex gets expressed on the cell surface and functions as primary recognition site for T cells. In the pursuit to find T cell help,

the activated B cells migrate towards the boundary of the T cell zone as both lymphocytes occupy distinct areas of the lymphoid tissue (1). This migration is supported by the CC-chemokine receptor 7 (CCR7) expressed on B cells which recognizes the CC-chemokine ligand 19 (CCL19 and CCL21), produced by stromal cells in the T cell area (45). Similarly, antigen-experienced helper T cells, referred to as follicular helper T cells (T_{fh}), mirror the movement and get attracted to the B cell follicle by expression of CXCR5 (46, 47). When antigen-presenting B cells encounter T_{fh} cells with matching specificity, help is provided by secretion of IL21 and CD40L – CD40 interaction (1, 48). As a consequence, B cell survival is increased, co-stimulatory molecules are expressed and the B cell moves back to the interfollicular regions with their associated T_{fh} cell where they form a germinal centre (3).

However, the combination of BCR engagement and a lack of survival signals induced from CD40 ligation leads to activation induced cell death (AICD), another tolerance mechanism that prevents the production of autoreactive antibodies (49). In the germinal centre the process of affinity maturation produces B cells with high affinity to the antigen presented earlier to T_{fh} cells (3). The variable region of the immunoglobulin gene acquires somatic hypermutations which modulates the affinity, while simultaneously only B cells with the highest affinity are selected for survival. Furthermore, class switch recombination is induced by the activation-induced cytidine deaminase (AID) to change the heavy constant region of the encoded immunoglobulin (50). This customization of the antibody class enables the selection of the effector function which is best suited for combating the respective pathogen. The end results are high affinity, long-lived plasma cells that secrete efficacious antibodies and long-lived memory B cells providing protection against reinfection by the same pathogen. Alternatively, B cells accumulate in extrafollicular foci where they differentiate into short-lived plasmablasts that already secrete antibodies of different isotypes but with lower affinity due to little somatic hypermutation and limited access to affinity maturation (51, 52). Memory B cells are known for their longevity and the efficient response to repeated antigen exposure, but even long-lived antibody-secreting plasma cells are thought to contribute to the immunological memory. Migration back to the bone marrow allows for the colonization of a survival niche where proliferation is arrested but antibody production continues (4, 52).

1.3 Antibody mediated immune response

The antibody generation is of vital importance for host defence against infectious agents and represents the humoral response of the adaptive immune system. Antibodies prevent pathogen

entry through binding and direct neutralization but also facilitate the clearance of infected cells by interconnecting several antimicrobial processes from the innate with the adaptive immune system (1, 2, 5). As described above, a specialized subset of terminally differentiated B cells, termed plasmablasts and plasma cells secrete antibodies with diverse effector functions. The antibody production is regulated at multiple maturation stages and displays the main determinant for the development and survival of the emerging B cell. All antibodies consist of two functional domains: the fragment antigen binding (Fab fragment) domain that provides the specific antigen interaction, and the fragment crystallizable (Fc fragment) region which activates immune cells and soluble components of the humoral immunity (5, 54). Both domains are interconnected by a hinge region which allows a certain degree of flexibility for the interaction with the target antigen. Fab fragments possess two identical arms, each of which has a heavy and a light chain composed of a constant and a variable immunoglobulin domain. The constant and variable domain are constructed from two β-sheets folded onto each other with three hypervariable loops extended at the N-terminus of the variable domain that constitute the antigen binding site (1, 55). The three hypervariable regions, also known as complementarity-determining regions (CDR), from the heavy combined with the three CDRs from the light chain confer the antigen specificity (56). Antibodies mostly bind to conformational epitopes, which represents a discontinuous sequence of amino acids brought together by the tertiary structure of a protein (1). The binding of an antibody to the antigenic target is mediated by non-covalent forces, primarily determined by the CDRs, however the neighbouring framework regions on the β-sheet and variable glycosylation patterns can influence the steric constraints, and thus the binding specificity of the antibody (1, 57).

Another key feature of the humoral immune response is the vast diversity of the antibody repertoire which offers protection against virtually any invading pathogen. The combinatorial diversity created by the somatic rearrangement of the V(D)J gene segments during early B cell development in the bone marrow is one of the mechanisms that facilitate the immense antibody repertoire (58, 59). The Fc region determines the effector functions of an antibody and is ultimately selected in the late, antigen-dependent phase of the B cell development in the secondary lymphoid organs (5). All five immunoglobulin classes: IgM, IgD, IgG, IgA and IgE, defined by their heavy chain constant region, can be expressed first as transmembrane receptors before being secreted as soluble antibodies (1). Affinity maturation in the germinal center is accompanied by the activation of AID which regulates two important processes for antibody diversification. First it induces deamination of cytosine bases in the variable region of the

immunoglobulin, leading to mismatch repair or base-excision repair and ultimately somatic hypermutations (1, 60). Secondly, AID initiates class switch recombination in which the exon of the heavy chain variable region is fused with a different heavy chain constant gene (50). The constant regions are encoded in a cluster of gene segments with flanking DNA repeats, called switch regions, that enable non-homologous recombination after double strand breaks are introduced by the initial action of AID (61, 62). Each immunoglobulin isotype provides unique features for the antibody function, for example the penta- or hexameric IgM have enhanced avidity but low affinity for antigens and are considered primary activators of the complement system (5, 63). IgA on the other hand is a weak complement activator but can be linked into dimers by disulfide bridges and secreted in the mucosal tissue (1, 5). IgG are the most common antibody isotype found in the blood circulation and can be further divided into the subclasses IgG_1 – IgG_4 which in turn have their own functional advantages. The more flexible hinge region of an IgG_3 allows improved antigen complexation and enhanced binding by complement components while rendering the antibody more susceptible to proteolytic cleavage. Therefore, IgG_3 exhibits the lowest half-life of all four subclasses. IgG_1 shows the second highest effector potency, followed by IgG_2 whereas IgG_4 provides rather regulatory functions and is incapable of activating complement (1, 2, 5, 64, 65).

Fc domains of antibodies can be fine-tuned by posttranslational modifications in the form of additional glycans, which impact the stability, half-life and interaction-profile of the antibody (5, 66). Exchange of an individual glycosylation, namely the removal of fucose from an IgG_1 Fc domain has been shown to dramatically improve Fc receptor binding and subsequently antibody-dependent cellular cytotoxicity (ADCC) (67). One of the three major mechanisms deployed by antibodies to prevent the spread of pathogens and to clear already infected cells is opsonization. Binding the target and making it accessible for phagocytosis by innate immune cells prevents the evasion of pathogens and viral infections from the immune surveillance. This effector function is coordinated by a membrane-expressed Fc sensor that recognizes the Fc domain of an antibody and the immune cell that actually expresses said Fc receptor (FcR) (5, 68). There are different types of FcR which are classified according to the antibody isotype they recognize, for example Fcγ receptors bind the constant region of IgG antibodies. The antibody recognition domain belongs to the glycoproteins of the immunoglobulin superfamily and in case of the Fcγ receptor it contains a ligand-binding α-chain (68, 69). The receptor functions as a complex with additional subunits that facilitate the expression of the extracellular α chain and intracellular domains that mediate signal transduction. The Fcγ receptors I and IIA

(CD64 and CD32A) are expressed by several immune cells, including macrophages, neutrophils and eosinophils and stimulate phagocytosis of opsonized particles as well as cell activation of the immune cell through intracellular ITAM signalling (5, 68, 70). A different set of innate immune cells, called natural killer (NK) cells express the FcγRIII (CD16) receptor which mediates ADCC of opsonized targets by releasing cytoplasmic granules that contain perforin and granzymes for the lysis of cells (71, 72). In contrast to these activating Fc functions, FcγRIIB (CD32B) represents an inhibitory receptor that originated from multiple gene duplications and recombination with an immunoreceptor tyrosine-based inhibitor motif (ITIM) as cytoplasmic tail (72). The receptor expression on B cells provides a feedback loop, as binding of immune complexes to the FcγRIIB increases the threshold for activation and downregulates antibody production (73). Similar adjustments of the activation-threshold have been observed for macrophages and neutrophils, whereas dendritic cells employ CD32B for the efficient uptake and processing of antigens (72).

These antibody-mediated mechanisms constitute an interface with the innate immunity. Hence, they have a direct impact on pro-inflammatory responses and the removal of infected cells. As discussed before, direct neutralization of viral particles and toxins is another effector function of antibodies. The Fab domain of an antibody binds a specific antigen target to prevent the entry of a pathogen, inhibit bacterial toxins or the formation of a biofilm (5). Even though neutralization depends only on paratope-epitope recognition, the disposal of the generated immune complex from the extracellular space has to be supported by FcR functions to guarantee full protective efficacy (72, 74). Complement activation is another protective mechanism of antibodies which amplifies opsonization and disrupts the membrane integrity of a target cell, leading to cell lysis (5). The complement system has an antibody-independent contribution to the humoral immune response and is of particular importance in the scope of this work, hence it will be addressed separately in the following section.

1.4 The complement system

The complement system is part of the innate immunity and the early defence mechanisms against infections, as it opsonizes target cells, coordinates phagocytosis, attacks membrane integrity and triggers an inflammatory response (1, 2, 75, 76). Additionally, complement components enhance (complement) antibody-mediated effector mechanisms, such as opsonization, but also processes like B cell activation, antigen-presentation of follicular dendritic cells and T cell homeostasis (75, 77, 78, 79). Thus, complement activation has a

systemic influence on multiple biological processes and its importance is demonstrated by the increasing number of new therapeutic approaches in recent years (75, 76). The complement system consists of an enzymatic cascade that relies on soluble and membrane-bound proteins to assemble in complexes with proteolytic activity for the production of bioactive fragments. Depending on the initial molecule that activates the complement cascade, three separate pathways can be distinguished: the lectin, the alternative and the classical pathway (5, 75, 76, 80). The classical pathway utilizes antibody opsonization as recognition pattern for the recruitment of the first complement components, consisting of C1q and the associated zymogens C1r and C1s (75, 81). The primary target of C1q is a hexameric immunoglobulin structure, either provided by IgM or clustered IgG_1, IgG_2 and IgG_3, whose binding leads to conformational changes in the C1 complex that generates the enzymatic activity of the two zymogens (75, 82). As a consequence, the soluble complement components C4 and C2 are cleaved and the resulting products C4b and C2a form a C3 convertase, a membrane-associated complex, that facilitates the proteolytic cleavage of C3. The larger C3b fragment combines with the existing C3 convertase to form the C5 convertase while the smaller C3a protein functions as anaphylatoxin with immunomodulatory and pro-inflammatory capacity (76, 83, 84). The lytic pathway of the complement cascade starts with the dissociation of C5 into C5b and C5a, both of which have comparable functions to their C3 equivalents. C5b binds non-covalently to the C5 convertase and recruits C6 and C7 to form a complex that causes conformational change in C7 and allows the insertion of its lipophilic extension into the membrane. Now the transmembrane proteins C8 and C9 follow as last components of the membrane attack complex (MAC) to create a pore for the osmotic lysis of the target cell (75, 76, 85).

All three enzymatic cascades converge at C3, therefore all three promote the effector arms of the complement activation in terms of phagocytosis, inflammation and membrane attack (80). The lectin pathway is initiated by the pattern recognition receptor mannose-binding lectin (MBL) and ficolin that interact with carbohydrate structures on the surface of microbes. Association with serine proteases activates the enzymatic cascade through proteolytic cleavage of C4 and continues on as described for the classical pathway (75, 76). The alternative pathway employs different enzymatic complexes and can progress in a fluid phase in parallel to the membrane-bound complement cascade. Continuous activation in the fluid phase results from the spontaneous hydrolysis of C3 which co-operates with factor B and factor D for the cleavage of subsequent C3 proteins (75, 86). Alternatively, an amplification loop is generated by

covalently bound C3b that interacts with the same two factors plus properdin, the only known positive regulator of complement activation (76).

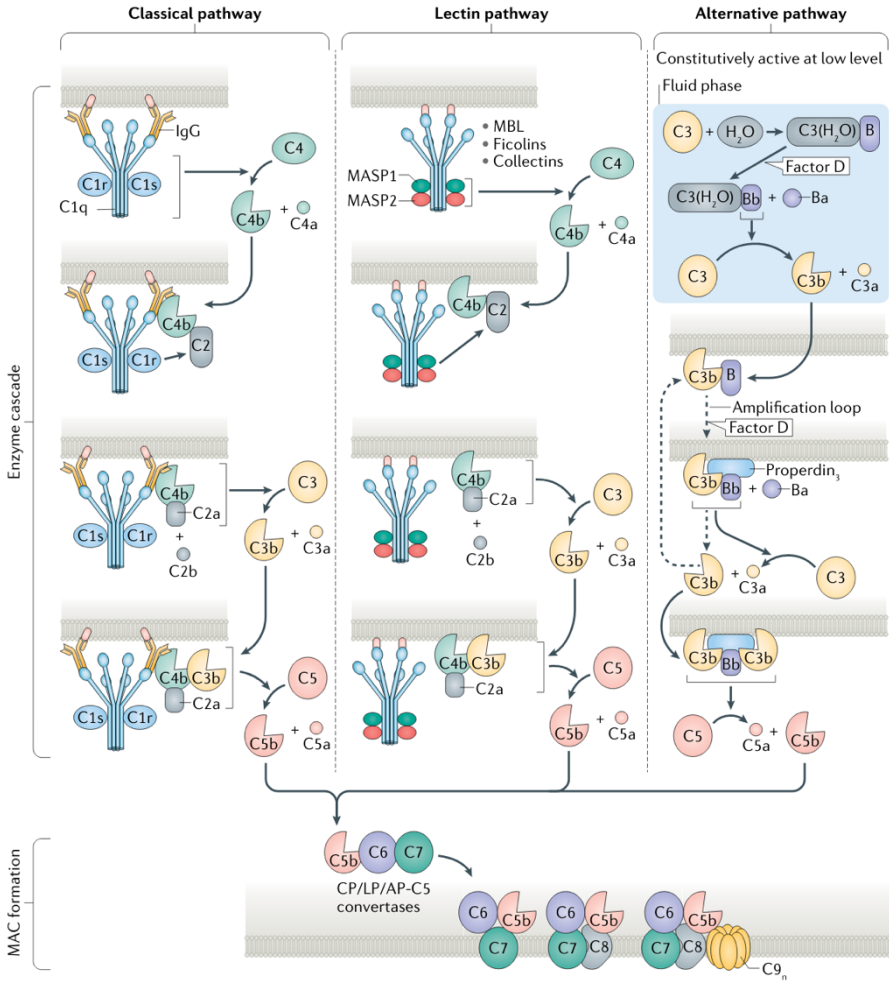

Figure 1: Schematic of the different complement pathways
Depiction of the principal components involved in the three different cascades which are distinguished by their differential initiation. All three pathways employ the similar components, converge at the proteolytic cleavage of C3 and the C5. The formation of the membrane attack complex as terminal effector function of the complement system is displayed as well.
Adapted from Dalakas et al., Nature Reviews Neurology, 2020 (75)

This alternative membrane-associated C3 convertase complex facilitates the rapid increase of available C3a and C3b and therefore the effector mechanisms of the terminal complement cascade. Opsonization with C3b and C4b stimulates immune cell phagocytosis via complement receptor 3 and 4 (CR3 and CR4) expressed on monocytes, macrophages and neutrophiles (76). The complement receptor 1 (CR1) is predominantly found on erythrocytes and mediates the clearance of C3b-coated immune complexes. The C3b-opsonized complex is loaded onto red blood cells and transported to the spleen where phagocytosis and degradation by macrophages takes place (87). As previously alluded to, complement activation supports different processes of the adaptive immunity through the complement receptor 2 (CR2), also known as CD21. The

B cell co-receptor complex consists of CD21, CD19 and CD81 and binds to C3 fragments which leads to the relocation into close proximity of a BCR (88, 89). Subsequently the cytoplasmic domain of CD19 is phosphorylated by tyrosine kinases of the activated BCR and induces downstream signalling to enhance B cell activation, differentiation and antibody production.

In light of the potential self-amplification a tight regulation of the complement cascade is required to avoid inadvertent damage. Most regulatory mechanisms target either the assembly or the degradation of the C3 convertase. For example, the complement regulatory protein DAF (decay accelerating factor or CD55) competes with factor B of the alternative pathway for the binding to C3b, as does factor H (76, 90). Additionally, factor H acts as cofactor for the serine protease factor I which cleaves C3b into the inactive protein fragment iC3b and disintegrates the C3 convertase (1, 91). Surface expression of the CR1 exerts also regulatory activity by accelerating the dissociation of the C3 convertase and supporting the factor I induced proteolysis (76, 92). These complement-regulatory proteins provide some control over the fast-acting and self-amplifying properties of the complement system, which render it an important constituent of the immune system. However, self-directed or dysregulated complement activation can result in collateral tissue damage and represent the fundamental pathomechanism described for inflammatory and autoimmune diseases. Abnormal development of B cells constitutes a further cause for the emergence of autoimmune diseases and is discussed in the next chapter.

1.5 Autoimmunity – breach of central and peripheral tolerance

Autoimmunity is the general concept of an immune response against the host's own, healthy cells, tissues or components which in turn leads to symptoms of disease. Self-antigens are recognized by autoreactive lymphocytes and incite for example B cells to produce disease-causing autoantibodies. Autoimmunity can be classified according to the predominant immune effector pathway that mediates the disease. In addition to the disease mechanism, the classification is dependent on whether the pathology is restricted to specific organs or has a systemic impact (1, 2). Hashimoto's thyroiditis and graves' disease, for example, represent organ-specific autoimmune diseases mediated by autoantibodies, whereas type I diabetes and psoriasis are also organ-specific but caused by autoreactive effector T cells. Rheumatoid arthritis (RA) and systemic lupus erythematosus (SLE) on the other hand belong to the category of systemic autoimmune diseases (1, 93). In general, autoimmunity arises spontaneously,

meaning the exact events that trigger the self-targeting immune response are not known. Some disorders may result from molecular mimicry, a postulated mechanism in which pathogen-derived peptides show sequence similarities with epitopes on host molecules and lead to the production of cross-reactive antibodies (94, 95). However, convincing evidence for this mechanism is scarce and only reported in a limited number of cases with neurological disease (96). Inflammation is another driving factor of autoimmune diseases, especially in RA and SLE, as chronic tissue injury breaks down compartmentalization and generates constant exposure to otherwise inaccessible self-antigens. The progression of the autoimmune response can lead to the recruitment of new lymphocytes and thus epitope spreading, a broadening in epitope recognition on the same antigen (1, 97).

Theoretically, all of these deleterious immune responses should be prevented by the different tolerance mechanisms along the development and activation of immune effector cells. The generation of antibodies and receptor motifs with broad specificity offer a physiological advantage by tightening the host defence against pathogens with congruent surface structures and allows the detection of minimal aberrations from the healthy condition (1,96). Therefore, a leakiness of the tolerance presents a tight balance between high sensitivity and self-harm. The earliest B cell tolerance mechanisms occur in the bone marrow where the newly rearranged V(D)J gene segments of the heavy and light chain produce BCRs of any given specificity and therefore have to be tested for self-reactivity (11, 12). This central tolerance checkpoint removes about two-thirds of all immature B cells from the emerging population (29). Clustering of the B cell receptor induces either direct clonal deletion through apoptosis, an anergic state of functional unresponsiveness or receptor editing (11, 12, 26, 27). However, receptor editing only allows the substitution of the light chain, hence cell death or anergy seem to be inevitable if the CDR of the heavy chain already exhibits high affinity to a self-antigen. The second tolerance checkpoint takes place in the periphery, which also reduces the number of autoreactive B cells through similar mechanisms (11). BCR activation without additional stimulation by extrinsic factors such as regulatory T cells, BAFF or CR2 ligation either deletes of inactivates the self-recognizing B cell (9, 51, 88). Both the central and peripheral tolerance exert damage control by purging self-reactive B cells while maintaining the BCR repertoire as comprehensive as possible.

The germinal center (GC) reaction on the other hand is involved in the removal but also the de novo generation of autoreactive B cells through the process of affinity maturation (51, 98). The GC is a specialized structure in the secondary lymphoid organs that forms after successful antigen presentation by B cells to activated T_{fh} cells (1). The anatomy of the GC is divided in

a light zone containing follicular dendritic cells (FDC), T_{fh} cells and tingible body macrophages and a dark zone that is mostly populated by extensively proliferating B cells (3, 99, 100). Activated germinal center B cells express the chemokine receptor CXCR4 which interacts with the CXCL12 ligand of stromal cells and retains B cells in the dark zone of the GC for a limited time (101). The activation of AID leads to the accumulation of somatic hypermutations and class switch recombination during this proliferation period (50). Migration to the light zone is regulated by CXCR4 reduction and the chemokine interplay of CXCR5 on B cells and CXCL13 of FDC (101). Here the selection process for high affinity BCR is mediated by antigen-expressing FDC, activated T_{fh} cells and a pro-apoptotic gene expression program in GC B cells. The downregulation of the cell death regulator BCL-2 couples B cell survival to an increased dependency on external stimulation by the CD40 signalling pathway (3, 51, 102). Thus, B cells with higher affinity capture more antigen presented by FDC and in turn are capable of presenting a higher density of MHC class II complexes to T_{fh} cells for CD40 activation. Low affinity B cells get outcompeted for T cell help, undergo apoptosis and get phagocytosed by tingible body macrophages. This dynamic process of mature activated B cells entering the germinal center, circulation of GC B cells through the different zones for further rounds of affinity maturation and apoptosis of low affinity B cells produces highly efficacious antibodies, but offers ample opportunities for autoreactive B cells as by-product (1, 2, 51, 100).

Most control mechanisms reported in the GC were established in animal models, as contribution of tolerance mechanisms by human GC in the context of autoantibody production is extraordinarily difficult to study. Dysregulation of the central T cell tolerance is a prerequisite for autoreactive T helper cells that respond to follicular B cells and allow formation of GC (1, 51, 96). Both the quality and the quantity of T_{fh} cells play a role in the SLE-phenotype of different mouse models. Reduced numbers of T_{fh} cells are accompanied by decreased GC numbers and importantly an amelioration of the disease phenotype (51, 103). Furthermore, the expression of surface receptors and chemokine production, such as CD95L (FAS ligand) or IL-21 by T_{fh} cells have been shown to be instrumental for the SLE-like disease in mice (51, 104, 105). Different lines of research provide evidence for the necessity of dysregulated germinal center reactions for the onset of autoimmune disease in humans. Patients with autoantibodies against receptors or channel proteins expressed in the central nervous system, such as aquaporin 4, GABA or LGI1 exhibit memory B cells and plasma cells with extensive somatic hypermutations (96, 106). The reversion of the autoantibody sequence to germline resulted in a loss of binding, which strongly suggested affinity maturation towards autoreactivity in the

GC (107). In patients with SLE high affinity, somatic hypermutated DNA-specific antibodies are found together with hyperactive GCs in the secondary lymphoid organs. Additionally, GCs are littered with apoptotic bodies providing readily accessible nuclear antigen for continued B cell maturation (98, 108, 109).

A third piece of evidence comes from B cell depleting therapies with anti-CD20 monoclonal antibodies which have been used extensively for different disease types. Some autoimmune diseases such as rheumatoid arthritis, multiple sclerosis and a certain subclass of myasthenia gravis showed improved clinical symptoms, but in particular patients with SLE do not benefit from the treatment and some experience severe disease flares on drug cessation (8, 80, 110, 111). Plasma cells no longer express CD20, thus autoimmune diseases that result from long-lived plasma cells that produce highly mutated and class switched autoantibodies are likely not effected by anti-CD20 therapies.

1.6 Myasthenia Gravis – A prototypic autoimmune disorder

Myasthenia Gravis (MG) is a neuromuscular autoimmune disease in which antibodies against components of the neuromuscular junction (NMJ) disrupt the signal transmission from nerve to muscle, leading to the characteristic manifestation of muscle weakness and increased fatigability (112, 113). The incidence of this rare neurological autoimmune disorder ranges from 150-300 cases per million and is consistent in most examined populations (114, 115). Patients are classified into different subgroups depending on the age of onset, effected muscle groups, thymus pathology and the presence of specific antibodies (112, 116). The two major subgroups according to age display a bimodal pattern with early-onset MG showing a peak at 30 years of age and late-onset MG manifesting after the age of 50 (80, 117). Early-onset MG is more common in females than in males, it is associated with thymic hyperplasia and a specific MHC class I haplotype, thus including a genetic predisposition (118, 119). In contrast, late-onset MG comprises a patient subset with normal or atrophic thymus, a rather even prevalence between genders with a slight shift towards men and an association with MHC class II genes (118, 119).

The disease presents the clinical hallmark of muscle weakness with varying degrees of severity and including different muscle groups. In ocular MG the eye muscles are affected leading to ptosis – the drooping of the eyelids and double vision, which is diagnosed as diplopia (112). A broader range of symptoms is detected in patients with generalized MG. In addition to the extraocular muscles the involvement of the cranial nerve impacts muscles of the head and neck

area associated with speech and swallowing but also the axial and limb muscles can be affected (112, 116). The abnormal weakening of particular muscle groups progresses throughout the day or after repetitive use and can be detected by electrophysiological measurements (112, 120). Exacerbation of symptoms can result in a myasthenic crisis, a life-threatening condition characterized by respiratory failure that requires ventilation and intensive care (121). Even though MG is a heterogenous disease with multiple subgroups all of them have a common denominator, namely antibodies against extracellular proteins at the NMJ that induce pathogenicity. In 85% of patients these autoantibodies target the acetylcholine receptor (AChR) located at the post-synaptic membrane of the NMJ (122). The percentage of AChR-positive MG patients increased in the past years due to the emergence of cell-based assays with higher sensitivity compared to the commercially available radioimmunoassay (RIA) which is still used as standard diagnostic tool (117). The second most common antibody target is the muscle-specific kinase (MuSK) protein, present in 4-8 % of individuals with myasthenic symptoms (80, 112). Followed by a third subset of patients with antibodies against the lipoprotein receptor protein 4 (LRP4), whose frequency is highly variable, depending on the experimental method and the examined population (123, 124). Similar to anti-agrin and anti-titin, antibodies targeting LRP4 are regularly identified in combination with AChR- and MuSK-specific antibodies, limiting the prevalence of exclusively LRP4 to less than 4% of all MG cases (123). The pathogenic potential of antibodies has already been demonstrated in the late 1970s through passive transfer experiments of the immunoglobulin fraction from MG patient sera into animal models that subsequently developed severe muscle weakness (125, 126, 127). The diverse symptoms diagnosed in MG can be attributed to the antibody characteristics, the multitude of effector functions and the complex interplay with the neuromuscular signal transmission which will be discussed next in more detail.

1.6.1 Disruption of signal transmission at the neuromuscular junction

The NMJ facilitates the transmission of action potentials arriving at the pre-synaptic nerve terminal to the motor end plate of a muscle fiber. The AChR at the post-synaptic membrane is a neurotransmitter-gated ion channel that transduces a chemical signal into an electrical signal. The opening of voltage-dependent calcium channels triggers the release of acetylcholine (ACh) from pre-synaptic vesicles. Almost instantly the ACh molecules diffuse across the synaptic cleft and bind to the α-subunit of the AChR. The specific binding to the receptor generates the endplate potential that promotes sodium channel opening, influx of cations along the

electrochemical gradient, which ultimately depolarizes the membrane and causes the muscle to contract (112, 128, 129). The key component in this signaling process, the muscle-type AChR, is a 290 kDa heteropentamer composed of two α-subunits and one each of β-, δ- and ε-subunit (adult type, whereas the fetal AChR incorporates a γ instead of the ε-subunit) that spans the plasma membrane (129, 130). Its high density along the crest of the folds formed on the post-synaptic membrane in conjunction with the rapid diffusion and hydrolysis of ACh by the acetylcholinesterase produce a near perfect on-off switch for the transmission of nerve impulses (129).

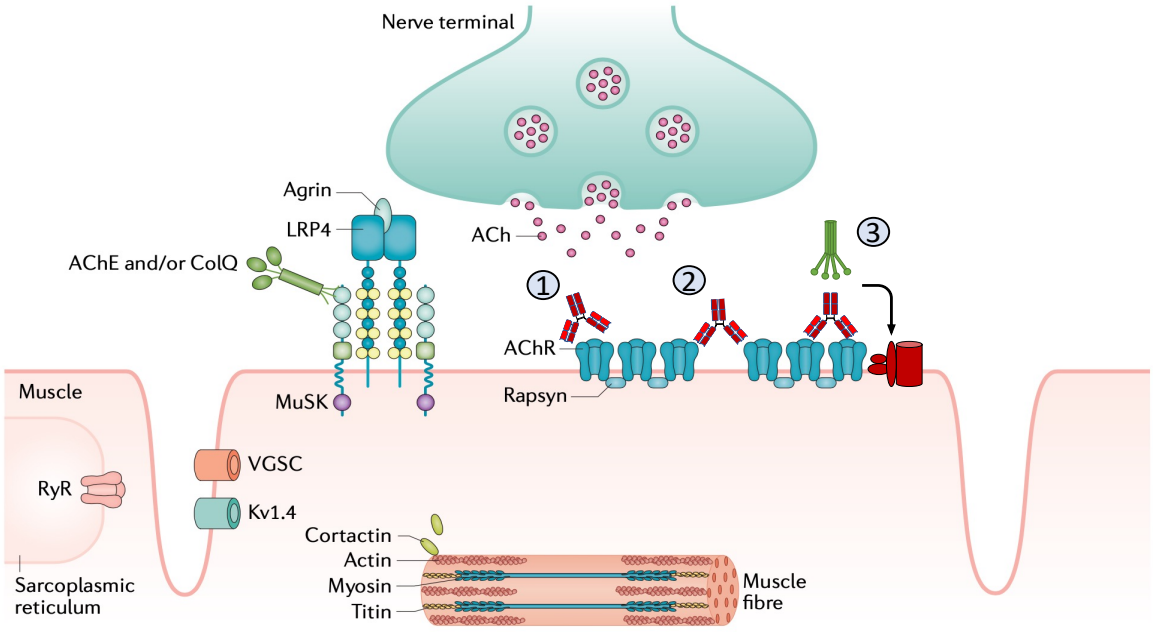

Figure 2. Schematic depiction of neuromuscular junction in myasthenia gravis.
Proteins targeted by autoantibodies and expressed at the post-synaptic membrane, including the acetylcholine receptor (AChR). The presumed modes of action that induce myasthenia gravis are highlighted: 1) direct receptor blockade; 2) antigenic modulation via receptor cross-linking; 3) complement activation with formation of a membrane-attack complex.
Adapted from Gilhus et. al., Nature Reviews Disease Primers, 2019 (112)

A polyclonal antibody response against the AChR is found in most MG patients with elevated levels of all four IgG subclasses (112, 131). The distribution of the AChR-specific antibody isotypes is dominated by IgG_1 and IgG_3, which differs from the global pattern as IgG_2 are underrepresented but follows the antibody profile of a prototypic T-cell dependent humoral response against protein-antigens (131, 132, 133, 134). Determining the explicit epitope of anti-AChR antibodies has been inherently difficult as most antibodies recognize conformational epitopes which eliminates the usage of denatured, soluble proteins (135, 136). Additionally, the expression of individual AChR subunits while retaining the conformational integrity has only been achieved in the past year and was solely demonstrated for α- and β-

subunit targeting antibodies (137). Nevertheless, animal studies suggested that antibodies targeting the a-subunit are most pathogenic and pointed towards a group of overlapping epitopes spanning across amino acids 67–76 of the extracellular α-subunit domain (138, 139). Subsequent research on patient sera confirmed this so-called main immunogenic region (MIR) were more than 50% of antibodies bind and which seems to be indicative of disease severity (135).

Compelling evidence was collected in the early days of MG research that suggested three modes of action driving the pathogenicity: first, direct receptor antagonism by blocking of the ACh binding site; second, antigenic-modulation with accelerated internalization and degradation of the AChR induced by receptor cross-linking; and third, complement activation leading to damage of the post-synaptic membrane. It is well established that myasthenic serum has the capacity to interfere through direct AChR blockade, still, it is considered the least relevant of the three proposed mechanisms. One reason is the limited occurrence of antibodies with the necessary characteristics, highlighted by the fact that no human-derived, monoclonal antibody has been isolated that mediated (exclusive) receptor blockade in a functional assay (140, 141, 142). Furthermore, MIR targeting antibodies do not directly interfere with ACh binding and despite of excessively high antibody titers patients can show well-preserved channel activity, which supported the assumption of a limited clinical relevancy (138, 143).

The involvement of complement activation was initially discovered by the presence of complement component depositions at degenerated NMJ in patient muscle biopsies as well as in animal models of the disease (126, 127). Furthermore, C9 complement component which is part of the terminal membrane-attack complex, was associated with the deteriorating post-synaptic membrane of myasthenic individuals (143). The predominance of the complement activating IgG subclasses 1 and 3 offers an explanation why most antibodies against the AChR induce the complement cascade. Yet, additional evidence supporting the importance of complement-mediated pathology in MG was provided by animal models either lacking genes encoding complement components or treated with inhibitory antibodies (144, 145, 146, 147). Furthermore, the recent advent of several complement inhibitors as new therapeutic strategies for MG are a strong indicator for the increasing acknowledgement of complement activation as essential driver of the disease.

The turnover of AChR on the post-synaptic membrane has been shown to be skewed towards increased internalization and degradation after treatment with MG patient derived IgG. The de novo synthesis becomes unable to compensate the loss of AChR due to the accelerated

internalization, a process also demonstrated in the diaphragm of rats treated with serum of animals immunized against the AChR (125, 148). The importance of receptor cross-linking was additionally shown by the comparison of different antibody preparations. Through proteolytic cleavage of AChR-specific antibodies monovalent Fab fragments and bivalent F(ab')2 fragments were produced, of which only the bivalent IgG antibody fragments retained the capacity to induce pathogenicity in animal experiments (149). These results were reproduced with monoclonal antibodies and even confirmed for antibodies targeting AChR-subunits other than the α-subunit (150, 151, 152). Still, antibodies directed against the MIR were the most potent in cross-linking and thus facilitating internalization and receptor depletion (138, 153.).

Bivalent IgG_1 and IgG_3 autoantibodies directed against the α-subunit are at the core of AChR-associated MG pathology. On the contrary, MG associated with anti-MuSK antibodies presents a vastly different pathomechanism and distinct clinical characteristics. MuSK is a single-subunit transmembrane protein responsible for AChR clustering, the development and the maintenance of the NMJ (154). The extracellular domain of MuSK is activated by the LRP4-agrin complex, which initiates phosphorylation and downstream recruitment of the scaffold protein rapsyn (154). Animal models with targeted disruption of the gene encoding the expression of MuSK or rapsyn did not produce viable offspring due to a of lack NMJ formation (155, 156). Patients with anti-MuSK antibodies show a different pattern of clinical symptoms in which the neck and respiratory muscles are affected primarily. The age of onset is in the range of 30-39 years and this subgroup is rarely reported in patients older than 70 (112, 157). Most MuSK-targeting antibodies belong to the IgG_4 subclass which does not activate complement but undergoes a process known as Fab-arm exchange. This mechanism generates bispecific, yet functionally monovalent IgG_4 antibodies through reciprocal swapping of a single Fab-arm with a randomly encountered IgG_4 in the serum (158). Studies with cultured myotubes demonstrated that bivalent, monospecific MuSK antibodies cross-link and activate MuSK phosphorylation, which induces AChR clustering and thereby counteracts the pathogenic effect (159). The different pathomechanisms, antibody profiles and distinct physiological processes interrupted at the NMJ in MuSK MG compared to AChR-associated MG also have implications on effective treatment which will be discussed in the following chapter.

1.6.2 Therapeutic interventions and challenges in the field of myasthenia gravis

Historically, the disease-specific treatment for MG relied on a combination of symptomatic treatment to improve the ability of a patient and general immunosuppression to limit the autoimmune response. The first line of treatment consists of acetylcholinesterase inhibitors to increase the availability of ACh in the synaptic cleft, which is well received by all MG subgroups except from patients with anti-MuSK antibodies (117, 160). For this patient subgroup acetylcholinesterase inhibitors do not only show limited effectiveness, but can also provoke exacerbation of weakness and potentially lead to a cholinergic crisis (161). In case of thymoma or early-onset MG, thymectomy is also considered a standard procedure that can provide substantial clinical improvements (80). If symptoms are not adequately controlled the treatment is escalated to immunosuppressive therapeutics including corticosteroids such as prednisone and non-steroidal immunosuppressants like azathioprine and cyclosporine (112, 162). Rescue therapies for patients experiencing a myasthenic crisis and therefore in need of rapid symptom relief consists of plasma exchange, intravenous immunoglobulin (IVIG) and high-dose daily administration of corticosteroids (121). Even though immunosuppressive treatments are well established with widespread clinical experience and considerable efficacy, they pose a risk for a multitude of adverse side-effects including hypertension, diabetes, osteoporosis and an increased risk of infection (80, 112). Approximately 10-15% of patients are refractory to conventional immunotherapy, thus experiencing persistent weakness and increased risk of disease relapse and symptom exacerbation (116). The treatment landscape, especially for patients with refractory MG, evolved rapidly in the past years with the development of new molecular therapies.

Rituximab is a well-established B cell depleting antibody that targets CD20-expressing lymphocytes and showed efficacy in 50-80% of MG patients across different open-label studies (163, 164). The response appeared to be heterogenous, however participants with anti-MuSK antibodies demonstrated a more robust benefit in comparison to other MG subgroups (165). Since rituximab depletes circulating B cells that express CD20, which includes naïve and memory B cells, the treatment response hints towards different B cell subsets that produce the pathogenic antibodies found in MuSK- compared to AChR-associated MG (8). Another monoclonal antibody that was first developed as a treatment for paroxysmal nocturnal hemoglobinuria but gained FDA approval in 2017 for generalized MG is the complement C5 inhibitor eculizumab (166). Results of a phase III ("REGAIN" trial), placebo-controlled, double-blinded clinical trial of eculizumab for patients diagnosed with AChR-associated,

refractory generalized MG failed to deliver significant changes in the primary efficacy end point, but provided robust improvement across several diagnostic evaluations that scored quality of life and perceived disease burden (167). Since the "REGAIN" trial, additional data has been collected from open-label extensions and clinical practice providing clear evidence that eculizumab is more effective in patients with AChR antibodies than B cell depletion via rituximab (168). Two other drugs, ravulizumab and zilucoplan, targeting the complement component C5 were approved in 2018 and 2023 respectively for treatment of adults with generalized MG (169, 170). While ravulizumab represents an additionally engineered version of eculizumab, zilucoplan is a small, synthetic macrocyclic peptide that exhibits strong affinity for the C5 component and prevents the proteolytic cleavage (171, 172). This drug offers several advantages, including rapid action, subcutaneous self-administration and most notably unresponsiveness to IgG depleting agents which enables the possibility of a combined treatment with neonatal Fc receptor (FcRn) inhibitors (169). Efgartigimod and rozanolixizumab belong to the family of FcRn inhibitors that bind to said receptor with high affinity and prevent other IgG antibodies from being captured. Binding to the FcRn shields IgG from degradation in lysosomes and enables the release back to the circulation providing an effective increase of the antibodies' half-life (173). The "MycarinG" phase III clinical trial of rozanolixizumab reported significant amelioration in pre-specified domains measuring weakness and fatigability of different types. Interestingly all 21 enrolled patients with MuSK autoantibody-positive generalized MG responded to the treatment and measured greater improvement scores than the overall population (174).

New treatment options have emerged for patients with MG but all of the recently approved drugs were designed with the intent of treating patients who are unresponsive to conventional therapies, thus targeting the late stages of the pathological cascade. Moreover, each of the clinical trials cited above contained a proportion of participants that did not benefit from treatment with the drug in question. Such deficiencies point towards gaps in knowledge of the underlying pathomechanism leading to imprecise patient stratification and potentially wrong treatment strategies. The heterogeneity of MG that comprises several targets at the NMJ with multiple epitopes and a variety of antibody classes with distinct characteristics still presents a major challenge to this day. Total AChR antibody concentrations measured in patients do not correlate with symptom severity and even an analysis with a higher level of detail achieved by investigating the epitope pattern provided only limited insight (112, 116, 117, 160). Antibodies against the α-subunit are the most pathogenic when compared individually, but MG patients

produce a polyclonal autoantibody response and each of the other subunit-targeting antibodies comprise a pathogenic capacity (175, 176). In contrast, fluctuations of antibody titers in MuSK-MG patients appear to reflect disease activity, showing that similar tools can be informative when applied to a well-defined subgroup with a distinct pathomechanism (157). The demand for an individualized approach necessitates the development of new diagnostic tools and sensitive biomarkers, which would help predict the disease course, the response to a given therapy and facilitate an improved MG classification system (112). To this end the establishment of national and international registries as well as the standardization of patient evaluation, diagnostics and treatment strategies was suggested to improve the understanding of the disease (80). Still the biggest challenge is to identify the primary cause of the disease. Already in the 1970s autoantibodies against the NMJ were determined as the cause of pathogenicity, yet the sequence of events that mediate the collapse of tolerance mechanisms and prompt the development of autoreactive B cells remain poorly understood. Shedding light on these processes would pave the way for novel antigen-specific or even generally applicable therapeutic approaches that restore tolerance and reduce autoimmunity.

2. Objective of the thesis

The aim of this study was to investigate two fundamental questions: 1. Why do antibodies against the AChR lead to muscle weakness? 2. Why do individuals produce antibodies against their own proteins?

The lab of Prof. Derfuss established a suit of methods to identify membrane-antigen specific B cells from the peripheral blood of a donor. The application of this so-called membrane-antigen capture assay in combination with fluorescence activated cell sorting enabled the isolation of single B cells from patients and healthy donors specific for the AChR. As described in the introduction, MG is a prototypic autoimmune disease induced by autoantibodies against proteins expressed at the post-synaptic membrane of the NMJ. Even though the target of the disease-causing autoantibodies is well-known and the basic processes that generate the pathology have been described decades ago, there is a lack of knowledge about the precise molecular mechanisms and their significance for mediating disease symptoms. These insufficiencies are reflected in the unaccounted observation that high anti-AChR antibody titers do not correlate with disease severity or the inadequate disease-specific treatment options. By the time this project started, six anti-AChR IgG antibodies had been identified and

commercially produced as patient-derived, monoclonal antibodies. This collection of autoantibodies provided the prerequisite for dissecting the mechanisms of autoantibody-mediated pathology and thus examining the first question of the present study. We investigated the different antibody-mediated effector functions with particular focus on the three postulated modes of action for pathogenicity in MG: direct receptor blockade, antigenic modulation and complement activation. None of the single autoantibodies showed the capability to induce myasthenic symptoms in vivo and provided limited efficacy in different in vitro assay for the assessment of the pathomechanisms. However, the synergistic combination of antibodies with different AChR subunit-specificities induced disease-causing levels of complement activation and indicated a novel mechanism for triggering the complement system.

In the second part of the research project, we connected the investigation of the underlying mechanism for enhanced complement activation by antibody combinations with the characterization of AChR-specific IgM antibodies. By screening MG patient and healthy donor samples with the membrane-antigen capture activated cell sorting (MACACS) method we additionally encountered clonally expanded, somatically hypermutated, AChR-specific IgM B cells, prompting a multitude of questions about their functional properties and the general pathogenesis of the disease. We constructed three competing hypotheses to explain the observed complement enhancement, whereas each of the three models predict different outcomes for complement activation depending on predetermined features of the combined antibodies. The combination of anti-AChR IgG and IgM antibodies constituted a particularly strong experimental approach and allowed the simultaneous examination of the three proposed models as well as the pathogenic potential of the hypermutated, AChR-specific IgM antibodies. Most of the recombinant human monoclonal IgM antibodies demonstrated AChR-specific binding, yet little capacity to activate the complement system and a lack of binding activity when expressed as IgG. Coupled with the sequence analysis that provided valuable information about the V(D)J gene usage, somatic hypermutations and clonal relations, we gained a first insight into the phenotype of this previously unknown B cell population.

3. Results

3.1 Results I: Receptor clustering and pathogenic complement activation in myasthenia gravis depend on synergy between antibodies with multiple subunit specificities

Acta Neuropathologica (2022) 144:1005–1025
https://doi.org/10.1007/s00401-022-02493-6

ORIGINAL PAPER

Receptor clustering and pathogenic complement activation in myasthenia gravis depend on synergy between antibodies with multiple subunit specificities

Natalie Rose[1,2] · Sebastian Holdermann[1,2,3] · Ilaria Callegari[1,2,3] · Hyein Kim[1,2,3] · Isabelle Fruh[4] · Ludwig Kappos[1,2,3] · Jens Kuhle[2] · Matthias Müller[4] · Nicholas S. R. Sanderson[1,2,3] · Tobias Derfuss[1,2,3]

Received: 24 June 2022 / Revised: 17 August 2022 / Accepted: 2 September 2022 / Published online: 8 September 2022

Abstract
Myasthenia gravis is an autoimmune disorder defined by muscle weakness and fatigability associated with antibodies against proteins of the neuromuscular junction (NMJ). The most common autoantibody target is the acetylcholine receptor (AChR). Three mechanisms have been postulated by which autoantibodies might interfere with neurotransmission: direct antagonism of the receptor, complement-mediated destruction of the postsynaptic membrane, and enhanced internalization of the receptor. It is very likely that more than one of these mechanisms act in parallel. Dissecting the mechanisms of autoantibody-mediated pathology requires patient-derived, monoclonal antibodies. Using membrane antigen capture activated cell sorting (MACACS), we isolated AChR-specific B cells from patients with myasthenia gravis, and produced six recombinant antibodies. All AChR-specific antibodies were hypermutated, including isotypes IgG_1, IgG_3, and IgG_4, and recognized different subunits of the AChR. Despite clear binding, none of the individual antibodies showed significant antagonism of the AChR measured in an in vitro neuromuscular synapse model, or AChR-dependent complement activation, and they did not induce myasthenic signs in vivo. However, combinations of antibodies induced strong complement activation in vitro, and severe weakness in a passive transfer myasthenia gravis rat model, associated with NMJ destruction and complement activation in muscle. The strongest complement activation was mediated by combinations of antibodies targeting disparate subunits of the AChR, and such combinations also induced the formation of large clusters of AChR on the surface of live cells in vitro. We propose that synergy between antibodies of different epitope specificities is a fundamental feature of this disease, and possibly a general feature of complement-mediated autoimmune diseases. The importance of synergistic interaction between antibodies targeting different subunits of the receptor can explain the well-known discrepancy between serum anti-AChR titers and clinical severity, and has implications for therapeutic strategies currently under investigation.

Keywords Myasthenia gravis · IgG_4 · Complement · Clustering · Human induced pluripotent stem cells · Live cell imaging

Introduction

Myasthenia gravis (MG) is a debilitating autoimmune disease associated with autoantibodies against components of the synapses between motor neurons and muscles (neuromuscular junctions, NMJ), making it one of the few autoimmune diseases in which the nature of the autoantigen provides an explanation for the symptoms. Various proteins can be involved, but four out of five patients [9, 44] have antibodies against subunits of the acetylcholine receptor (AChR). The receptor is a ligand-gated ion channel of four closely related subunits, alpha (α), beta (β), delta (δ) and epsilon (ε), each a four-pass transmembrane protein. Each receptor is a pentamer formed by two α, and one each of the

Natalie Rose and Sebastian Holdermann contributed equally.

Nicholas S. R. Sanderson and Tobias Derfuss contributed equally.

✉ Nicholas S. R. Sanderson
nicholas.sanderson@unibas.ch

1 Department of Biomedicine, University Hospital Basel and University of Basel, Basel, Switzerland

2 Neurologic Clinic and Policlinic and MS Center, University Hospital Basel, University of Basel, Basel, Switzerland

3 Research Center for Clinical Neuroimmunology and Neuroscience (RC2NB), University Hospital and University of Basel, Basel, Switzerland

4 Chemical Biology and Therapeutics, Novartis Institutes for BioMedical Research, 4002 Basel, Switzerland

other subunits [42]. There is inter-individual variation in the proportions of autoantibodies targeting the four subunits of the receptor [21, 43]. Action potentials arriving along the motor nerve result in the release of acetylcholine, which diffuses across the synaptic cleft of the neuromuscular junction, binds to the AChR and induces the opening of the channel, leading to depolarization and contraction of the muscle. Neural control of skeletal muscle is therefore completely dependent on the AChR, but how autoantibodies disrupt this process is not clear. Three mechanisms have been postulated, namely: direct blockade of the receptor, destruction of the receptor-bearing membrane by antibody-driven complement activation, and depletion of the receptors by antibody-mediated cross-linking and internalization [6, 7, 23, 40]. Sera from patients with anti-AChR-associated myasthenia gravis show evidence of all three of these mechanisms, in varying proportions [5, 28, 41].

Important advances have been made by studying whole sera or crude antibody preparations extracted from sera [17, 43], but understanding the relationship between antibodies and pathomechanisms requires examining the properties of individual patient-derived antibodies. For example, the isolation of antibodies against the muscle-specific kinase (MuSK), which are found in a small subset of myasthenic patients, has enabled the elucidation of their epitope specificity, and their effects on AChR clustering and MuSK phosphorylation [15, 40].

The isolation of autoantibodies against AChRs can be achieved by similar methods [25], but this approach requires that the antigen be prepared in a soluble form. In the case of AChR, this is complicated by the multi-membrane-pass, heteropentameric nature of the antigen. We therefore developed methods for isolating B cells specific for AChR from MG patients, using intact, membrane-expressed AChR as bait antigen, and examined the pathogenic potential of their anti-AChR antibodies in molecular mechanistic detail.

Materials and methods

Patients and healthy donors

Peripheral blood samples were collected from 12 healthy controls, six female and six male participants with an average age of 42, and 17 patients with clinically confirmed myasthenia gravis showing AChR-autoantibody RIA measurements above 0.5 nmol/l, with 6 female and 12 male participants and an average age of 62 (Supplementary Table 1).

Peripheral blood was drawn into S-Monovette tubes containing 1.6 mg EDTA per ml blood (01.1605.100) for isolation of PBMC, and into S-Monovette tubes with clot activator (01.1601.100, both from Sarstedt) for serum preparation. PBMC isolation and serum preparation were performed as previously described [1, 47]. PBMC were stored in liquid nitrogen until use, serum was stored at − 20 °C. The project was reviewed and authorized by the Ethikkommission Nordwest und Zentralschweiz.

Plasmids and cell lines

TE671 rhabdomyosarcoma cells were obtained from ATCC (LGC, Wesel, Germany) and cultured in complete RPMI medium (10% heat-inactivated fetal calf serum (FCS), 100 units/ml of penicillin and 100 µg/ml of streptomycin; all from Gibco), at 37 °C in 5% carbon dioxide. β, δ, and ε subunits of AChR cloned into pcDNA3.1-hygro, and α subunit cloned into pEGFP-N1 for an intracellular eGFP tag were a gift from David Beeson [20] and used to transfect TE671 cells to produce TE-AChR-GFP. pCMV3 containing the open reading frame of human CD40 ligand was purchased from Sino Biological. TE cells were stably transfected, sorted for CD40L expression, and irradiated with 72 Gy for mitotic inactivation and kept frozen in liquid nitrogen until use. pUltra was purchased from Addgene (24,129).

Identification of antigen-specific B cells using MACACS

AChR-specific B cells were isolated by the method described by Zimmermann et al. (2019). B cells were enriched from thawed PBMC by negative selection (Pan B cell isolation kit, human, Miltenyi). Five donors were selected from among anti-AChR-seropositive patients, on the basis of no recent immunosuppressive therapy (azathioprine within 6 months, glucocorticoids within 2 months, anti-CD20 ever). TE-AChR-GFP were labeled with cell trace blue (Thermo Fisher cat# C34568), and the extracellular AChR labeled with A647-conjugated α-bungarotoxin (α-BTX, B35450, ThermoFisher), then washed with complete RPMI medium. B cells were added to the adherent monolayer of labeled TE-AChR-GFP and incubated for 3 h. B cells were then retrieved and incubated for 20 min on ice with PE-conjugated anti-human CD69 diluted 1:100 in cold separation buffer. B cells were sorted on a FACSAria III Cell Sorter (BD Biosciences), gating on scatter to select live, single cells and on cell trace blue negative to exclude TE-AChR-GFP cells. Cells that were double positive for GFP and A647 were sorted into 1.5 ml Eppendorf tubes containing 700 µl RPMI-40 (RPMI with 40% FCS, 100 units/ml of penicillin, 100 µg/ml of streptomycin, and 50 ng/ml recombinant human IL-21 all from Gibco). The monoclonal antibody 8B4, an IgG1 specific for the hemagglutinin of Influenza A/California/07/2009 [47], was isolated by exactly the same process, from a healthy donor shortly after seasonal influenza immunization.

Ex vivo B cell activation and high-throughput screening of single B cell supernatants

B cells were plated in flat-bottomed 384-well plates at a density of 1 B cell per well in the presence of 5000 irradiated TE-CD40L and 50 ng/ml recombinant human IL-21 in 75 µl RPMI-40. The outer wells of each plate were filled with 120 µl sterile H_2O, plates were wrapped in aluminum foil to limit evaporation, and placed in a humidified incubator with 5% CO_2 and 8% O_2 at 37 °C for 12 days.

15 µl of B cell culture supernatant from each well was incubated with 10 µl separation buffer containing 5000 TE-AChR-GFP for 30 min at room temperature in the dark. Cells were washed and incubated with goat PE anti-human IgG at 1:200 (109-116-098), A647 anti-human IgA at 1:400 (109-605-011), and A594 anti-human IgM at 1:200 (109-585-129; all from Jackson ImmunoResearch), washed again and fixed in 4% PFA in PBS. Cells were acquired on a Cytoflex flow cytometer (Beckman Coulter).

cDNA generation, Illumina sequencing and antibody preparation

After the screening, all but 10 µl of cell culture supernatant was removed and transferred to storage plates using a ViaFlo 384 pipetting apparatus (Integra). B cells were lysed in 20 µl of 15 mM Tris–HCl, pH 8.0 containing 0.5 U/µl of recombinant murine RNAse inhibitor (NEB, M0314L). Plates containing lysed B cells were stored at − 80 °C, plates containing supernatant at − 20 °C. RNA was isolated from lysed samples using the Quick-RNA MicroPrep Kit (Zymo). In brief, samples were thawed at room temperature, then mixed with 100 µl lysis buffer. 130 µl 100% ethanol was added and the mixture transferred to the column. After centrifugation, the column was treated with DNAse for 15 min at room temperature. The column was first washed with RNA prep buffer, then twice with RNA wash buffer before the RNA was eluted in 15 µl H_2O. 4.5 µl RNA was used to generate cDNA using the SMART-Seq® v4 Ultra® Low Input RNA Kit for Sequencing by Takara following the manufacturer's instructions at half the volume per reaction. Illumina library preparation (Nextera XT DNA Library Preparation Kit) and sequencing on a NexSeq500 (Illumina) were exactly as described by Callegari et al. [1].

Immunoglobulin gene sequences were extracted from the raw sequencing reads using custom scripts in R. Fastq files from the sequencer were aligned using the QasR and Rsamtools packages to an artificial mini genome containing the genomic sequences of constant regions from δ, µ, γ, α, and ε heavy chain genes, and κ and λ light chain genes, and the number of reads aligning to each were used to infer the classes and subclasses. Variable regions were reassembled using tools from the ShortRead and BioStrings Packages. Assembled variable regions were checked for V(D)J open reading frames using IgBlast (NCBI). DNA constructs encoding the inferred amino acid sequence from leader to several bases into the constant region were synthesized by IDT with restriction sites at the termini to enable in-frame cloning into pUltra plasmids already containing the appropriate constant regions. Plasmids were transfected into HEK cells to produce the encoded antibodies, and when more than one light chain and one heavy chain was found in the same well, all possible combinations were examined for AChR binding. Adherent HEK293T/17 (ATCC) were cultured in medium supplemented with 10% heat inactivated FCS and 100 units/ml penicillin and 100 µg/ml streptomycin (DMEM-10) in 12 or 6 well plates. Cells were transiently transfected with 1.5 µg plasmids encoding the heavy and light chain of a recombinant antibody in 1.5 ml DMEM-10 using 150 µl jetprime buffer and 3 µl jetprime reagent (PPLU114-07, Polyplus transfection). After 48–72 h, the supernatants were harvested and binding of antibodies to AChR was verified. Antibodies with the expected binding properties were then custom-manufactured according to our sequences by SinoBiological (Eschborn, Germany), purified by protein-A affinity chromatography, and their purity assessed by reducing and non-reducing SDS-PAGE gel electrophoresis. The antibody B12L described by Makino et al. [25], referred to in the nomenclature of the current work as $aG_1$12, and the anti-influenza hemagglutinin antibody 8B4, were made by Sino Biological in IgG_1 subclass. Sequences of variable regions of heavy and light chains for all antibodies whose cloning is described are shown in Supplementary Table 2. To produce the naturally occurring IgG_4 $bG_4$02 as an IgG_1, the heavy constant gamma 4 region was replaced with a construct encoding the heavy constant gamma 1 (Uniprot accession P01857.1).

Flow cytometry of antibody binding, complement activation, and epitope determination

HEK cells transfected with the human adult AChR, incorporating an α-subunit fused with GFP (AChR-GFP), were used for flow cytometric assays. 80,000 cells diluted in 40 µl of DMEM-10 were seeded in a U-bottomed 96-well plate. For the antibody binding assay, 10 µl of serum or antibody was added and incubated for 30 min on ice. After three washing steps with cold PBS, bound antibody was labeled with DyLight™ 405 donkey anti-human IgG (JIR: 115-295-166) in a 1:200 dilution and finally analyzed via flow cytometry. In the case of the in-vitro complement activation assay, the mix of HEK cells with antibodies or serum was supplemented with 10 µl of human serum as source of complement components. Cells were incubated for 2 h at 37 °C and 5% carbon dioxide. After three repeated washing steps with PBS, complement activation were tested by labeling of

C3 complement component deposition with a mouse monoclonal anti-complement C3/C3b/iC3b antibody (BioLegend Cat. No. 846402) for 30 min on ice. Following another three washing steps, secondary antibodies Rhodamine Red™-X goat anti-mouse IgG (JIR: 115-295-166) and DyLight™ 405 donkey anti-human IgG (JIR: 115-295-166) were used for labeling. Finally, after 20 min of incubation on ice and two rounds of washing with PBS, data for a target of 10,000 cells were acquired on a Cytoflex cytometer (Beckman Coulter), stored as.fcs files and analyzed using FlowJo (Becton Dickinson). To determine epitope specificity of the human-only anti-AChR antibodies, HEK cells were transfected with four plasmids, one encoding a human subunit, and three encoding rat orthologs of the other three subunits. Labeling and flow cytometry were otherwise the same as above. To determine epitope specificity by competitive blocking, HEK cells transfected with AChR-GFP were first incubated for 30 min with 2 µg/ml of a commercial, monoclonal, subunit-specific antibody (α: mAb35, BioCell; β, BioRad, cat MCA1329GA), washed once, and then labeled and analyzed as above.

Human induced pluripotent stem cell (iPSC) generation and maintenance

The iPS line 90/1.2 (Invitrogen #C-013-5C) was derived from adult human dermal fibroblast lines from Invitrogen. Fibroblasts were reprogrammed using the CytoTune-iPS Reprogramming Kit (Invitrogen, cat-#A1378001). All cell lines were checked for normal karyotype and pluripotency. iPS cells were cultured on laminin 521 (Biolamina, cat-# LN521) coated dishes in mTeSR plus (Stem Cell Technologies, cat-# 05825) supplemented with 1% Pen/Strep (P/S) (ThermoFisher, cat-# 15070-063). Cells were dissociated with TrypLE (Gibco, cat-# 12604-013) every 3–4 days and plated at a density of 20,000/cm^2 in the presence of 10 µM ROCK inhibitor (Calbiochem, cat-# Y-27632). The medium was replaced every other day.

The fast green fluorescent calcium indicator GCaMP6f open reading frame [2] was placed under the control of the CAG promoter, with a puromycin resistance gene and cloned into an AAVS1-targeting vector [12]. After co-transfection of the targeting vector with a Cas9 construct [34] and a guide (gtc acc aat cct gtc cct ag) against AAVS1 into a doxycycline-inducible MyoD iPS cell line, colonies were picked after puromycin (1 µg/ml) (Gibco, cat-# A11138-03) selection. Correct integration to the AAVS1 locus was validated via PCR analyses.

Human Ngn2 cDNA was synthesized according to sequences available from the Ensembl database (Ensembl Gene ID ENSG00000178403 or accession number NM_024019.3) and cloned under the control of TRE tight (Tetracycline Response Element) promoter in a PiggyBac/Tet-ON all–in-one vector. This vector contains a CAG rtTA16 cassette allowing constitutive expression of Tet-ON system and an Hsv-tkNeo cassette for generation of stable IPS clones. Differentiation to neurons was performed as reported previously [32]. Briefly, iPS cells were plated on Matrigel-coated cell culture plate in DMEM/F12 (ThermoFisher, cat-# 31331) supplemented with 2% B27 (ThermoFisher, cat-# 17504-044) and 1% N2 (ThermoFisher, cat-# 17502-048), 10 ng/ml of Human Epidermal Growth Factor (hEGF) (ThermoFisher, cat-# PHG0315), 10 ng/ml of basic human Fibroblast Growth Factor (hFGF) (ThermoFisher, cat-# CTP0263) and 1% penicillin/streptomycin (P/S) containing 10 µM ROCK inhibitor for 1 day and 1 µg/ml doxycycline (Sigma, cat-# D9891) for 3 days. Human Myoblast Determination Protein 1 (MYOD1) cDNA was synthesized according to Accession number NM_002478.5, cloned into the inducible vector and transfected into iPS cells as above. For differentiation, cells were cultivated in KSR Medium composed of Minimum Essential Medium α (ThermoFisher, cat-# 12571063), 5% Knockout™ serum replacement (KSR) (ThermoFisher, cat-# 10828028), 1% P/S, 55 µM β-mercaptoethanol (ThermoFisher, cat-# 21985023) and supplemented with 1 µg/ml doxycycline for 3 days to generate myoblasts. These myoblasts were further amplified in KSR Medium containing 20 ng/ml hFGF (ThermoFisher, cat-# CTP0263) for an additional 4 days in the same medium as described above.

40,000 myoblasts were seeded in a laminin-coated 384-well plate in KSR medium supplemented with ROCK inhibitor and doxycycline. One day later, medium was switched to myoblast differentiation medium: DMEM F12-Glutamax (Gibco, cat-# 31331028) with 5% FBS (HyClone, cat-# SH30070.02), 0.2% ITS (BD, cat-# 354351, 0.1% BSA (Sigma, cat-# A1595), 1% P/S, CHIR99021 (2uM) (Sigma, cat-# 1046), Dorsomorphin (1 uM), (Stemgent, cat-# 04_0024), Dibutyryl-cAMP (1 mM) (Sigma, cat-# D0627). Three days later, iNGN2 neurons, differentiated for 3 days in proliferation medium, were plated on top of myotubes in a 1:1 ratio and further differentiated in neuronal differentiation medium composed of NeurobasalTM Medium (ThermoFisher, cat-# 21103049), supplemented with 2% B27, 1% N2, 1% P/S, 10 ng/ml of human BDNF, GDNF and NT3 (R&D Systems, cat-# 248-BD, 212-GD and 267-N3, respectively) for approximately 3 weeks at 37 °C in 5% CO_2. Medium was replaced every 2–3 days. MAP4K4 inhibitor (i.e. GNE-495) was added at 5 µM between day 5 and 14. 2 µM Cytosine β-D-arabinofuranoside (AraC) (Sigma, cat-# C1768) was added at day 5–12 to protect the culture from proliferating cells.

Functional drug screening system read out from human iPSCs

Sera or antibody diluted in neuronal differentiation medium was added after about 3 weeks to the co-culture and was

incubated for 3 h. For FDSS, medium was replaced by Ca^{2+} buffer (50 ml HBSS 10x (ThermoFisher, cat-# 14065049), 10 ml HEPES 1 M (ThermoFisher, cat-# 15630056), 440 ml dH_2O and 375 µl $CaCl_2$ (1 M). After 40 min, all plates were read by FDSS/µCELL Functional Drug Screening System (Hamamatsu, cat-# C13299) after injection of 0.5 µM AMPA (Sigma, cat-# A6816). Analysis was done with Hamamatsu software.

Live cell imaging of cluster formation

HEK cells seeded in an 8-well chambered coverslip (Ibidi 80826) were transfected with the human AChR subunits α-GFP, β, δ, and ε, and allowed to express the receptor overnight at 37 °C in 5% carbon dioxide. On the following day the chambered coverslip was placed in a humidified chamber with controlled temperature and carbon dioxide concentration for imaging with a Nikon A1R confocal microscope. A 40 ×, 0.6 NA air objective was used and stacks of 8 planes spanning the focal plane of the cells were continuously acquired over the course of 10 min. Two cycles of such image acquisition were performed per well. The first cycle after a 10 min incubation with α-BTX, and the second after a change of medium and addition of single or combinations anti-AChR antibodies. Thereby two data sets of confocal images were generated, one showing the AChR distribution on the cell surface before and the other after antibody addition.

Passive transfer myasthenia gravis in Lewis rats

Procedures involving live animals were reviewed and permitted by the cantonal animal research commission. Four-week-old female Lewis rats obtained from Janvier Labs received only one intraperitoneal injection of PBS, or a human monoclonal antibody dissolved in PBS under isoflurane anesthesia. Monoclonal antibodies included 8B4, $bG_4 02$, $bG_4 02\text{-}G_1$, $aG_1 01$ or a combination of $bG_4 02\text{-}G_1$ and $aG_1 01$. Each rat received 4 mg/kg of total antibody, i.e. 4 mg/kg of each single antibody, or 2 mg/kg of each antibody in the case of combinations. For the animal experiments with a behavioral endpoint the rotarod performance as well as weight loss and clinical score were assessed every 12 h. Each animal was scored based on guidelines for pre-clinical assessment of anti-AChR antibody induced myasthenia gravis as reported elsewhere [18, 25]. The clinical scale was defined as follows: 0, no weakness; 1, first signs of a weakened grasp and fatigable after several trials; 2, incomplete paralysis of hind limbs and clinical signs of weakness; 3, severe clinical signs of weakness with no ability to grip, hindlimb paralysis and moribund; 4, death. Animals were euthanized if they reached clinical score 3 with severe muscle weakness. One animal was found dead already at the 24 h testing time point. Rats were examined and trained on the rotarod machine to establish the baseline starting 72 h prior to injection, and 48 h after the injection all rats were sacrificed by transcardial perfusion fixation with 4% paraformaldehyde (PFA). Subsequently, the gastrocnemius muscle, the soleus muscle and the diaphragm were isolated and stored in 4% PFA until further analysis. In the second experiment for investigating complement activation, the same procedure was performed but the animals were sacrificed at 12 h.

Immunofluorescent labeling of rat muscle sections and iPSC cocultures

The gastrocnemius muscle stored in 4% PFA was cryoprotected in an ascending concentration series of 10%, 20% to 30% sucrose-PBS solution. After snap-freezing, the rat muscles embedded in OCT (CellPath) on dry ice were cut into 30 µm thick cryosections with a Leica cryostat. Rat muscle sections stored at − 80 °C for immunofluorescent labeling were thawed for 10 min at room temperature, washed twice with PBS and incubated with 0.1 M glycine in PBS for another 10 min. Following a 10 min incubation with ice-cold 80% methanol and two PBS washing steps, the rat muscle sections were blocked with a solution containing 1% FCS, 3% BSA and 0.3% Triton X-100 in PBS for 1 h. Primary antibodies to label rat C3 complement deposition (mouse anti-rat IgG, clone 12E2, Novus Biologicals, NBP1-05140) and SV2A (rabbit anti-rat IgG, Novus Biologicals, NBP1-82964) were diluted in blocking solution for a final concentration of 1 µg/ml and 0.3 µg/ml, respectively and incubated for 16 h at 4 °C in a humid chamber at 4 °C. After washing with PBS, the sections were soaked with goat anti-mouse IgG (H + L) Rhodamine Red™-X (Jackson ImmunoResearch 115–295-166, final concentration 4 µg/ml), goat anti-rabbit IgG Alexa Fluor 488 (Jackson ImmunoResearch 111-545-144, final concentration 4 µg/ml) and α-BTX (ThermoFisher B35450, final concentration 1 µg/ml) diluted in blocking solution for 16 h at 4 °C. Finally, the muscle sections were washed with PBS, labeled in PBS-containing 1 µg/ml DAPI, mounted with Fluoromount-G and sealed with a coverslip. Depending on the analysis, images were acquired with a Nikon A1R scanning microscope with a 60 ×, 1.4 NA OI objective using voxel dimensions set to Nyquist sampling, a Nikon Crest V3 spinning-disc confocal microscope with a 40 ×, 0.95 NA air objective or a Nikon Eclipse TI2 equipped with a 20 ×, 0.75 NA air objective. For investigating human antibody binding at the neuromuscular junction, the sections were not treated with primary antibodies, but directly incubated with α-BTX and goat anti-human IgG FITC (Jackson ImmunoResearch 109-096-098, final concentration 4 µg/ml). Further processing and image acquisition were performed as described for analyzing complement deposition.

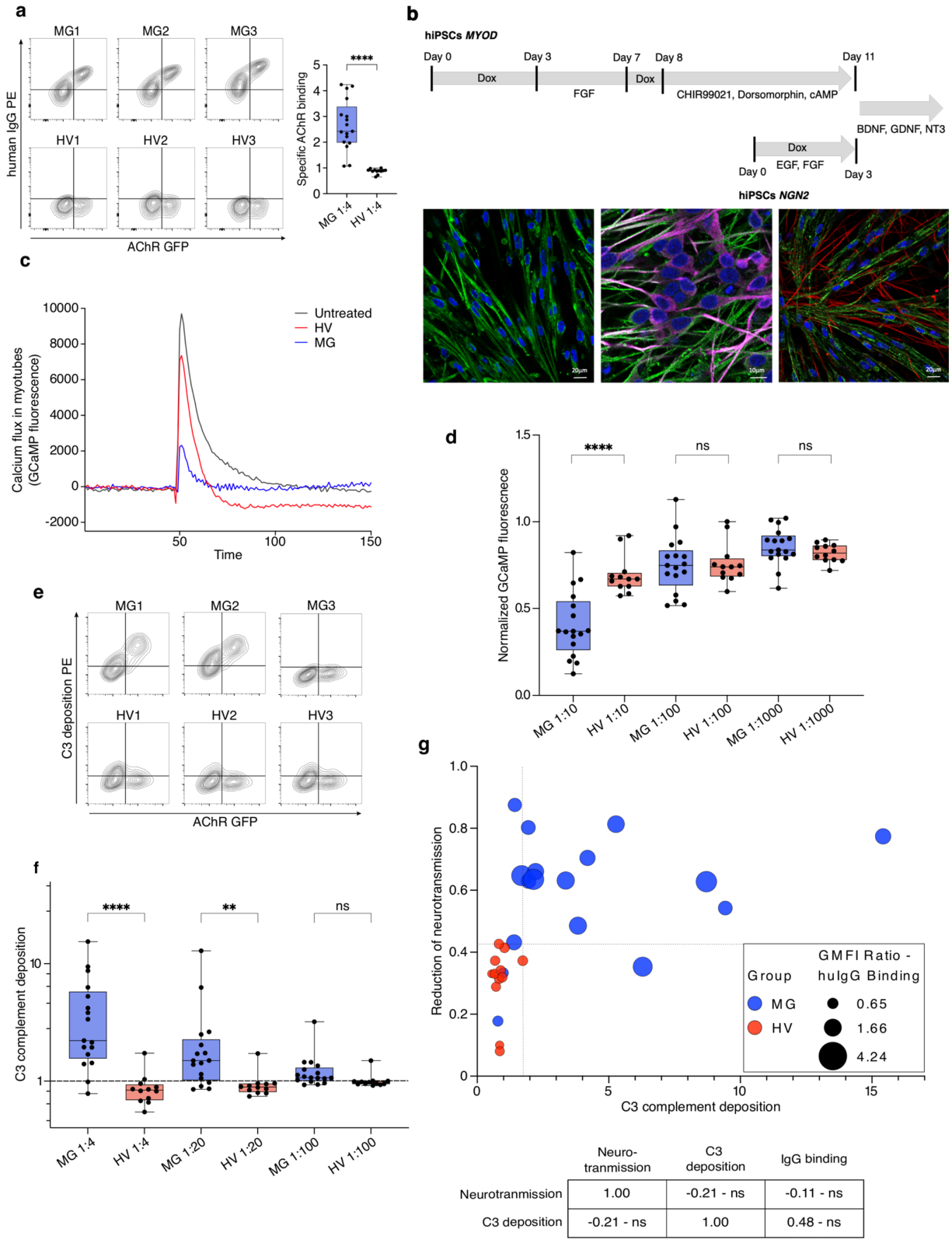

	Neuro-tranmission	C3 deposition	IgG binding
Neurotranmission	1.00	-0.21 - ns	-0.11 - ns
C3 deposition	-0.21 - ns	1.00	0.48 - ns

◂**Fig. 1** Inhibition of neuromuscular signal transmission and induction of complement activation by serum from patients with MG. **a** Live cell flow cytometry of specific antibody binding to AChR. Sera from 3 MG patients and 3 healthy controls were incubated with TE671 cells expressing human AChR-GFP. The horizontal axis depicts the fluorescence intensity of GFP and the vertical axis the fluorescence intensity of the anti-human IgG secondary antibody. The box and whisker plot on the right shows the specific AChR binding (the geometric mean fluorescence intensity (GMFI) ratio, i.e., the fluorescence signal for anti-IgG immunofluorescence on AChR-transfected cells divided by the signal on non-transfected cells) in serum from 17 MG patients and 12 healthy control sera. Demographic information about these donors is shown in Supplementary Table 1. Results shown in d and f come from the same donors. The difference between the groups was significant (****$p<0.0001$) by two-tailed Mann–Whitney U test. **b** The hiPSC-derived neuromuscular system. Schematic figure shows timeline of co-culture generation. hiPSC MYOD and hiPSC NGN2 cells were treated with doxycycline and growth factors to direct their differentiation to muscular and neuronal phenotypes, respectively. Co-culture started on day 13 with iND3 plating on iMD13. Fluorescence photomicrographs below the schematic timeline show cocultures labeled for neuronal or muscular markers. Shown in the left panel is a myotube culture before iND3 neurons were added. The typical muscular striations are visible after labeling the myogenic marker α-actinin (green). The middle panel shows a pure neuronal culture at 10 days labeled with markers for mature neurons, MAP2 (green) and Tuj-1 (pink). The right panel shows an image of the co-culture after 3 weeks. Myotubes are labeled for α-actinin (green) and neurons for NF200 (red), another marker for neurons. DAPI (blue) labels nuclei. See also live cell imaging of co-culture (Supplementary Video 1). **c** Effect AChR blockade on signal transduction in the iPSC-derived neuromuscular model. Myotubes express GCaMP, allowing intracellular calcium to be monitored by fluorescence quantification. The horizontal axis displays the time, with the AMPA stimulus added at time 50. The vertical axis shows the fluorescent signal corresponding to intracellular calcium in myotubes. The black trace is the signal in cocultures without serum added. The red trace shows the signal in cultures to which serum from a healthy donor was added. The blue trace shows the signal after addition of serum from a patient with MG. **d** The effect of MG serum on acetylcholine-dependent calcium flux in myotubes of the hiPSC-derived neuromuscular system. The vertical axis shows the normalized cholinergic transmission (peak height of the GCaMP calcium signal measured as explained in c, divided by the mean value of untreated wells). Each point shows the mean of 3 repeat measurements with one serum. The assay was performed at 3 different dilutions of serum from patients with myasthenia gravis (MG) or from healthy volunteers (HV) as shown below the horizontal axis. Differences between results using sera from the two sources were compared using a two-way ANOVA with multiple comparison correction according to Tukey (****$p<0.0001$). **e–f** Antigen-dependent complement activation by MG sera. **e** Sera from 3 MG patients and 3 healthy controls were incubated with HEK cells expressing human AChR-GFP, and complement deposition was measured with an anti-C3 antibody by flow cytometry. The vertical axis of each contour plot shows the anti-C3 signal, and the horizontal axis the AChR-GFP fluorescence. The top row shows results for sera from MG patients, and the lower row results from HV controls. **f.** Sera from 17 donors with MG and 12 healthy donors were measured as shown in e. The vertical axis shows C3 deposition (GMFI ratio, i.e., the fluorescence signal for anti-C3 immunofluorescence on AChR-transfected cells (the right side of each plot in e), divided by the signal on non-transfected cells (the left side of each plot in e). Differences between conditions were compared by Kruskal–Wallis test, followed by Dunn's multiple comparison (**$p=0.0063$, ****$p<0.0001$). **g** Relationships between anti-AChR IgG binding, complement activation, and signal transmission blockade. For each serum sample (healthy, "HV", red symbols; or myasthenic, "MG", blue symbols) complement activation measured by C3 deposition as shown in **e–f** is plotted against the reduction of cholinergic transmission as measured in **c–d**, with symbols whose size represents IgG binding to AChR, as shown in **a**. The table below the plot shows the Spearman's rank correlation coefficients and the p values calculated by two-tailed permutation test. None of the correlations between the three pairs of variables was significant

Cocultures of hiPSC-derived cells were fixed in 4% paraformaldehyde at room temperature for 10 min, followed 3 × DPBS (Sigma, cat-# 14190) washings, 5 min each. DPBS supplemented with 0.1% Tween and 2.5% BSA or for permeabilization 0.1% Triton X-100 and 1% BSA (blocking) was used for primary antibody labeling, overnight at 4 °C. The following antibodies were used: NF-200 (Abcam, cat-# Ab72996); α-Actinin (Abcam, cat-# Ab9465), Tuj1 (cat-# Sigma T8660); MAP2 (cat-# Abcam Ab5392). After three washing steps with DPBS, cells were incubated for 1 h with secondary antibodies (Invitrogen). Afterwards, cells were washed in DPBS and incubated with DAPI for 10 min. Ibidi mounting medium (IBIDI, cat-# 50001) was added to the wells and stored at 4 °C. Images were acquired with LSM900 microscope using Zen 3.2 (Blue edition) software.

Image analysis

Nikon NIS-Elements software and Fiji based on ImageJ2 were used for image analysis. Based on the SV2A signal a mask was designed to define the area of the NMJ. The α-BTX fluorescence signal intensity inside this mask was measured and the ratio to the colocalizing SV2A calculated. In total, eight images from three different gastrocnemius cryosections per animal were analyzed amounting to more than 600 NMJs tested for each injected group. For complement activation, the fluorescence signal intensity of C3 deposition was measured for a minimum of 100 NMJs per rat and four rats per condition. The structural analysis was performed on high magnification image stacks of 15 individual NMJs per animal. Initial processing included the generation of maximum intensity projections, the separation of the α-BTX channel, the reduction of background and selection of a threshold based on the signal intensity. From the resulting image, the number of individual objects, object area, and mean fluorescence intensity were measured. The analysis of the live cell imaging is based on the same approach. For each image acquired over the course of the 20 min of imaging, a threshold level of α-BTX signal was calculated with the RenyiEntropy function of ImageJ, and areas of signal exceeding this threshold, of an area between 0.8 and 10.0 square microns, were defined as "clusters", whose area and number were extracted using an automated macro in Fiji. R scripts were applied to calculate the total area, mean area and total number of clusters in each image, and plot the data as bubble charts.

Statistics

GraphPad Prism was used for statistical analysis. Prior to performing statistical tests, the data were tested for normal distribution with the Normality and Lognormality test. Quantification of the AChR content of NMJs was compared using a One-Way ANOVA with a multiple comparison corrected according to Tukey. For C3 deposition and structural parameters either a Two-Way ANOVA or a Kruskal–Wallis test with a Dunn's multiple comparison was applied depending on the normal distribution of the dataset. Differences between MG patients and healthy volunteer serum in signal transmission in the iPSC-derived neuromuscular model were tested using a two-way ANOVA with a multiple comparison corrected according to Tukey.

Results

Serum from patients with MG inhibits neuromuscular signal transduction and induces complement activation

To enable examination of antibodies interacting with antigen in its native conformation, we developed a suite of techniques based on expression of the native human AChR on live cells. Antibody binding was measured by flow cytometry on AChR-transfected cells. AChR-binding antibodies of the IgG class were detected in all patients who were AChR-seropositive by the clinical radioimmunoassay, and diagnosed with clinically definite MG (Fig. 1a, Table 1).

AChR antagonism was assessed by measuring the reduction in acetylcholine-induced calcium flux in a human iPSC-derived neuromuscular system. This system consisted of neuronal cells and myotubes generated by overexpression of MYOD1 as the myogenic and NGN2 as neurogenic master regulators, enabling in vitro modeling of the neuromuscular junction (Fig. 1b). Cholinergic neurotransmission was monitored by calcium imaging in myotubes stably expressing GCaMP. Due to spontaneous electrical activity, individual myotubes occasionally depolarize, resulting in brief peaks of fluorescence (see Supplementary Video 1). Following stimulation of the presynaptic neurons with α-amino-3-hydroxy-5-methyl-4-isoxazolepropionic acid (AMPA), all myotubes in the culture depolarize and fluoresce together, yielding a strong signal that can be recorded and quantified. Any reduction in responsiveness of the myotubes to acetylcholine release from the stimulated neurons is observed as a reduction in the magnitude of this signal (Fig. 1c). Compared to sera from healthy donors, sera from patients with MG impeded neurotransmission from neurons to myotubes significantly (Fig. 1d). Direct AChR antagonism by serum constituents was independent of complement, because heat-inactivated sera showed the same results as fresh sera (Supplementary Fig. 1).

Antigen-dependent complement activation was measured by incubating cells expressing AChR, or untransfected control cells, with sera from patients and healthy controls, and measuring C3 deposition on the cell surface by flow cytometry (Fig. 1e). Sera from patients with myasthenia gravis induced complement activation specifically on AChR-transfected cells, while sera from healthy volunteers did not. At dilutions up to 1:20, this difference was significant (Fig. 1f).

Sera from the majority of patients (65%) evinced both complement activation and receptor antagonism, but neither parameter was significantly correlated with total specific antibody binding, or with each other (Fig. 1g). Receptor antagonism in 3/17 patients, (18%), and complement deposition in 5/17 (29%) were within the range of the healthy

Table 1 Patient and donor information, of whom serum was tested individually to provide representative results shown in Fig. 1a, e

Participant	Sex	Age	Diagnosis	Thymus status	Disease onset	Besinger Score	Immuno-therapy	RIA AChR antibody titer (nmol/l)
MG1	M	63	Ocular AChR MG	No thymoma	02/2018	6	None	16.5
MG2	M	35	Generalized AChR MG	Thymoma	06/2018	8	None	27.4
MG3	F	39	Generalized AChR MG	Slight thymic hyperplasia	2014	6	None	366
HC1	F	38	Healthy control	–	–	–	–	–
HC2	F	36	Healthy control	–	–	–	–	–
HC3	M	44	Healthy control	–	–	–	–	–

Furthermore, anti-AChR specific B cells were isolated from these 3 MG patients and used for the production of recombinant monoclonal anti-AChR antibodies. Patients who provided serum and the B cells from which monoclonal antibodies were isolated, and healthy controls who provided serum. Comparisons of AChR binding and AChR-dependent complement activation between patients and controls are shown in Figs. 1a, e, respectively

controls. In two patients (11%), both values were in the normal range. These patients also had minimal total AChR-specific antibody binding (the two lowest values in Fig. 1a).

Isolation of anti-AChR specific B cells by MACACS

Following the observation that patient sera mostly contain activities mediating both receptor antagonism and complement activation, it became apparent that investigation of either mechanism would require the isolation of monoclonal antibodies. To this end, we used the method of membrane antigen capture activated cell sorting (MACACS) described by Zimmermann et al. [47]. This method exploits the ability of live B cells to extract their cognate antigen from cell membranes, becoming highly activated in the process (Fig. 2a, b). By screening PBMC from 5 seropositive donors by this method, we isolated six AChR-specific antibodies from three donors with myasthenia gravis (Table 2). The antibodies, of classes IgG_1, IgG_3, and IgG_4 are somatically hypermutated (7–19 amino acid replacements per heavy chain), and include two members of one expanded clone from one donor (Table 2). As an approximate indicator of affinity, we plotted AChR-specific

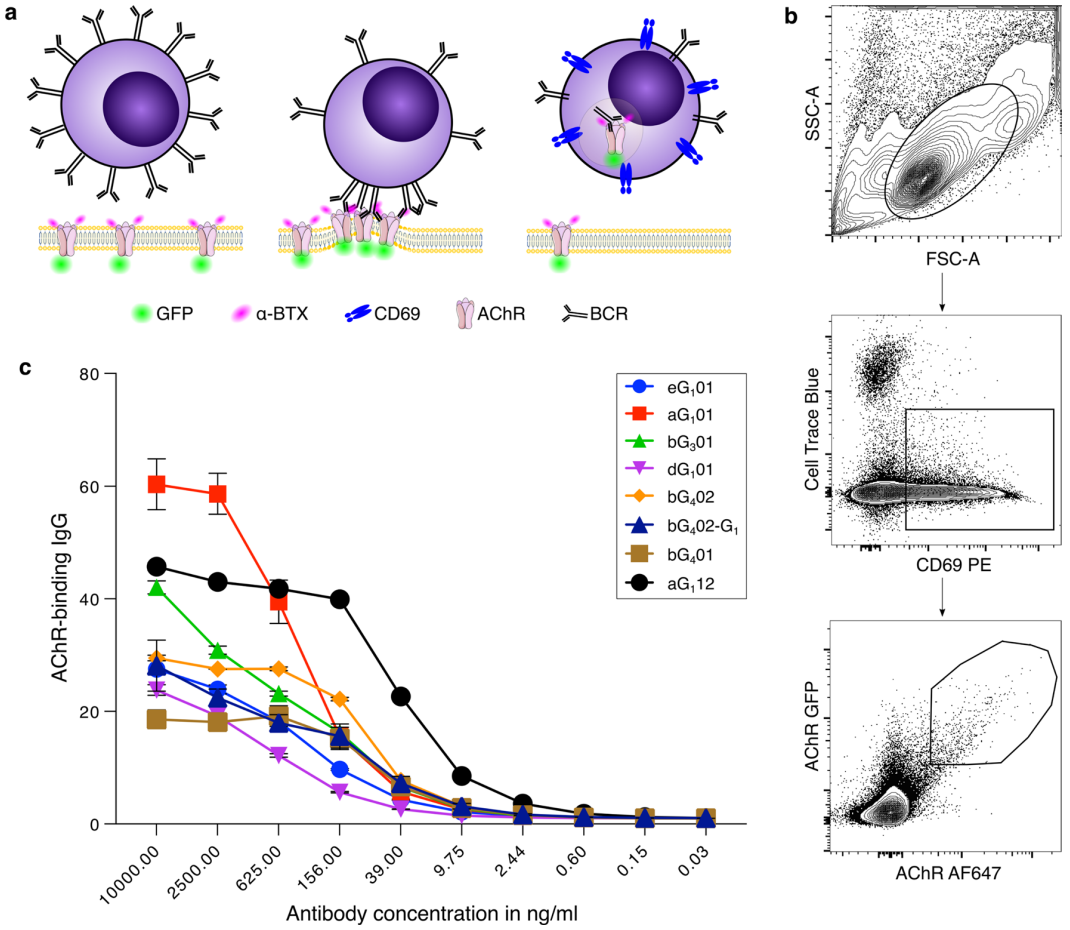

Fig. 2 Isolation of AChR-specific B cells from MG patients by MACACS. **a** Schematic illustration of membrane antigen capture by a B cell. AChR-specific B cells recognize their cognate antigen in the membrane of a live cell, bind and extract it. This process leads to B cell activation, CD69 upregulation, and the acquisition of GFP signal. **b** Representative FACS plots showing the gating for B cells enriched by MACACS. The first plot shows forward and side scatter, the second plot shows the cell trace blue label used to exclude antigen donor cells, plotted against CD69. The third plot shows two markers used to detect antigen-specific cells, i.e., AChR-GFP, and α-BTX. Cells in the polygonal gate in the third plot were sorted and used to prepare monoclonal antibodies, as described in Materials and Methods. **c.** Binding of monoclonal antibodies to AChR. Serial dilutions (shown on the horizontal axis) of each of the six monoclonal antibodies prepared from B cells isolated as above were incubated with AChR-GFP expressing HEK cells and specific binding calculated as GMFI ratio of anti-human-IgG signal on AChR-expressing cells divided by signal on non-transfected cells. As a positive control $aG_1 12$ antibody described by Makino et al. [25] was used, and we also included the antibody $bG_4 02$ artificially switched from IgG_4 to IgG_1 ($bG_4 02$-G_1)

Table 2 Antibody characteristics; list of anti-AChR specific antibodies isolated from the peripheral blood of MG patients

Antibody ID	Patient ID	Isotype	Aa replacements in V region	CDR3 aa length	α-subunit block (%)	β-subunit block (%)	Rat cross-reactivity	Subunit specificity
$aG_1$01 1J7	MG3	IgG1	19	23	66	1	Yes	α
		κ	16	10				
$bG_3$01 3I3	MG2	IgG3	11	25	3	68	No	β
		k	2	5				
$bG_4$01 5D2[a]	MG1	IgG4	9	17	26	65	No	β
		λ3	3	9				
$bG_4$02 6J2[a]	MG1	IgG4	12	17	16	66	Yes	β
		λ3	7	9				
$bG_4$02-G_1 6J2 IgG1	MG1	IgG1	12	17	17	71	Yes	β
		λ3	7	9				
$dG_1$01 5H10	MG1	IgG1	7	17	42	15	No	δ
		κ	7	9				
$eG_1$01 2M18	MG1	IgG1	11	9	17	10	No	ε
		κ	1	9				

[a]Clonally related with shared use of H and L chain V(D)J combinations

binding at a range of concentrations and extracted the concentration required for half maximal specific binding (EC50), yielding values between 58 and 783 ng/ml (Fig. 2c).

Antibody binding experiments with HEK cells expressing the rat AChR showed that two patient-derived antibodies recognize receptors from both species, and four recognized only the human receptor. This enabled us to elucidate the subunit specificity of the human-only antibodies using chimeric receptors of mixed human and rat subunits (Supplementary Fig. 2) assuming that replacement of the target subunit with the human ortholog would confer binding on the otherwise non-binding rat receptor. To confirm these results, and to identify the targets of the rat- and human-reactive antibodies, we examined competitive blockade of the patient-derived antibodies by commercial monoclonal antibodies of known subunit specificity. The combined results from the two approaches suggested that one patient-derived monoclonal antibody targeted the α subunit, three antibodies the β, and one each the δ, and ε (Table 2). Based on the subclasses and the deduced epitope specificity, antibodies were assigned names reflecting these properties, e.g., $aG_1$01 is the first α-binding antibody of subclass IgG_1 (Table 2).

Single antibodies have limited effect on pathomechanisms

None of the monoclonal anti-AChR antibodies interfered with cholinergic neurotransmission in the hiPSC model, even at a 100-fold higher concentration than needed to achieve maximum binding to AChR-transfected HEK cells (Fig. 3a). Only two antibodies, $aG_1$01 and $bG_3$01, mediated complement activation in vitro (Fig. 3b), and neither was as potent as the positive control antibody. None of the four antibodies isolated from patient MG1 were capable of inducing complement activation, even though all of them showed strong specific binding, and the donor's serum was potent in the same complement assay (Fig. 3b, Supplementary Fig. 3).

We examined the pathogenic potential of the two rat-cross-reactive, patient-derived, AChR-binding antibodies in a passive transfer MG model. The cross-reactive antibodies $aG_1$01 and $bG_4$02 were administered to Lewis rats and the animals' health and motor performance was evaluated over the course of 48 h, in comparison with rats injected with PBS vehicle, or a control human-derived IgG_1 (8B4, specific for influenza hemagglutinin). All rats remained healthy, and none showed a significant decline in motor performance as measured by rotarod, compared to animals given vehicle control or the control antibody (Fig. 3c). Histological examination revealed elevated C3 deposition in muscles of animals given $aG_1$01, but not in any of the other three groups (Fig. 3d), as was seen in vitro (Fig. 3b). We also confirmed human IgG deposition at the neuromuscular junction in rats injected with $aG_1$01 or $bG_4$02, and its absence in animals given the vehicle control or the control antibody (Fig. 3e).

Combining antibodies enhances complement activation synergistically

In view of the observation that serum MG1 induced strong AChR-dependent complement activation (Supplementary Fig. 3), but the four individual anti-AChR monoclonal antibodies isolated from the same donor did not (Fig. 3b), we

hypothesized that complement activation is dependent on the synergistic effect of multiple antibodies combined.

The combination of $dG_1 01$ and $eG_1 01$, each at half the concentration (i.e., same final concentration as the previously tested single antibodies), and each with negligible ability to activate complement alone, induced strong complement activation (Fig. 4a).

We tested all possible binary combinations of the patient-derived monoclonal antibodies, and added a well-characterized anti-α IgG_1 isolated by Makino et al. [25], known to be pathogenic and able to activate complement. We observed combination-dependent complement activation of varying magnitude, from minimal activation similar to the single antibodies, up to a 40-fold increase over baseline (Fig. 4b). The $bG_4 02$ antibody, originally isolated as an IgG_4, was additionally tested after artificial class switch to IgG_1, to enable examination of the effect of different epitope specificities, independent from the constant regions.

Combinations of antibodies with differing AChR-subunit specificity seemed to be required to produce a synergistic effect on complement activation. The two combinations of two antibodies targeting the same subunit i.e., $bG_3 01 + bG_4 02\text{-}G_1$, and $aG_1 12 + aG_1 01$, did not result in enhanced complement activation (Fig. 4b–d and Table 2). The strongest enhancement of complement activation was seen in combinations of the α-binding antibody $aG_1 12$ with antibodies targeting one of the other three subunits (Fig. 4b).

Consistent with the well-known inability of IgG_4 to activate complement [3, 27] combinations involving the IgG_4 $bG_4 02$ showed less complement activity than the analogous combinations with the class-switched derivative $bG_4 02\text{-}G_1$ (Fig. 4b, c). However, in the context of combinations with an IgG_1 targeting the α subunit, for example $bG_4 01 + aG_1 01$, or $bG_4 02 + aG_1 12$, complement activation was if anything higher than the single α-binding antibody, despite the fact that the concentration of complement-interacting IgG_1 antibody was halved (Fig. 4b, c).

We also examined the effect of combining antibodies on direct receptor antagonism. No effect on this parameter was detected (Supplementary Fig. 5).

Autoantibody combination is pathogenic in vivo

The discovery that AChR-dependent complement activation by antibodies is so strongly affected by combinations of different epitope specificities raised the question of whether antibody combinations would have a similar impact on in vivo pathogenicity. We, therefore, used a passive transfer rat model to compare the pathogenicity of antibodies administered alone or in combination. We chose the combination of $aG_1 01$ and $bG_4 02$ because both recognize the rat receptor as well as human, and neither induced significant complement activation alone. The $bG_4 02$ antibody was expressed as an IgG_1 to avoid the confound of comparing antibodies of different classes. The results mirrored the in vitro complement experiments; single antibodies had no significant effect on clinical score or rotarod performance, but the combination of the two antibodies was potently pathogenic (Fig. 5a, b), leading to a significant decrement in rotarod performance by 12 h after injection, and a significant increase in clinical score at 24 h after injection.

To examine the histological processes underlying the behavioral impact of the antibodies, we labeled gastrocnemius muscle cryosections from animals in this experiment with Alexa Fluor 647-conjugated α-bungarotoxin (α-BTX) to visualize the AChR, and antibodies against synaptic vesicle glycoprotein 2A (SV2A) to visualize the presynaptic nerve terminal (Fig. 5c). We delineated the NMJs based on SV2A labeling intensity above an automatically calculated threshold, and within this area measured the ratio of α-BTX signal to SV2A signal. This analysis revealed a significant loss of AChR content on the postsynaptic membrane in rats injected with the combination of both antibodies compared to vehicle controls, or to animals given single antibodies (Fig. 5d).

An obvious question was whether complement activation at the NMJ in vivo would also follow the pattern seen in vitro. At the 36-h time point used for behavioral analysis, the NMJ was already severely degraded, stymying the simple approach of labeling the same tissue for complement analysis. Accordingly, the experiment was repeated with a separate cohort of twelve animals, injected with $aG_1 01$ alone, or the combination of $aG_1 01$ and $bG_4 02\text{-}G_1$, or with PBS vehicle, and sacrificed at an earlier time point (12 h after antibody injection). Cryosections of gastrocnemius muscle were immunolabeled for SV2A and for the complement component C3. AChR at the endplates was visualized with α-BTX (Fig. 5e). First, we quantified the intensity of C3 labeling at individual NMJs in animals in the three conditions. Animals given $aG_1 01$ alone had significantly more C3 labeling than control treated animals but significantly less than animals given the combination of $aG_1 01$ and $bG_4 02\text{-}G_1$ (Fig. 5f). Even at the 12-h time point, detailed structural analysis of single NMJs demonstrated advanced disintegration in animals injected with both antibodies (Fig. 5g, h). The total area occupied by AChR was significantly reduced in animals given the combination of $aG_1 01$ and $bG_4 02\text{-}G_1$, while in animals injected with $aG_1 01$ alone, this parameter was not significantly different from the control group. Overall reduction in AChR-containing area was accompanied by fragmentation of the NMJ in both the single antibody and the combination conditions compared to the vehicle control, but this difference was only statistically significant for the combination condition (Fig. 5h).

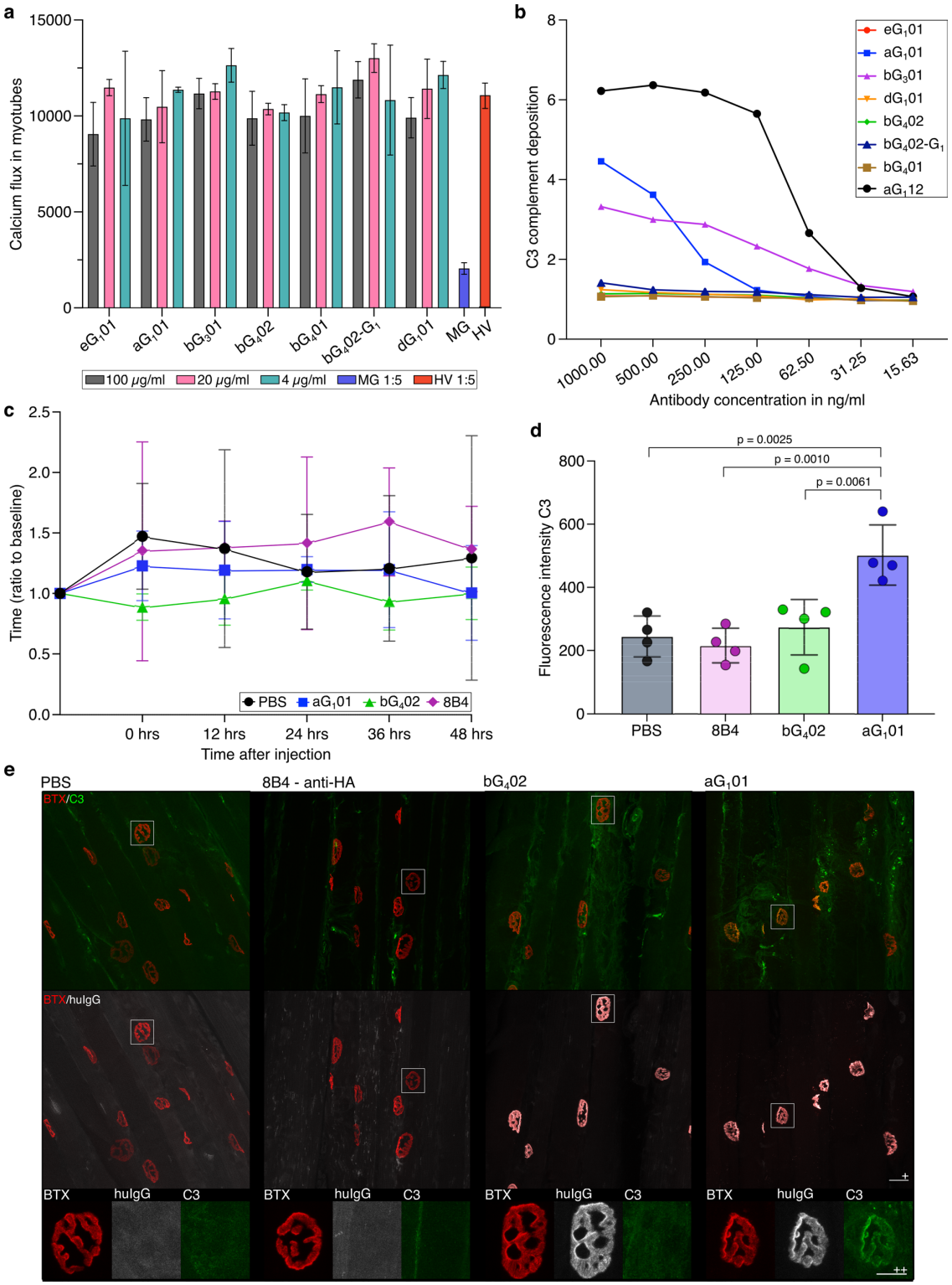
a
Calcium flux in myotubes
15000
10000
5000
0
eG1 01
aG1 01
bG3 01
bG4 02
bG4 01
bG4 02-G1
dG1 01
MG
HV
100 µg/ml
20 µg/ml
4 µg/ml
MG 1:5
HV 1:5
b
C3 complement deposition
8
6
4
2
0
eG1 01
aG1 01
bG3 01
dG1 01
bG4 02
bG4 02-G1
bG4 01
aG1 12
1000.00
500.00
250.00
125.00
62.50
31.25
15.63
Antibody concentration in ng/ml
c
Time (ratio to baseline)
2.5
2.0
1.5
1.0
0.5
0.0
PBS
aG1 01
bG4 02
8B4
0 hrs
12 hrs
24 hrs
36 hrs
48 hrs
Time after injection
d
Fluorescence intensity C3
800
600
400
200
0
p = 0.0025
p = 0.0010
p = 0.0061
PBS
8B4
bG4 02
aG1 01
e
PBS
8B4 - anti-HA
bG4 02
aG1 01
BTX/C3
BTX/huIgG
BTX
huIgG
C3

◂**Fig. 3** Pathogenic potential of single monoclonal AChR-specific antibodies derived from B cells from MG patients. **a** Effect of monoclonal AChR-specific antibodies on cholinergic transmission in the iPSC derived neuromuscular assay. Co-cultures of iPSC-derived neurons and myotubes were incubated for 3 h with the indicated concentrations of monoclonal antibodies, and the effect on AMPA-induced cholinergic signaling was assessed as in Fig. 1c, d. Vertical axis shows the acetylcholine-dependent calcium flux in myotubes as measured by GCaMP signal after AMPA stimulation. Bars show mean values from three replicates with each of the antibodies indicated below the horizontal axis, and the error bars show the SD. Sera from a patient (MG) or a healthy volunteer (HV) diluted 1:5 were included as positive and negative controls. **b** Antigen-dependent complement deposition on live cells measured by flow cytometry. Cells expressing AChR-GFP and untransfected control cells were incubated with serial dilutions of single AChR-specific monoclonal antibodies and supplemented with human serum as source of complement. Activation of the complement cascade was assessed by flow cytometry analysis of C3 deposition visualized with fluorescent secondary antibodies. The GMFI ratio was calculated as described in Fig. 1f. In vivo investigation of pathogenicity of single antibodies. **c** Passive transfer myasthenia gravis in rats. Graph shows rotarod performance of animals given PBS vehicle (black lines and circles), the anti-hemagglutinin IgG_1 control antibody 8B4 (purple lines and diamonds), the anti-α IgG_1 $aG_1$01 (blue lines and squares) or the anti-β IgG_4 $bG_4$02 (green lines and triangles). The horizontal axis shows the time after antibody administration, and the vertical shows the relative time animals remained on the rod (ratio of time on rod at measurement, divided by average time for the three trials before antibody administration) at each of the five timepoints after injection. Each point is the mean of four animals in each condition. Error bars show the standard error of the mean. No significant difference was observed in mean times between groups at any time point (two-way ANOVA with repeated measures, $n=4$ per group). **d** Complement deposition at neuromuscular junctions. Cryosections from gastrocnemius muscles from the animals whose behavior is shown in c were labeled with α-BTX to visualize the AChR, and immunolabeled with a mouse anti-rat C3 antibody to reveal complement deposition. C3 labeling was quantified at at least 100 NMJ per animal, and the vertical axis shows the mean value per animal across NMJs. *P* values were calculated by one-way ANOVA, followed by Tukey's test. Error bars show standard deviation. An analogous figure, with values for individual NMJ is shown in Supplementary Fig. 4. **e** Histopathological impact of monoclonal antibody administration. Cryosections as described in d were immunolabeled, in addition to C3(green), for human IgG (white), and α-BTX (red). From left to right, the first image comes from a rat injected with PBS, the second from a rat injected with 8B4, the third $bG_4$02 and the fourth $aG_1$01. All three anibodies were injected at 4 mg/kg. The scale bar (+) represents 20 µm. Below each image is an enlarged view of an NMJ with a scale bar (++) of 10 µm

Differential subunit specificity of anti-AChR antibody combinations promotes receptor clustering

Compared with the even distribution over the NMJ in animals given single antibodies, bungarotoxin labeling in animals given the pathogenic combination of antibodies was strikingly focused into patches of 1–10 μm^2 in area (Fig. 5e). This could be due to direct immune-mediated destructive fragmentation of the postsynaptic membrane, or to antibody-mediated cross-linking of the receptors shown conceptually in Fig. 6a. To investigate this second possibility, we developed a live cell imaging model for examining antibody-mediated receptor clustering in vitro, enabling real-time monitoring of the phenomenon, and avoiding the possible confound of immune destruction.

We transfected HEK cells with AChR and labeled the extracellular domains of the receptor with α-BTX to allow tracking of receptor location by live cell microscopy. The distribution of α-BTX-labeled AChR on the surface of cells was monitored over the course of 10 min before adding either single or combinations of two antibodies, followed by another 10 min of live cell imaging. Single images from before and after antibody addition are shown in Fig. 6b. The formation of large clusters of receptors following antibody-mediated crosslinking can be observed as localized increases in α-BTX signal density, which we tracked as a function of time after antibody addition (Fig. 6c). We tested eight individual antibodies and various combinations. None of the single antibodies had any significant effect on the distribution of the receptor. Combinations of antibodies such as $aG_1$12 and $bG_4$02, on the other hand, mediated strong clustering (Fig. 6b, c). We investigated this quantitatively for the combination of antibodies ($aG_1$01 and $bG_4$02-G_1) used in the in vivo model, and this combination induced a significantly greater increase in the size and the number of AChR clusters compared to single antibodies (Fig. 6d). The artificial class switch had no effect on the phenomenon, since the combination of $aG_1$01 and the original $bG_4$02 IgG_4 induced a similar degree of clustering (Fig. 6e). The pattern of strong clustering by the combination, and no effect of the single antibodies were seen in four out of five tested pairs of antibodies, independent of the IgG subclass (Fig. 6e).

Discussion

The MACACS technique has several advantages over more traditional techniques using labeled soluble antigen. Antigen-specific B cells are strongly enriched because the BCR affinity has to be high enough to extract the membrane antigen from the target cell, and sorting is facilitated because antigen capture leads to an activation of the B cell and CD69 up-regulation [1, 47]. Particularly when the target antigen is a multi-pass membrane protein or protein complex, expression of antigen in live cells enables the isolation of antibodies against a wide variety of epitopes without a priori assumptions about relative epitope importance. This technique allowed us to isolate six monoclonal anti-AChR antibodies of subclasses IgG_1, IgG_3 and IgG_4. Targets included all subunits of the AChR, and all six antibodies showed evidence of affinity-driven hypermutation. We could then investigate whether the pathogenically relevant properties shown by patients' sera could be assigned to specific antibodies.

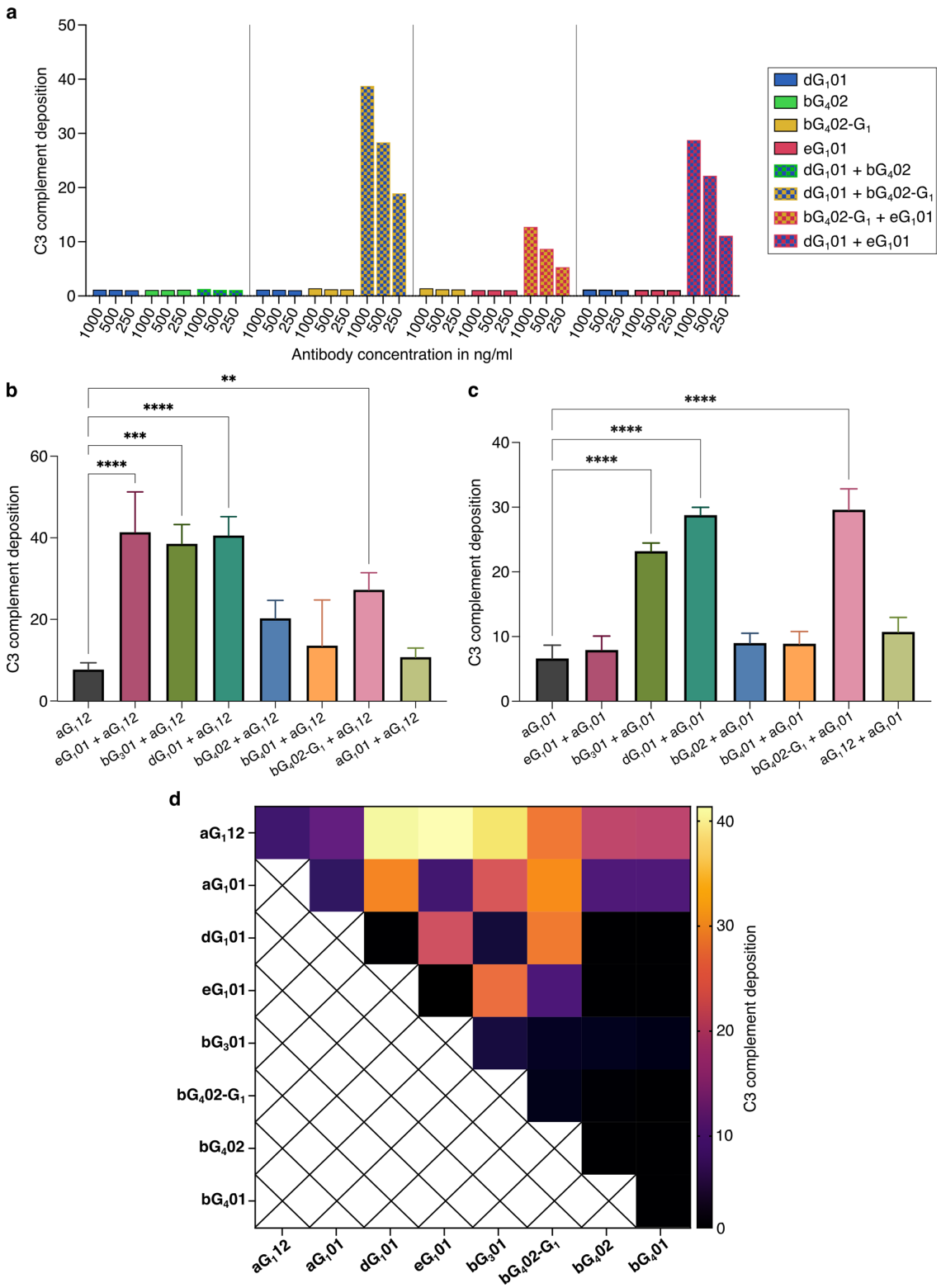
a
C3 complement deposition
Antibody concentration in ng/ml
dG1 01
bG4 02
bG4 02-G1
eG1 01
dG1 01 + bG4 02
dG1 01 + bG4 02-G1
bG4 02-G1 + eG1 01
dG1 01 + eG1 01
b
C3 complement deposition
aG1 12
eG1 01 + aG1 12
bG3 01 + aG1 12
dG1 01 + aG1 12
bG4 02 + aG1 12
bG4 01 + aG1 12
bG4 02-G1 + aG1 12
aG1 01 + aG1 12
c
C3 complement deposition
aG1 01
eG1 01 + aG1 01
bG3 01 + aG1 01
dG1 01 + aG1 01
bG4 02 + aG1 01
bG4 01 + aG1 01
bG4 02-G1 + aG1 01
aG1 12 + aG1 01
d
aG1 12
aG1 01
dG1 01
eG1 01
bG3 01
bG4 02-G1
bG4 02
bG4 01
C3 complement deposition

◂**Fig. 4** Influence of antibody combinations on complement activation. **a** C3 deposition measured for three different concentrations of AChR-specific monoclonal antibodies, singly or in combination. The concentrations shown on the horizontal axis are the total amount of antibody used, e.g., the very first bar shows the results for 1000 ng/ml of $dG_1$01, and the 7th bar 500 ng/ml of each = 1000 ng/ml total antibody. The vertical axis shows the GMFI ratio of C3 immunofluorescence as described in Fig. 1f. Statistical comparison of the ability of single anti-α monoclonal antibodies to activate complement, compared with combinations of these antibodies with other monoclonals targeting different subunits. **b** Shows results for $aG_1$12, and **c** the analogous results for $aG_1$01. Differences between singles and combinations were analyzed by one-way ANOVA followed by Dunnett's test (**$p < 0.01$, ***$p < 0.001$, ****$p < 0.0001$). Bars show means of three values from three independent experiments, each with a single measurement for each antibody or combination. Error bars show standard deviations. **d** Heatmap comparing C3 deposition induced by single AChR-specific monoclonal antibodies, and by all possible combinations. Measurements were repeated in three independent experimental runs with a total antibody concentration in each assay of 500 ng/ml

Single antibodies showed surprisingly little ability to activate complement, or to cause disease in a passive transfer animal model. This changed, however, when antibodies were combined. Combinations of antibodies targeting disparate subunits led to extensive complement activation in vitro, and to a severe behavioral phenotype in vivo. This finding was unexpected, but not completely unprecedented; earlier experiments suggested that rats immunized with a combination of α and β subunits developed myasthenic signs more rapidly than those immunized against α only [19]. Synergy in complement activation between antibodies against different epitopes of single antigens has been observed in the field of anti-cancer antibodies [16], between antibodies against rhesus antigens in hemolytic disease [31], and between antibodies against bacteria [8], but the mechanisms underlying this synergy are not understood. It is well established that isolated IgG molecules are weak inducers of complement, and that some form of multimeric IgG is required to initiate complement signaling [4, 37]. In studies of antibodies interacting with antigen on artificial liposomes, Diebolder et al. (2014) concluded that an optimal complement-activating configuration of IgG is a hexamer of antibodies. According to this model, the individual IgG monomers assemble via interactions between their Fc domains into a wheel-like configuration, with the Fc domains arranged towards the hub, and the Fab domains at the rim. One Fab of each antibody is modeled as binding the antigen, while one Fab arm interacts with the complement C1 component. This configuration would not result in any crosslinking, making it difficult to reconcile with our results, or with the well-established importance of receptor cross-linking in MG [6]. Studies of antibodies interacting with antigens engineered into hexamers with a DNA origami system [33] suggested that the majority of binding configurations involved three antibodies, each bivalently bound to two of the six targets, and not the kind of hexamers described by Diebolder et al. [4]. It is possible that the importance of the hexameric antibody binding configuration is dependent on antigen density. In the NMJ, antigen concentration is very high, with receptor densities estimated in the order of 10,000 receptors per square micrometer [30]. This would put corresponding epitopes on neighboring receptors at distances of the order of 10 nm apart, well within the range of antigen separation for bivalent antibody binding defined by Shaw et al. [33]. We therefore hypothesize that combinations of AChR antibodies are highly complement activating not because they assemble in hexameric configurations, but because they mediate the formation of large, cross-linked lattices of receptor. At the NMJ, the AChR is in some sense "clustered" under normal conditions by the postsynaptic protein rapsyn, under the regulation of a network of other proteins [38]. However, this kind of clustering must be somehow functionally different from that induced by antibodies, since the latter and not the former mediate antigenic modulation [6].

An example of the importance of the two-dimensional supramolecular organization of antigen in the membrane for the activation of complement has been described by researchers working on the aquaporin-4 (AQP4) autoantibody response in neuromyelitis optica [29, 35]. This disease is often associated with autoantibodies against the membrane water channel (AQP4 is expressed in two isoforms, M1 and M23). M1-AQP4 exists as isolated homotetramers in the membrane, while M23-AQP4 tetramers spontaneously assemble into large clusters. Cells transfected with M23-AQP4 are subject to complement-dependent cytotoxicity by patient-derived anti-AQP4 monoclonal IgG, but cells transfected with M1-AQP4 are not [29]. Because this difference is observed even when the cytotoxic antibody binds with similar affinity to the two isoforms, it seems likely that the difference lies in the ability of stable supramolecular platforms of antigen and antibody to act as signal initiation centers for the complement cascade by increasing the local ratio of complement activation versus deactivation by complement regulatory proteins. We propose that in myasthenia gravis, the assembly of AChR into stable two-dimensional arrays that are the substrate of complement-activating antibody clusters is mediated by the cross-linking effect of the antibodies. This requires combinations of antibodies that recognize disparate subunits, as shown in Fig. 6a.

The importance of receptor cross linking rather than antibody density can explain why the addition of a complement-non-activating IgG_4 can have a positive effect on the degree of complement activation in combination with IgG_1 targeting other subunits. A clear prediction of the multi-epitope dependency model is that patients whose myasthenic symptoms are caused by complement activation will have autoantibodies against more than one subunit.

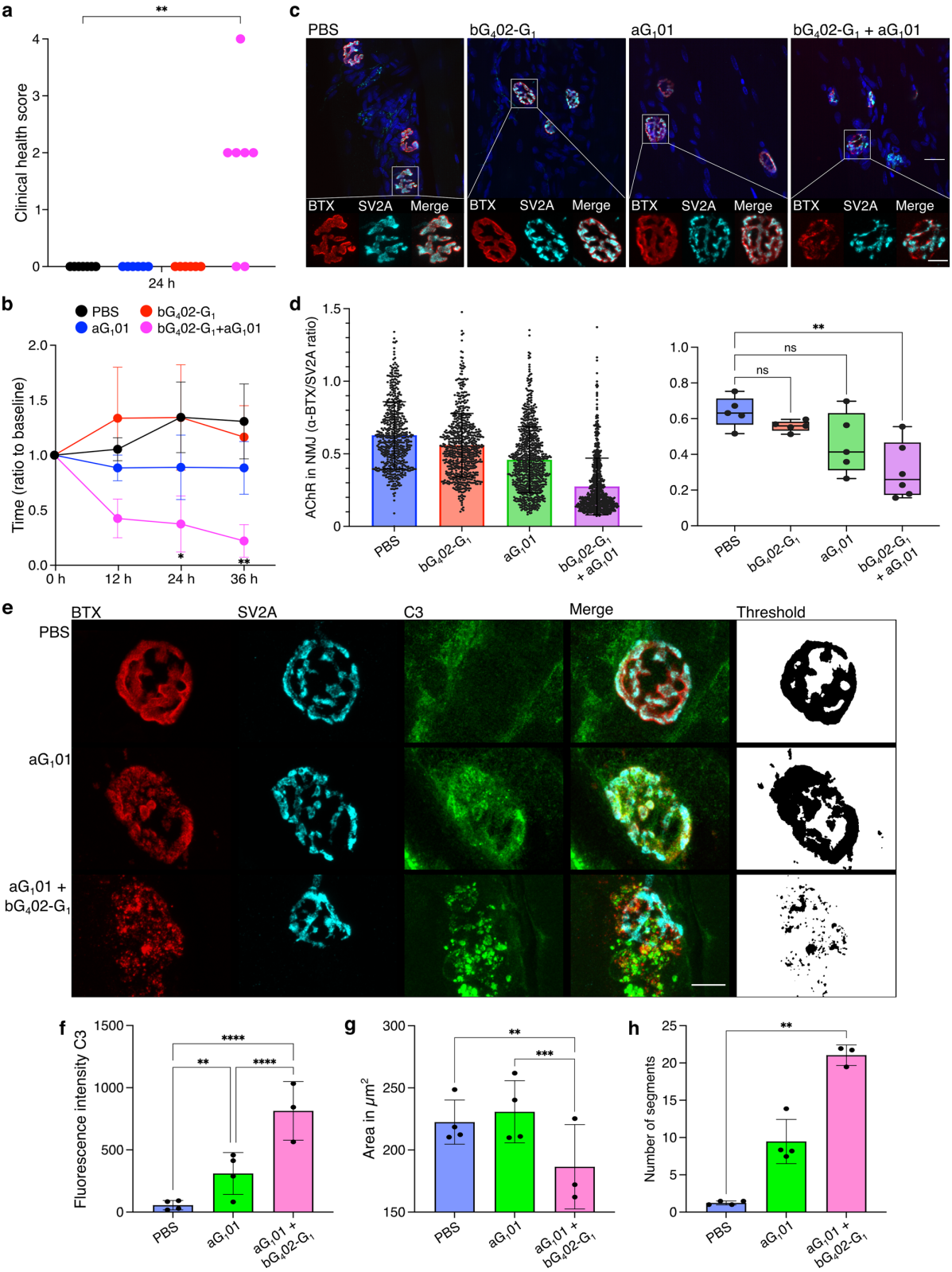
a
Clinical health score
24 h
**
b
PBS
bG4O2-G1
aG1O1
bG4O2-G1+aG1O1
Time (ratio to baseline)
0 h
12 h
24 h
36 h
c
PBS
bG4O2-G1
aG1O1
bG4O2-G1 + aG1O1
BTX
SV2A
Merge
d
AChR in NMJ (α-BTX/SV2A ratio)
ns
e
BTX
SV2A
C3
Merge
Threshold
aG1O1 +
bG4O2-G1
f
Fluorescence intensity C3
g
Area in μm2
h
Number of segments

◂**Fig. 5** Influence of antibody combination on pathogenicity in a PTMG rat model. **a**–**d** The effect of two single, patient-derived, AChR-specific, monoclonal antibodies, was compared with the combination of both. Female Lewis rats were injected with PBS ($n=7$), 4 mg/kg $aG_1 01$ ($n=6$), 4 mg/kg $bG_4 02\text{-}G_1$ ($n=6$), or the combination of 2 mg/kg of each ($n=7$). $bG_4 02\text{-}G_1$ is an IgG1, prepared by switching $bG_4 02$ to IgG_1 to avoid the confound of different classes. **a**. Clinical scores ranging from 0 to 4 (0 = healthy, 4 = dead, see "Materials and methods") at 24 h after injection. Differences between each condition and PBS were subjected to Kruskal–Wallis test, followed by Dunn's multiple comparison (**$p=0.0028$). **b** Rotarod performance was tested every 12 h over 36 h following injection, as shown on horizontal axis. The vertical axis shows the relative time animals remained on the rod (ratio of time on rod at measurement, divided by average time for the three trials before antibody administration). Each point displays the mean of all animals tested (6–7 animals per group, pooled from two independent experiments) and error bars show standard error of the mean. If indicated, the differences between antibody-injected and vehicle control groups were signifcantly different (*$p=0.0439$, **$p=0.0089$) according to Kruskal–Wallis test, followed by Dunn's multiple comparison. **c** Deterioration of NMJ following monoclonal antibody administration. Cryosections from gastrocnemius muscles from the animals whose behavior is shown in **a**, **b**, sacrificed at 36 h after injection, were labeled with DAPI (blue) to visualize nuclei, α-BTX (red) to visualize AChR, and immunolabeled for SV2A (cyan) to visualize the presynaptic side of the synapse. The four images left to right come from animals given PBS, $aG_1 01$, $bG_4 02\text{-}G_1$, and $aG_1 01 + bG_4 02\text{-}G_1$. Below each image is a series of enlarged images of a single NMJ showing the α-BTX, the SV2A, and the overlay. Scale bar = 10 µm. **d** Relative amount of AChR per NMJ in each of the conditions. The ratio of α-BTX to SV2A fluorescence intensity within the NMJ was calculated for approximately 100 NMJs per animal and each NMJ is represented by one dot on the column scatter plot on the left. The vertical axis shows this ratio. The box and whisker plot on the right shows mean values for each animal, and differences between conditions were subjected to one-way ANOVA followed by Dunnett's test to compare each condition with PBS (**$p=0.0013$). **e–h** Similar experiment with shorter duration to enable histological evaluation of complemen activation at NMJ. **e** Representative high magnification confocal images of rat gastrocnemius muscle cryosections from animals injected with PBS (upper row, $n=4$), $aG_1 01$ (middle row, $n=4$) or the combination of $aG_1 01$ and $bG_4 02\text{-}G_1$ (lower row, $n=3$). Cryosections were labeled with α-BTX, and immunolabeled for SV2A and C3. The monochrome images to the right of the figure show examples of thresholded images based on the fluorescence intensity of the α-BTX label which were used for the structural analysis shown in **g**–**h**. Scale bar = 10 µm. **f** Fluorescence intensity of immunolabeled C3 deposition localized at the NMJ. Results of at least 100 NMJs analyzed per animal are summarized. Differences between experimental groups were statistically significant as indicated (**$p=0.0031$, ****$p<0.0001$) using a two-way ANOVA with a multiple comparison corrected according to Dunnett. One animal of the cohort injected with the antibody combination was excluded from analysis because serum human IgG measurement was negative. **g** Total NMJ size measured as area labeled by α-BTX. **h** Disintegration of NMJs expressed as number of fragments per NMJ. Single data points in g-h display the means of 15 analyzed NMJs per animal. Differences between groups were subjected to Kruskal–Wallis test with Dunn's multiple comparison test (**$p<0.005$, ***$p<0.0005$, ****$p<0.0001$)

The subunit specificities of antibodies in patients' sera have been assessed by two methods: by competition with experimental monoclonal antibodies of known subunit specificity [10, 39, 46], and by measuring binding to chimeric receptors containing only one human subunit [23]. Tzartos et al. [43] examined the ability of monoclonal antibodies deemed MIR-, β-, or γ-specific to inhibit binding of antibodies from sera from 86 patients, and concluded that 78%, 20%, and 36% of the 86 sera were inhibited at least 50% by the anti-MIR, anti-β, and anti-γ antibodies respectively. Application of a lower threshold of 10% inhibition would suggest that approximately 99%, 84%, and 95% of sera contain antibodies against the three subunits. These authors detected no correlation between antibody specificity and disease severity.

According to a similar competitive inhibition study by Whiting et al. [46], the least inhibition was exerted by an anti-γ antibody, and the greatest by anti-α, with the anti-β and anti-δ showing intermediate inhibition. These results too, support the conclusion that most patients have antibodies against several subunits. These authors reported "no apparent influence of duration of disease, clinical severity, or previous immunosuppressive treatment over anti-AChR specificity". Heidenreich et al. [11] report inhibition percentages by monoclonals against α, β, γ, and δ, for 20 individual sera. All twenty sera are at least 30% inhibited by antibodies against at least two subunits. These data too, support the prediction that all patients have autoantibodies of multiple subunit specificities.

A corollary to the prediction of multiple specificities is that a person who has antibodies against only one subunit ought to be healthy. Detection of anti-AChR antibodies in non-myasthenia patients is rare, with for example zero positive results out of 427 serum assays from patients with non-myasthenia neurological diagnoses [14]. In summary, the available evidence supports the hypothesis of requirement for multiple subunit specificities for the initiation of MG pathology. This hypothesis predicts that therapeutic approaches designed to interfere with cross-linking [22], especially if combined with a complement-inhibiting strategy [36] are likely to be effective. Also potentially effective in disrupting antibody-crosslinking and receptor clustering might be strategies based on soluble decoy antigens [24].

The antibodies we isolated were, in combination, highly complement activating, but not receptor blocking. Since we did observe direct receptor blockade by sera, we assume that this pathomechanism is relevant, and we expect that future studies with receptor-blocking monoclonal antibodies will be needed to address this. In humans, the therapeutic success of the complement inhibitors eculizumab and ravulizumab in a large proportion of myasthenia patients also points to a pivotal role of complement [13, 26, 45]. While cloning and testing of single recombinant antibodies is not feasible in clinical practice, in vitro testing of sera for their effect on complement activation could provide a tool for assessing this pathway in individual patients. Ultimately, these functional

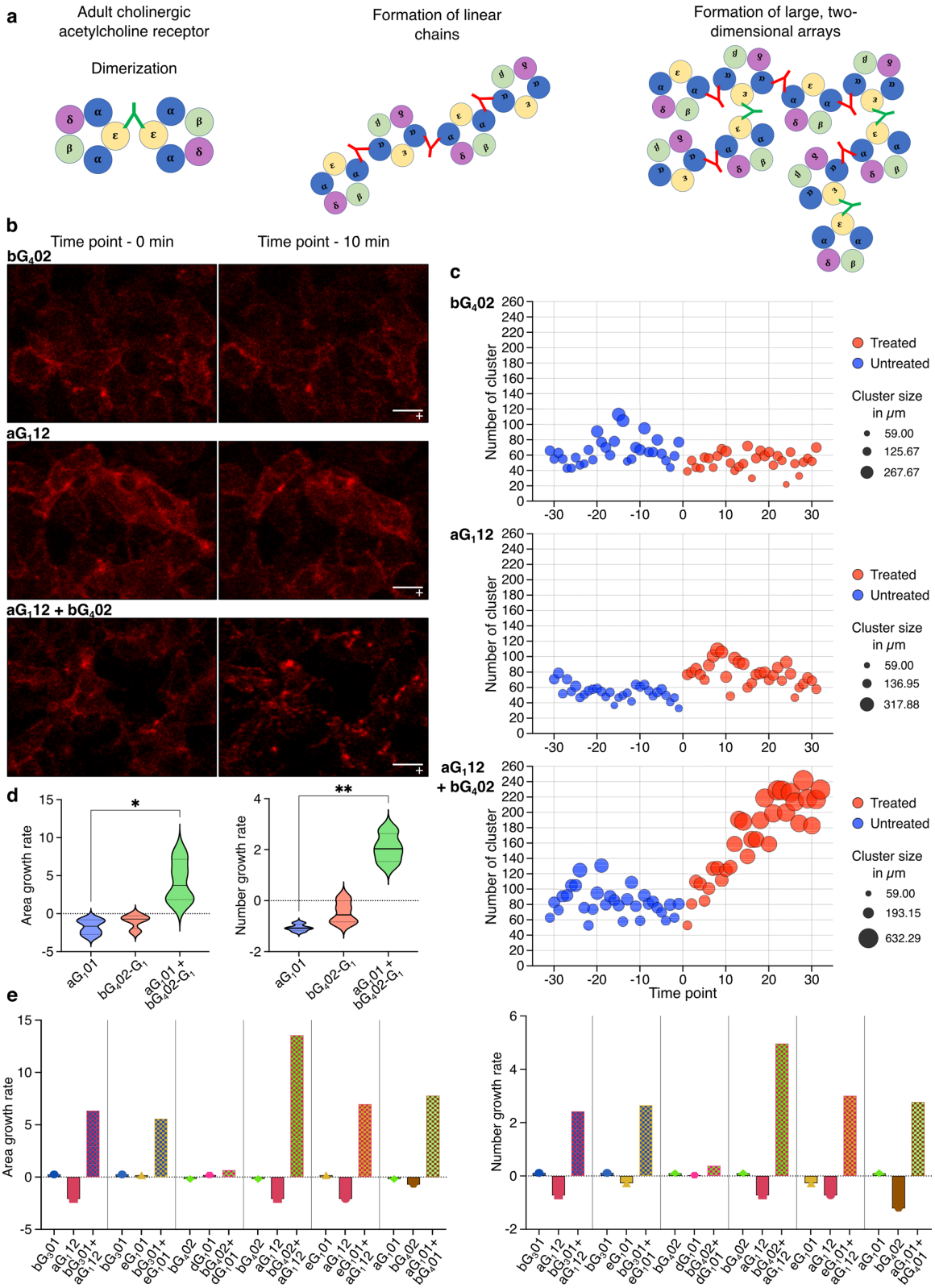
a
Adult cholinergic acetylcholine receptor
Dimerization
Formation of linear chains
Formation of large, two-dimensional arrays
b
Time point - 0 min
Time point - 10 min
bG4 02
aG1 12
aG1 12 + bG4 02
c
bG4 02
aG1 12
aG1 12 + bG4 02
Number of cluster
Time point
Treated
Untreated
Cluster size in μm
59.00
125.67
267.67
136.95
317.88
193.15
632.29
d
Area growth rate
Number growth rate
aG1 01
bG4 02-G1
aG1 01 + bG4 02-G1
e
Area growth rate
Number growth rate

◂**Fig. 6** Induction of receptor clustering by anti-AChR antibodies. **a** Hypothetical model of antibody-mediated receptor clustering depending on subunit specificity and combinational synergy. Single, non-α subunit specific antibodies mediate dimerization; α-specific antibodies mediate formation of linear chains; and combinations of antibodies with differing subunit specificity mediate formation of extensive two-dimensional arrays. **b** Live cell imaging of AChR cluster formation induced by antibodies. Images on the left show AChR-transfected HEK cells labeled with α-BTX (red) at time point zero, i.e., after ten minutes of live cell imaging, and before addition of antibody. Images on the right were captured from the same cultures, 10 min after addition of the antibodies indicated to the left of the images, i.e., 4 µg/ml $bG_4$02, 4 µg/ml $aG_1$12 or the combination of 2 µg/ml of each (4 µg/ml total IgG in each case) scale bar = 10 µm. Supplementary video 2 is a movie compiled from the live cell imaging data shown in the lower row of this figure. **c**. From each image, clusters of AChR, defined as areas of signal exceeding a given threshold were extracted as described in Materials and Methods, and their numbers and sizes plotted as a function of time in the bubble plots on the right. The vertical axis shows the number of clusters, and the size of each bubble corresponds to the average size of the clusters in each image. Each bubble depicts the quantification of one image acquired at one time point during the 20 min of live cell imaging (approximately 3 frames per minute). Blue bubbles represent images taken before, and red bubbles taken after antibody addition. **d, e** Bar graphs showing the growth rate (slope of graph of parameter plotted against time) of either the number or the size of clusters induced by anti-AChR antibodies. **d** Violin plots depicting the growth rates of size and number of clusters of four separately performed experiments for $aG_1$01 and $bG_4$02-G_1. The bold line within the violin depicts the median, dotted lines the quartiles. Significant differences between single antibodies and the combinations were assessed by Kruskal–Wallis test with Dunn's multiple comparison test (*$p = 0.0181$; **$p = 0.0051$). **e** Similar information as shown in d, for five combinations of antibodies, as shown below the horizontal axis. Each combination was tested once

assays might be more meaningful than measuring titers of anti-AChR antibodies in patients.

Supplementary Information The online version contains supplementary material available at https://doi.org/10.1007/s00401-022-02493-6.

Acknowledgements We are grateful to the patients of the neurologic clinic of the University Hospital Basel for the kind donation of their samples, and to the clinical staff for facilitating their collection. We thank David Beeson and Susan Maxwell for the gift of the AChR plasmids, and Tomohiro Makino for extensive advice on the project. Flow and microscopy cores of the Department of Biomedicine at the University of Basel provided expert technical support, and computational resources were provided by sciCORE (http://scicore.unibas.ch/) scientific computing center at University of Basel. We thank Tim Roloff and Adrian Egli for Illumina sequencing completed at the Applied Microbiology Research lab, Department of Biomedicine, University of Basel. Rats were cared for by staff at the University of Basel Animal Facility in Mattenstrasse, Basel. Funding for this project was provided by the Swiss National Science Foundation (grant numbers 169674, 189043), Alexion Pharmaceuticals, and the Neuromuscular Research Association Basel (NeRAB).

Funding Open access funding provided by University of Basel.

References

1. Callegari I, Schneider M, Berloffa G, Mühlethaler T, Holdermann S, Galli E et al (2022) Potent neutralization by monoclonal human IgM against SARS-CoV-2 is impaired by class switch. EMBO Rep. https://doi.org/10.15252/EMBR.202153956
2. Chen TW, Wardill TJ, Sun Y, Pulver SR, Renninger SL, Baohan A et al (2013) Ultrasensitive fluorescent proteins for imaging neuronal activity. Nat 4997458(499):295–300. https://doi.org/10.1038/nature12354
3. Dalakas MC, Alexopoulos H, Spaeth PJ (2020) Complement in neurological disorders and emerging complement-targeted therapeutics. Nat Rev Neurol 16:601–617. https://doi.org/10.1038/s41582-020-0400-0
4. Diebolder CA, Beurskens FJ, De Jong RN, Koning RI, Strumane K, Lindorfer MA et al (2014) Complement is activated by IgG hexamers assembled at the cell surface. Science (80-) 343:1260–1263. https://doi.org/10.1126/science.1248943
5. Drachman DB, Adams RN, Josifek LF, Self SG (1982) Functional activities of autoantibodies to acetylcholine receptors and the clinical severity of myasthenia gravis. N Engl J Med 307:769–775. https://doi.org/10.1056/nejm198209233071301
6. Drachman DB, Angus CW, Adams RN, Michelson JD, Hoffman GJ (1978) Myasthenic antibodies cross-link acetylcholine receptors to accelerate degradation. N Engl J Med 298:1116–1122. https://doi.org/10.1056/nejm197805182982004
7. Engel AG, Arahata K (1987) The membrane attack complex of complement at the endplate in myasthenia gravis. Ann N Y Acad Sci 505:326–332. https://doi.org/10.1111/j.1749-6632.1987.tb51301.x
8. Faleri A, Santini L, Brier S, Pansegrau W, Lo SP, Scarselli M et al (2014) Two cross-reactive monoclonal antibodies recognize overlapping epitopes on Neisseria meningitidis factor H binding protein but have different functional properties. FASEB J 28:1644–1653. https://doi.org/10.1096/fj.13-239012
9. Gilhus NE, Tzartos S, Evoli A, Palace J, Burns TM, Verschuuren JJGM (2019) Myasthenia gravis. Nat Rev Dis Prim. https://doi.org/10.1038/s41572-019-0079-y
10. Heidenreich F, Vincent A, Roberts A, Newsom-Davis J (1988) Epitopes on human acetylcholine receptor defined by monoclonal antibodies and myasthenia gravis sera. Autoimmunity 1:285–297. https://doi.org/10.3109/08916938809010682
11. Heidenreich F, Vincent A, Willcox N, Newsom-Davis J (1988) Anti-acetylcholine receptor antibody specificities in serum and in thymic cell culture supernatants from myasthenia gravis patients. Neurology 38:1784–1788. https://doi.org/10.1212/WNL.38.11.1784
12. Hockemeyer D, Wang H, Kiani S, Lai CS, Gao Q, Cassady JP et al (2011) Genetic engineering of human pluripotent cells using TALE nucleases. Nat Biotechnol 298(29):731–734. https://doi.org/10.1038/nbt.1927

13. Howard JF, Utsugisawa K, Benatar M, Murai H, Barohn RJ, Robeson K et al (2017) Safety and efficacy of eculizumab in anti-acetylcholine receptor antibody-positive refractory generalised myasthenia gravis (REGAIN): a phase 3, randomised, double-blind, placebo-controlled, multicentre study. Lancet Neurol 16:976–986. https://doi.org/10.1016/S1474-4422(17)30369-1
14. Howard FM, Lennon VA, Finley J, Matsumoto J, Elveback LR (1987) Clinical correlations of antibodies that bind, block, or modulate human acetylcholine receptors in myasthenia gravis. Ann N Y Acad Sci 505:526–538. https://doi.org/10.1111/J.1749-6632.1987.TB51321.X
15. Huijbers MG, Vergoossen DL, Fillié-Grijpma YE, Van Es IE, Koning MT, Slot LM et al (2019) MuSK myasthenia gravis monoclonal antibodies: valency dictates pathogenicity. Neurol Neuroimmunol Neuroinflamm. https://doi.org/10.1212/NXI.0000000000000547
16. Klitgaard JL, Koefoed K, Geisler C, Gadeberg OV, Frank DA, Petersen J et al (2013) Combination of two anti-CD5 monoclonal antibodies synergistically induces complement-dependent cytotoxicity of chronic lymphocytic leukaemia cells. Br J Haematol 163:182–193. https://doi.org/10.1111/bjh.12503
17. Kordas G, Lagoumintzis G, Sideris S, Poulas K, Tzartos SJ (2014) Direct proof of the in vivo pathogenic role of the AChR autoantibodies from myasthenia gravis patients. PLoS ONE. https://doi.org/10.1371/JOURNAL.PONE.0108327
18. Kusner LL, Losen M, Vincent A, Lindstrom J, Tzartos S, Lazaridis K et al (2015) Guidelines for pre-clinical assessment of the acetylcholine receptor-specific passive transfer myasthenia gravis model-recommendations for methods and experimental designs. Exp Neurol 270:3–10. https://doi.org/10.1016/j.expneurol.2015.02.025
19. Lazaridis K, Baltatzidi V, Trakas N, Koutroumpi E, Karandreas N, Tzartos SJ (2017) Characterization of a reproducible rat EAMG model induced with various human acetylcholine receptor domains. J Neuroimmunol 303:13–21. https://doi.org/10.1016/j.jneuroim.2016.12.011
20. Leite MI, Jacob S, Viegas S, Cossins J, Clover L, Morgan BP et al (2008) IgG1 antibodies to acetylcholine receptors in "seronegative" myasthenia gravis. Brain 131:1940–1952. https://doi.org/10.1093/BRAIN/AWN092
21. Lennon VA, Griesmann GE (1989) Evidence against acetylcholine receptor having a main immunogenic region as target for autoantibodies in myasthenia gravis. Neurology 39:1069–1076. https://doi.org/10.1212/wnl.39.8.1069
22. Losen M, Labrijn AF, Van Kranen-Mastenbroek VH, Janmaat ML, Haanstra KG, Beurskens FJ et al (2017) Hinge-deleted IgG4 blocker therapy for acetylcholine receptor myasthenia gravis in rhesus monkeys. Sci Rep. https://doi.org/10.1038/S41598-017-01019-5
23. Loutrari H, Kokla A, Tzartos SJ (1992) Passive transfer of experimental myasthenia gravis via antigenic modulation of acetylcholine receptor. Eur J Immunol 22:2449–2452. https://doi.org/10.1002/eji.1830220939
24. Luo J, Lindstrom J (2015) AChR-specific immunosuppressive therapy of myasthenia gravis. Biochem Pharmacol 97:609–619. https://doi.org/10.1016/J.BCP.2015.07.011
25. Makino T, Nakamura R, Terakawa M, Muneoka S, Nagahira K, Nagane Y et al (2017) Analysis of peripheral B cells and autoantibodies against the anti-nicotinic acetylcholine receptor derived from patients with myasthenia gravis using single-cell manipulation tools. PLoS ONE. https://doi.org/10.1371/journal.pone.0185976
26. Muppidi S, Utsugisawa K, Benatar M, Murai H, Barohn RJ, Robeson K et al (2019) Long-term safety and efficacy of eculizumab in generalized myasthenia gravis. Muscle Nerve 60:14–24. https://doi.org/10.1002/mus.26447
27. Van Der NeutKolfschoten M, Schuurman J, Losen M, Bleeker WK, Martínez-Martínez P, Vermeulen E et al (2007) Anti-inflammatory activity of human IgG4 antibodies by dynamic Fab arm exchange. Science 317:1554–1557. https://doi.org/10.1126/science.1144603
28. Newsom-Davis J, Pinching AJ, Vincent A, Wilson SG (1978) Function of circulating antibody to acetylcholine receptor in myasthenia gravis: investigation by plasma exchange. Neurology 28:266–272. https://doi.org/10.1212/wnl.28.3.266
29. Phuan PW, Ratelade J, Rossi A, Tradtrantip L, Verkman AS (2012) Complement-dependent cytotoxicity in neuromyelitis optica requires aquaporin-4 protein assembly in orthogonal arrays. J Biol Chem 287:13829–13839. https://doi.org/10.1074/jbc.M112.344325
30. Popot JL, Changeux JP (1984) Nicotinic receptor of acetylcholine: structure of an oligomeric integral membrane protein. Physiol Rev 64:1162–1239. https://doi.org/10.1152/physrev.1984.64.4.1162
31. Rosse WF (1969) Fixation of the first component of complement (C'la) by human antibodies. J Clin Investig 47:2430–2445. https://doi.org/10.1172/jci105926
32. Russell OM, Fruh I, Rai PK, Marcellin D, Doll T, Reeve A et al (2018) Preferential amplification of a human mitochondrial DNA deletion in vitro and in vivo. Sci Rep 81(8):1–10. https://doi.org/10.1038/s41598-018-20064-2
33. Shaw A, Hoffecker IT, Smyrlaki I, Rosa J, Grevys A, Bratlie D et al (2019) Binding to nanopatterned antigens is dominated by the spatial tolerance of antibodies. Nat Nanotechnol 14:184–190. https://doi.org/10.1038/s41565-018-0336-3
34. Smurnyy Y, Cai M, Wu H, McWhinnie E, Tallarico JA, Yang Y et al (2014) DNA sequencing and CRISPR-Cas9 gene editing for target validation in mammalian cells. Nat Chem Biol 108(10):623–625. https://doi.org/10.1038/nchembio.1550
35. Soltys J, Liu Y, Ritchie A, Wemlinger S, Schaller K, Schumann H et al (2019) Membrane assembly of aquaporin-4 autoantibodies regulates classical complement activation in neuromyelitis optica. J Clin Investig 129:2000–2013. https://doi.org/10.1172/JCI122942
36. Song C, Xu Z, Miao J, Xu J, Wu X, Zhang F et al (2012) Protective effect of scFv-DAF fusion protein on the complement attack to acetylcholine receptor: a possible option for treatment of myasthenia gravis. Muscle Nerve 45:668–675. https://doi.org/10.1002/mus.23247
37. Strasser J, De Jong RN, Beurskens FJ, Wang G, Heck AJR, Schuurman J et al (2019) Unraveling the macromolecular pathways of IgG oligomerization and complement activation on antigenic surfaces. Nano Lett 19:4787–4796. https://doi.org/10.1021/acs.nanolett.9b02220
38. Takamori M (2020) Myasthenia gravis: from the viewpoint of pathogenicity focusing on acetylcholine receptor clustering, transsynaptic homeostasis and synaptic stability. Front Mol Neurosci. https://doi.org/10.3389/FNMOL.2020.00086
39. Takata K, Stathopoulos P, Cao M, Mané-Damas M, Fichtner ML, Benotti ES et al (2019) Characterization of pathogenic monoclonal autoantibodies derived from muscle-specific kinase myasthenia gravis patients. JCI Insight. https://doi.org/10.1172/jci.insight.127167
40. Toyka KV, Drachman DB, Griffin DE, Pestronk A, Winkelstein JA, Fishbeck KH et al (1977) Myasthenia gravis. Study of humoral immune mechanisms by passive transfer to mice. N Engl J Med 296:125–131
41. Tsujihata M, Yoshimura T, Satoh A, Kinoshita I, Matsuo H, Mori M et al (1989) Diagnostic significance of igg, C3, and C9 at the limb muscle motor end-plate in minimal myasthenia gravis. Neurology 39:1359–1363. https://doi.org/10.1212/wnl.39.10.1359
42. Tzartos SJ, Barkas T, Cung MT, Mamalaki A, Marraud M, Orlewski P et al (1998) Anatomy of the antigenic structure of a

large membrane autoantigen, the muscle-type nicotinic acetylcholine receptor. Immunol Rev 163:89–120. https://doi.org/10.1111/j.1600-065X.1998.tb01190.x

43. Tzartos SJ, Seybold ME, Lindstrom JM (1982) Specificities of antibodies to acetylcholine receptors in sera from myasthenia gravis patients measured by monoclonal antibodies. Proc Natl Acad Sci USA 79:188–192. https://doi.org/10.1073/pnas.79.1.188
44. Vincent A, Palace J, Hilton-Jones D (2001) Myasthenia gravis. Lancet 357:2122–2128. https://doi.org/10.1016/S0140-6736(00)05186-2
45. Vu T, Meisel A, Mantegazza R, Annane D, Katsuno M, Aguzzi R et al (2022) Terminal complement inhibitor ravulizumab in generalized myasthenia gravis. NEJM Evid. https://doi.org/10.1056/EVIDOA2100066
46. Whiting PJ, Vincent A, Newsom-Davis J (1986) Myasthenia gravis: monoclonal antihuman acetylcholine receptor antibodies used to analyze antibody specificities and responses to treatment. Neurology 36:612–617. https://doi.org/10.1212/WNL.36.5.612
47. Zimmermann M, Rose N, Lindner JM, Kim H, Gonçalves AR, Callegari I et al (2019) Antigen extraction and B cell activation enable identification of rare membrane antigen specific human B cells. Front Immunol. https://doi.org/10.3389/fimmu.2019.00829

3.2 Results II: Antigen array formation facilitates complement activation by antibody combinations with synergistic subunit specificity in myasthenia gravis (manuscript)

Abstract

Myasthenia gravis is an autoimmune disease of the neuromuscular junction associated with antibodies against proteins expressed at the post-synaptic membrane, most commonly the acetylcholine receptor. Several mechanisms have been described that disrupt the signal transmission from nerve to muscle endplate, among them the antibody-dependent complement activation. This pathomechanism induces the formation of a membrane attack complex with subsequent destruction of the receptor-bearing membrane, a process that has been demonstrated to be the main cause of the clinical symptoms.

Previously, we reported six monoclonal, AChR-specific IgG antibodies derived from myasthenia gravis patients of which none showed significant pathogenic capacity despite clear binding to the receptor. Only when combined in synergistic antibody pairs with distinct AChR-subunit specificities did we observe enhanced complement activation in vitro and myasthenic symptoms in a passive transfer myasthenia gravis rat model. In the present study we used a C5 complement inhibitor to show that the in vivo pathology mediated by the antibody combination was a direct result of complement-dependent cytotoxicity.

To unravel the underlying mechanism that enhances complement activation by antibody combinations we postulated three competing hypotheses and experimentally tested their validity. Combinations of antibodies comprised of IgG_1 and IgG_4 still generated elevated levels of C3 complement deposition and even the affinity of individual antibodies proved less important than synergistic subunit specificities. We included AChR-specific IgM antibodies isolated from myasthenia gravis patients and healthy donors to investigate the significance of a hexameric antibody shape for the initiation of the complement cascade. Most IgM were unable to induce antibody-mediated complement activation in spite of AChR-specific binding, arguing against the importance of the predominant hexamer model. In conclusion the antigen array hypothesis provided the most reliant model, describing an extended platform of stabilized and interconnected AChR which improves the antibody binding kinetics and leads to enhanced complement activation. Disruption of the antigen conformation as a therapeutic strategy may greatly reduce IgG-mediated complement pathology in myasthenia gravis and could exert profound impact on diseases with similar pathomechanisms.

Introduction

Myasthenia gravis (MG) is a debilitating autoimmune disease of the neuromuscular junction (NMJ), in which antibodies against proteins of the post-synaptic membrane interfere with the signal transmission from nerve to muscle end plate. In about 85% of patients these autoantibodies target the acetylcholine receptor (AChR), a ligand-gated ion channel that regulates the depolarization of the post-synaptic membrane and thus muscle contraction (Vincent A. and Newsom-Davis J., 1985). The pentameric AChR consists of four different subunits named α, β, δ, and ε, of which the α-subunit is incorporated twice. The clinical manifestation of the disease presents as weakness and increased fatigability of particular muscle groups, including the eye muscles, or muscles of the head and neck area associated with swallowing and speaking. In severe cases, symptom exacerbation can affect the respiratory system, leading to a life-threatening condition known as myasthenic crisis that requires intensive care (Iorio R., 2024). Compelling evidence has been collected during the 1970s and 1980s proposing three potential mechanisms that mediate the disease symptoms observed in MG: (1) direct receptor antagonism, (2) antigenic modulation, describing an increased internalization that results in AChR depletion and (3) complement activation leading to the assembly of a membrane-attack complex and destruction of the post-synaptic membrane (Toyka et al., 1975; Drachman et al., 1978). Autoantibody-dependent complement damage of the NMJ is considered the principal pathogenic mechanism in MG and the target of recently emerging therapeutic interventions (Kusner et al., 2008; Gilhus et al., 2019; Iorio R., 2024).

The complement system is a fundamental component of the humoral immune response and provides effector functions for host defense, including opsonization, inflammation, chemotaxis and cell lysis (Mastellos et al., 2024). In the classic pathway, the complement cascade is initiated by the binding of the C1 complex, consisting of the multimeric recognition molecule C1q and two associated zymogens C1r and C1s, to immunoglobulins of the IgM or IgG class (Dalakas et al., 2020). Single IgG antibodies bound to an antigen represent weak activators of the complement system, while increasingly large complexes showed enhanced proficiency, up to the formation of a hexameric structure that resembles the organization of an IgM molecule (Diebolder et al., 2014). This prevailing concept, introduced by Diebolder and colleagues predicts that IgG binding as functionally monovalent antibodies in a cartwheel shape provides the ideal conformational platform for the interaction with C1q and subsequent initiation of the complement system.

In the context of neuromyelitis optica, an autoimmune disease of the central nervous system

mediated by autoantibodies against the water channel aquaporin-4 (AQP4), complement-dependent cytotoxicity depends on antibody characteristics but also on the distribution of the antigenic target on the cell surface (Crane et al., 2010). Two isoforms of AQP4 have been described, including M23 with the propensity to form orthogonal arrays of particles (OAP) and facilitate complement activation, and M1 which disperses evenly, rendering cells less susceptible to complement-mediated lysis (Phuan et al., 2012; Soltys et al., 2017). Much less is known about the underlying mechanisms that contribute to complement activation in MG, partly because the isolation of individual AChR-specific autoantibodies posed a major challenge. We reported recently, that combinations of antibodies with synergizing subunit-specificities amplified complement activation in vitro through receptor clustering (Rose et al., 2022). Furthermore, we observed that individually non-pathogenic antibodies induced myasthenic symptoms in vivo when administered in combination, proving the significance of the combinational effect. In the present study, we therefore aim to elucidate the mechanistic foundations that enhance complement activation by revisiting the characteristics of IgG that synergize in activating complement and investigating the unique potential of anti-AChR IgM antibodies.

Materials and methods

Cell lines and plasmids

HEK293T/17 cells were obtained from ATCC (LGC, Wesel, Germany) and cultured in complete DMEM medium (supplemented with 10% heat-inactivated fetal calf serum (FCS), 100 units/ml of penicillin and 100 µg/ml of streptomycin, all from Gibco) at 37 °C and 10% carbon dioxide. TE671 rhabdomyosarcoma cells from ATCC were cultured in complete RPMI (same supplements as complete DMEM) at 37°C and 5% carbon dioxide. For the generation of a stable CD40L-expressing cell line TE671 cells were transfected with a pCMV3 plasmid containing human CD40 ligand, sorted and subsequently irradiated with 72 Gy for mitotic inactivation and kept in liquid nitrogen until use. The AChR subunits β, δ and ε were cloned into pcDNA3.1-hygro, the α-subunit was fused to GFP in a pEGFP-N1 expression plasmid to produce a cytoplasmic eGFP tag and all four of the subunits were a gift from David Beeson (Leite et al., 2008). For cloning of the heavy and light chain immunoglobulin gene sequences pVitro1-hygro-mcs (Invivogen) was used. Two additional restriction sites, SwaI and AflII with flanking tag regions were introduced at the two different cloning sites to enable ligation independent cloning.

Donors and B cell isolation

Peripheral blood samples were collected from two healthy controls, one male and one female with no diagnosis and no detectable AChR-specific antibodies in serum. Another three MG patient samples were used, two male and one female with clinically confirmed MG showing AChR-antibody titers above 0.5 nmol/L measured via radioimmunoassay. The peripheral blood was collected in S-Monovette tubes containing EDTA (01.1605.100) for the isolation of peripheral blood mononuclear cells (PBMC) and S-Monovette tubes with clot activator (01.1601.100, both from Sarstedt) for extraction of serum. The PBMC isolation was performed as described previously (Rose et al., 2022; Zimmermann et al., 2019) and stored in liquid nitrogen until use, while serum samples were kept at -20°C after isolation. AChR-specific B cell identification was performed according to the membrane-antigen capture activated cell sorting protocol described in Zimmermann et al. (2019). B cells were isolated from PBMC samples via negative selection with the Pan B cell isolation kit (Miltenyi), and directly used for co-culturing on a monolayer of TE-AChR-GFP cells labelled with cell trace blue (Thermo Fisher cat# C34568). Extracellular AChR was additionally labelled with A647-conjugated α-bungarotoxin (α-BTX, B35450, ThermoFisher) and after 3 hours of incubation the cells were retrieved, labelled for CD69 expression and subjected to fluorescence activated cell sorting on an Aria III Cell Sorter (BD Biosciences). The CTV-, AChR-GFP+, α-BTX+ and CD69 high B cell population was collected in a 1.5 ml Eppendorf tube containing 500 µl of RPMI-40 (complete RPMI with 40% FCS, 100 units/ml of penicillin, 100 µg/ml of streptomycin and 50 ng/ml recombinant human IL-21, all from Gibco) and seeded in a 384 flat-bottom well plate containing irradiated TE-CD40L expressing cells in a limiting dilution for single B cell distribution.

Screening of single seeded B cell supernatant, cDNA generation and Illumina sequencing

After 9 days in culture, 15 µl of supernatant from single wells was collected to measure antibody production via live-cell flow cytometry as reported in Rose et al. (2022). HEK cells transfected with AChR-GFP were incubated with the supernatant of single seeded B cells for 30 min., washed and labelled with goat PE anti-human IgG (109-116-098), AF647 anti-human IgA (109-605-011), and AF594 anti-human IgM (109- 585-129; all from Jackson ImmunoResearch (JIR)). Following a final washing and fixation with 4% PFA in PBS, AChR-specific binding of antibody was analyzed on a Cytoflex flow cytometer (Beckman Coulter). Positive wells were selected for the extraction of mRNA. All but 10 µl of cell culture supernatant was removed and B cells lysed in 20 µl of 15 mM Tris–HCl (pH 8.0) with 0.5 U/µl

recombinant murine RNAse inhibitor (NEB, M0314L). The samples were snap-frozen on dry ice and either stored at -80°C or directly utilized for RNA isolation with the help of the Quick-RNA MicroPrep Kit (Zymo). After purification of the RNA, the cDNA was generated using the SMART-Seq® v4 Ultra® Low Input RNA Kit for Sequencing from Takara following the manufacturer's guide but only applying half the volume recommended per single reaction. The library for Illumina sequencing were prepared exactly as described in Callegari et al. (2022) and paired-end 150 bp reads generated on a NextSeq 500 sequencer (Illumina). The sequencing reads from the single-cell transcriptome were mapped to immunoglobulin genes using a custom R script (Callegari et al., 2022), the packages Shortread (Morgan et al., 2009) and Biostrings, EZassembler (Masoudi-Nejad et al., 2006) and IgBLAST (https://www.ncbi.nlm.nih.gov/igblast/) to determine the V(D)J gene usage.

Cloning and production of recombinant antibodies

According to the deduced heavy and light chain sequences, two primer pairs were designed to amplify the immunoglobulin genes from the single cell cDNA used for sequencing. The primers targeted the 5' non-coding region of the V gene and the 3' non-coding region adjacent to the constant region and included a tag sequence for ligation independent cloning. After amplification and purification of the heavy and light chain using the Phusion polymerase (NEB, M0530S) and following the protocol provided by the manufacturer, single stranded overhangs were generated by the exonuclease activity of the T4 polymerase (NEB, M0203S). The pVITRO-hygro dual expression plasmid with the two enzymatic restriction sites, SwaI and AflII, (pVitro2LIC) for cloning the heavy and the light chain into the MSC1 and MSC2 sites was digested and likewise treated with the T4 polymerase to create complementary single stranded overhangs. Stellar Competent Cells (Takara, 636763) were transformed with the annealed but nicked expression plasmid and after replication the plasmid was purified for transfection into HEK cells. The JetPrime transfection reagent (Polyplus) was used according to the manufacturer's instructions to transfect adherent HEK cells cultured in 6-well plates with the pVitro2LIC containing both the heavy and light chain of the recombinant antibody. After 48h the cell supernatant was harvested, centrifuged at 2000g for 3 min and 1.5 ml collected for storage at -20°C.

Class switch of recombinant IgM to IgG

To achieve an immunoglobulin class switch from IgM to IgG without altering the binding specificity we fused the variable region of the mu heavy chain to a gamma 1 constant region as described in Callegari et al (2022). In this two-step process, we first amplified the variable region from the pVitro2LIC expression plasmid with a stable forward primer that targets the plasmid backbone and can therefore be used for any sequence cloned into the same MCS site. The reverse primer was designed to target the last 19 bases on the 3' end of the variable region J gene and comprised an additional tag which is complementary to the first 24 bases on the 5' end of the gamma 1 constant region. The gamma region of the IgG_1 was amplified in a similar fashion, as the antibody was previously cloned into pVitro2LIC as well. Utilizing a reverse primer binding to the backbone of the expression plasmid and a forward primer targeting the first 19 bases of the gamma 1 constant region we produced the second half of the class switched immunoglobulin sequence. In the second step the two products were fused with two outside primers matching the plasmid backbone and incorporating the tag sequence for LIC cloning as described above. The fused product was purified with the Marcherey Nagel Gel and PCR cleanup kit (740609), digested with the exonuclease activity of the T4 polymerase und cloned into pVitro2LIC that already contained the light chain gene sequence used for IgM synthesis. The final plasmid was transfected into adherent HEK cells and the supernatant harvested as outlined before.

ELISA quantification of IgM in HEK cell culture supernatant

For the assessment of the antibody concentration in the supernatant of transiently transfected HEK cells, 384-well plates were coated with goat anti-human IgM (Southern Biotec, 2023-01) antibody diluted to a final concentration of 1 µg/ml in PBS and kept at 4°C overnight. On the following day the plates were washed once with PBS, blocked with PBS- 1% BSA for 90 min at room temperature and washed another three times with PBS containing 0.05% Tween before being used for the incubation with 15 µl of serially diluted supernatant. After 2h of incubation at room temperature, the plate was washed three times with PBS 0.05% Tween, incubated again for 1h at room temperature with goat anti-human IgM-HRP (Southern Biotec, 2023-05) diluted to a final concentration of 1 µg/ml in PBS-0.1% BSA. Prior to the development the plate was washed another three times, then incubated with TBM ELISA substrate (SureBlue Reserve TBM Microwell Peroxidase Substrate, 53-00-00) for approximately 5 minutes at room temperature until a blue color shift became visible. The reaction was terminated with sulfuric

acid and the plate acquired immediately afterwards on an ELISA microplate reader (Agilent BioTek Synergy H1) at 450 nm.

Live-cell flow cytometry assay for AChR-specific binding, rat cross-reactivity and complement activation

Adherent HEK cells were transfected with all four AChR subunits, including the α-subunit fused with GFP, one day before being used for the live-cell flow cytometry assay. To test the rat cross-reactivity HEK were instead transfected with the orthologous rat AChR subunits, of which none is conjugated with a fluorophore and thus detection of AChR expression was measured through the binding of a separate rat AChR-specific antibody. A total of 80.000 transfected HEK cells and 20.000 coated polybead carboxylate microspheres diluted in 40 µl of PBS or complete DMEM were seeded in a U-bottom 96-well plate. For the AChR-specific binding serial dilutions of the supernatant were added to single wells and incubated for 30 min on ice. After three washing steps with PBS a secondary goat anti-human IgM conjugated with AF647 (109-605-129, JIR) was used in a 1:400 dilution to label bound antibody. Following a 30-minute incubation on ice, the cells were washed twice with PBS, fixed with 4% PFA in PBS and acquired on a Beckman Coulter Cytoflex flow cytometer equipped with a 96-well plate reader. The same protocol was used for the analysis of cross-reactivity to the rat AChR with the addition of mAb35 (BE0123, BioxCell), a rat IgG_1 with high specificity to human and rat AChR. This primary antibody was applied as control condition and labelled with an AF647-conjugated goat anti-rat IgG (112-605-003, JIR) at a 1:200 dilution. To assess in vitro complement activation dependent on antibody binding to the AChR, transfected HEK cells in complete DMEM were mixed with serial antibody dilutions and human serum as source of complement. The human serum was applied in a 1:20 dilution and the mix of antibody, cells and serum incubated for 2h at 37°C and 5% carbon dioxide. After three washing steps with PBS the complement activation was measured on cells with and without AChR-expression by labelling C3 complement component deposits with a mouse monoclonal anti-complement C3/C3b/iC3b antibody (846402, BioLegend). Following a 30-minute incubation on ice and another three repeated washing steps with PBS, the secondary antibodies RRX goat anti-mouse IgG (115-295-166, JIR) and AF647 goat anti-human IgM (109-605-129, JIR) were used for labelling. After the final incubation for 30 min on ice and two wash steps with PBS the cells were fixed with 4%PFA-PBS and measured on a Cytoflex flow cytometer (Beckman Coulter). The acquired data of each experimental run was stored as .fcs file and analyzed via FlowJo (Becton Dickinson).

Complement inhibitor and passive transfer myasthenia gravis in Lewis rats

The experimental protocols and procedures including live animals were reviewed and permitted by the cantonal animal research commission. Four-week-old female Lewis rats obtained from JanvierLabs were trained on the rotarod and their weight measured every 12h for 3 days to establish a baseline and minimize differences in performance due to the normal learning curve. The animals received only one intraperitoneal injection under isoflurane anesthesia that contained of PBS, human monoclonal antibody or rat monoclonal antibody with the addition of either a rat IgG_1 isotype control (BP0290, TNP6A7, BioXCell) or a C5 complement inhibitor (TPP-903, generously provided by Alexion Pharmaceuticals). The human antibody was represented by a combination of 1J7 and 6J2_IgG_1, 2 mg/kg of each antibody amounting to a total of 4 mg/kg per rat; mAb35, the rat AChR-specific antibody was administered in a final concentration of 3 mg/kg and 20 mg/kg of the isotype control or the C5 inhibitor were added respectively. In summary six different groups of animals, with 4 rats per condition were injected and the behavioral endpoint defined by weight loss, clinical healthy score and rotarod performance assessed every 12h. Each animal was scored according to the guidelines for pre-clinical assessment of anti-AChR antibody induced MG as delineated by Kusner et al. (2015) and Makino et al. (2017). The clinical health score was determined on a scale from 0 to 4, with 0. representing a healthy animal with no signs of weakness and 4. imminent death. If a clinical score of 3 with severe muscle weakness, hindlimb paralysis and moribund was reached, the animals were euthanized. All animals were sacrificed 24h after the injection by transcardial perfusion fixation with 4% PFA-PBS. Subsequently the gastrocnemius and soleus muscles of the hind limbs as well as the diaphragm were isolated and fixed in 4% PFA at 4°C until further analysis.

Immunofluorescence labelling of rat gastrocnemius muscle cryosections and image analysis

The rat gastrocnemius muscle stored in 4% PFA was cryoprotected by increasing concentrations of sucrose solution, starting with 10%, 20% and 30% of sucrose in PBS. The muscles were incubated for at least 6 hours in each sucrose-PBS solution before embedding in OCT (CellPath) and snap-freezing on dry ice. Cryosections with a thickness of 30 µm were cut on a Leica cryostat and affixed on Superfrost Plus Adhesion Microscope Slides (J1800AMNZ, Epredia). The sections were stored at -80°C until utilized for immunofluorescence labelling. Frozen tissue sections were thawed at room temperature for 10 min, washed once for 10 min with PBS and incubated in 0.1 M glycine solution in PBS for 10 min at room temperature. Afterwards the cryosections were treated with 80% ice cold (-20°C) methanol in PBS for 10

min, washed once more with PBS for another 10 min and blocked with a solution containing 1% FCS, 3% BSA and 0.3% Triton X-100 in PBS for 1 h. The same solution was used for the dilution of the primary antibodies, which included a mouse anti-rat IgG to label C3 complement deposition (NBP1-05140, Novus Biologicals) and rabbit anti-rat IgG against SV2A (NBP1-82964, Novus Biologicals) to label pre-synaptic vesicles. The antibodies were diluted in a final concentration of 1 µg/ml and 0.3 µg/ml, respectively and the slides incubated for 16 h overnight in a humidifying chamber at 4°C. On the following day the sections were washed three times with PBS for 10 min each and labelled with RRX-conjugated goat anti-mouse IgG (115–295-166, JIR), goat anti-rabbit IgG conjugated with AF488 (111-545-144, JIR) or alternatively goat anti-human IgG conjugated with FITC (109-096-098, JIR) all diluted to a final concentration of 4 µg/ml. Additionally, α-BTX conjugated with AF647 (B35450, ThermoFisher) with a concentration of 1 µg/ml was added to the antibodies diluted in blocking solution and the sections were incubated again for 16 h at 4 °C in a humidifying chamber. On the next day, the labelling protocol included a washing step with PBS, followed by a brief incubation in PBS-containing 1 µg/ml DAPI and a final washing step with PBS before the sections were mounted with Fluoromount-G and sealed with a coverslip. Images of the rat gastrocnemius muscle cryosections were acquired on a Nikon Eclipse TI2 equipped with a 20 ×, 0.75 NA air objective for analysis of the AChR content at the NMJ. Representative images of structural alterations of the NMJ were acquired with a Nikon A1R scanning confocal microscope with a 60 ×, 1.4 NA OI objective using voxel dimensions set to Nyquist sampling.

The image analysis was performed with the Fiji software based on ImageJ2 and a custom script described in Rose et al. (2022). In brief, five images of three different gastrocnemius cryosections were acquired per muscle for each animal and used for image analysis. The SV2A signal was employed to identify the NMJ and to define an area in which the AChR content was analyzed. The α-BTX fluorescence signal was measured according to the SV2A mask and normalized by calculating a ratio to the co-localizing SV2A fluorescence signal. For the analysis of complement activation, the fluorescence signal intensity of C3 depositions co-localizing at the NMJ were also measured with the help of the SV2A mask. The same mask was used for the analysis of both labels and a minimum of 100 NMJ were examined for each injected animal.

Statistics

The applied statistical tests are described in the figure legends. Generally, GraphPad Prism was used to perform statistical analysis, including a priori tests for normal distribution with the

Normality and Lognormality test. The quantification of the AChR content as determined by the α-BTX ratio and the C3 deposition at the NMJ were compared using a One-Way ANOVA with a multiple comparison corrected according to Tukey. The correlation between measured antibody characteristics such as specific binding strength, C3 deposition, rat AChR cross-reactivity and number of hypermutations was determined using the Spearman's rank correlation coefficients and the p values were calculated by a two-tailed permutation test.

Results

Inhibition of the terminal complement pathway prevents in vivo pathogenicity of anti-AChR antibody combinations with synergistic subunit-specificity

The discovery of in vivo pathogenicity mediated by a combination of anti-AChR antibodies with differing subunit-specificities raised the question of how myasthenic symptoms are induced in animals and what underlying mechanism is driving the pathology. We observed enhanced complement activation in vitro by antibody combinations, however, the causal relationship between complement activation and myasthenic symptoms in the passive transfer myasthenia gravis animal model remained unclear. The experimental setup reported in Rose et al. (2022) did not account for alternative pathomechanisms, such as antigenic modulation and direct receptor blockade, that could also be enhanced by antibody combinations. We therefore compared the in vivo pathogenicity of an antibody combination alone or co-administered with a complement C5 inhibitor to block the lytic pathway of the complement system. We chose the combination of 1J7 and 6J2 expressed as IgG_1 that has been shown to activate complement and cause disease symptoms in live rats (Rose et al., 2022) and included mAb35, a well-established and highly pathogenic rat anti-AChR antibody as positive and PBS as negative control. Animals injected with pathogenic antibodies and co-administered with an isotype control presented severe signs of muscle weakness and a significant increase in clinical scores after 24 h. These animals showed a dramatic decrement in rotarod performance already by 12 h after injection, whereas rats supplemented with the C5 complement inhibitor remained healthy and performed equal to animals of the control groups (Fig.1 a, b). To examine the condition of the NMJ and to verify the injection regiment we collected blood and isolated the gastrocnemius muscle from the hind limb of each rat. One animal injected with the isotype control in addition to mAb35 was excluded from the analysis, since serum IgG binding to AChR-expressing cells was found to be negative (Supplementary figure S.1). For the histological analysis of gastrocnemius muscle cryosections we labeled the AChR with AF647-conjugated α-BTX and

used antibodies against the synaptic vesicle glycoprotein 2A (SV2A) to visualize the pre-synaptic membrane. In addition, the cryosections were immunolabeled for C3 complement deposition (Fig.1 c). The SV2A labeling was used to delineate the NMJ and provided a reference for calculating the ratio of the fluorescence intensity signals. The analysis revealed a significant loss of AChR content at the NMJ in rats injected with the antibody combination or mAb35 and in conjunction with the isotype control compared to the vehicle control or animals treated with the complement inhibitor (Fig.1 d).

Examination over the course of 24 h is well-suited as primary end point for the behavioral analysis but inapt for the histological evaluation of complement activation as NMJ are already severely degraded and complement deposits mostly removed. Nevertheless, we decided to analyze C3 complement deposition by measuring the fluorescence intensity at the endplates. Animals with behavioral deficits and loss of AChR content showed only a minor increase of C3 labeling compared to the vehicle control. However, both animal cohorts that received pathogenic antibodies and the complement inhibitor showed a significant increase of complement deposition at the NMJ (Fig.1 d). The simultaneous labelling of gastrocnemius muscle cryosections with human IgG in addition to α-BTX and immunolabeling for C3 confirmed a co-localization of all three markers on the post-synaptic membrane and demonstrated no loss of structural integrity for animals co-administered with the C5 complement inhibitor (Fig.1 e).

Different AChR-subunit specificities of antibody combinations represent a key parameter for effective complement activation

In our previous work, we established that combinations of antibodies enhance C3 deposition when measured by an in vitro complement activation assay (Rose et al., 2022). The highest effect size was observed when a single activating antibody was combined with a second one that recognized a different AChR-subunit, as in the case of B12L and 2M18 (Fig.2 a). Subunit specificity appeared to be more important than the IgG subclass, as the combination of B12L with any β-subunit targeting IgG_4 showed stronger enhancement of complement activation than the combination with for example 1J7, an IgG_1 antibody targeting the α-subunit of the AChR. Although the concentration of the single complement-fixing IgG_1 was cut in half when combined with the IgG_4, the measured C3 deposition more than doubled. However, the synergistic effect of IgG_4 antibodies was not observed for combinations in which none of the two antibodies targeted the α-subunit, illustrated by the combination of 5H10 and 6J2 (Fig.2 d). When expressed in its native version, 6J2 is of the IgG_4 subclass, which did not activate

complement individually or in combination with 5H10. Yet, when expressed as IgG_1 a profound complement activation was mediated by the combination (Fig.2 a).

The relative binding strength of the individual anti-AChR IgG antibodies had no impact on complement activation of antibody combinations. The antibody concentration needed for half maximum binding as measured by live-cell flow cytometry and determined with a 4PL dose-response curve was used as approximate indicator of affinity (Fig.2 b). According to these results, 6J2 displayed a 10-fold higher affinity than 5H10, yet the combination of B12L and 5H10 generated twice as much C3 complement deposition than the combination of B12L and 6J2. Even substituting the IgG_4 subclass with IgG_1 was not sufficient to propel the synergistic effect to the level of 5H10 and B12L (Fig.2 a, b). As the example of 3I3 and 6J2 IgG_1 illustrated, even for antibodies with the same AChR-subunit specificity, the calculated affinity did not represent a reliable indicator for the enhancement of complement activation when used in combinations.

Accordingly, no correlation was identified between the relative binding strength and complement activation (Fig.2 c). There was likewise no significant correlation between the number of amino acid changes due to somatic hypermutations and the affinity as represented by the relative binding strength. The only significant correlation was identified for complement activation and amino acid substitutions, however it has to be noted that both antibodies with the highest values for amino acid replacements and complement activation target the α-subunit.

Competing hypothetical models predict how the structural relationship between the AChR and the antibody subunit specificity amplifies complement activation

The synergistic relationship between an α-subunit targeting IgG_1 antibody and an IgG_4 antibody with a different subunit specificity provided strong evidence for a yet unidentified mechanism that enhances complement activation. We constructed three competing hypotheses that predict different outcomes for complement activation, depending on the manipulated parameters of the experimental approach and varying antibody properties (Fig.3 a, b). The density hypothesis describes a reductionistic concept, in which the local density of antibodies on individual AChR is the main determining factor for complement activation. The maximum density of an antibody against the α-subunit is twice as high for a single AChR and additional antibodies against single, differing subunits facilitate an additive, linear increase of complement activation. The antigen array hypothesis represents the assumption, that combinations of antibodies lock AChR into an extensive interlinked platform, stabilizing the location and orientation of individual AChR and thereby manipulating the antibody on/off rate.

According to this concept, bivalent antibody binding provides an essential characteristic of anti-AChR antibodies for complement activation and while antibodies against single AChR-subunits only cross-link two receptors into dimers, α-subunit targeting antibodies already connect receptors into higher level structures. This effect is further potentiated by antibody combinations with distinct subunit specificities. The hexamer hypothesis is based on published results in the field of complement research that reported a hexameric model as most effective configuration of IgG molecules for the activation of the complement system (Diebolder et al., 2014). IgG assembled in a cartwheel shape, akin to the structure of an IgM, provide the ideal spatial configuration for the binding of C1q and the activation of the associated C1r and C1s zymogens. In the context of the AChR, the synergistic effect of combinations could be facilitated by anti-α-subunit antibodies that generate and stabilize the ring structure whereas antibodies against a single subunit form the inner spokes of the wheel and mediate binding to C1q.

From these three hypotheses, different predictions were deduced for changes in complement activation, following the addition of a secondary antibody with particular properties to an already present anti-α targeting IgG_1 antibody. The according prediction of each hypothesis with the different experimental approaches to test parameters such as varying IgG subclasses, functionally monovalent antibodies, or multiple antibodies with distinct subunit specificities are summarized in Fig.3 b. An insightful experimental approach to validate the hexamer hypothesis represented the investigation of complement activation caused by an anti-AChR IgM antibodies (Fig.3 a). This immunoglobulin class represented the ideal structural conformation, was thought to be the most proficient antibody class in terms of complement activation and yielded clear differences in the various predictions of the three competing hypotheses. The antibody density hypothesis postulated that adding an IgG to an IgM provides little benefit for complement activation because IgM have a higher dose-response and single IgM antibody molecules can already bind C1q efficiently. The antigen array hypothesis predicts a strong synergy between IgG and IgM antibodies and a maximum effect size for combinations with an IgM antibody, as avidity should relate to a high degree of receptor cross-linking. Conversely, the hexamer hypothesis does not predict a combination effect between IgM and an additional IgG, as IgM already provide the necessary structural substrate and simply binding to the AChR is required for efficient complement activation.

Isolation of anti-AChR IgM B cells from myasthenia gravis patients and healthy donors

Patients with MG have no detectable AChR-targeting IgM antibodies in the circulation, nevertheless, with the help of the membrane antigen capture activated cell sorting (MACACS) method we managed to isolate AChR-specific, IgM B cells from patients and healthy donors. This suit of methods exploits the B cells capacity to recognize and capture their cognate antigen, throughout which the B cells become transiently attached to the antigen-expressing cell surface. Thus, antigen-specific B cells are enriched and the subsequent activation marker in combination with the internalized fluorescently labeled membrane-antigen are used for fluorescence activated cell sorting. By screening PBMC samples with the MACACS method and consecutive sequencing and cloning of the cDNA, we produced 18 IgM antibodies, half of them derived from MG patients and the other half from healthy donors (Table 1). Each donor set included somatically hypermutated and germline IgM, as well as members of one expanded clone from the same donor according to the VDJ gene usage analysis.

The production and purification of IgM antibodies remains a major challenge due to the lack of efficient and cost-effective methods. In this preliminary study, we used a ligation independent cloning system to synthesize both the heavy and light chain from a single expression vector, which was transfected into adherent HEK cells. The antibody concentration in the harvested supernatant was determined via ELISA to ensure comparable conditions for ensuing in vitro experiments (Table 1, Supplementary figure S.2). Aside from two preparations that yielded less than 1000 ng/ml and two with more than 4000 ng/ml, all IgM concentrations ranged around the average of 2360 ng/ml. Following the recombinant antibody production, the two hypermutated IgM 1H11 and 2E16 showed no binding to cells expressing the AChR and were consequently excluded from experimental testing and statistical analyses.

AChR-specific IgM antibodies have limited capacity for complement activation

The discovery of naturally occurring AChR-specific, IgM B cells enabled us to test the predictions of the three hypotheses on complement activation by IgM antibodies without having to engineer them artificially. In the framework of this preliminary study, we used transient transfection of adherent HEK cells with the IgM-expressing plasmid to produce sufficient amounts of antibodies for subsequent experimental studies. First, we verified the antibody class and tested the AChR-specific binding with a live-cell flow cytometry assay that involved AChR-GFP expressing target cells and a fluorophore-conjugated secondary antibody against human IgM (Fig.4 a). The quantification of the AChR-specific binding by measuring the fluorescence intensity and calculating the GMFI ratio to cells without AChR-expression

depicted a range of different binding strengths (Fig.4 c). Considering the mutational load of the examined IgM, it appeared that antibodies with an accumulation of somatic hypermutations and amino acid changes presented higher binding strength, particularly in the cohort of IgM from healthy donors (Fig.4 b, c). However, it has to be noted that three of the four hypermutated IgM of the healthy donors are clonally related. In general, a similar number of hypermutations was found in IgM antibodies of the two donor groups, which ultimately did not indicate a tendency towards higher affinity depending on amino acid changes or the health status of the donor (Fig.4 b, Fig.5 a). In fact, the antibody with the intermediate mutational load of the three clonally related 1M9, 6G21 and 3O14 showed the highest GMFI ratio (Fig.4 b, c). And in the case of MG patient-derived IgM, the two antibodies with the most hypermutations ranked among the IgM with the weakest AChR-specific binding strength.

In summary, we could show that IgM antibodies specifically bind to the AChR, and therefore turned our attention to the effector functions of the IgM. According to literature, IgM represent the most proficient antibody class for complement activation (Goldberg et al., 2020; Oskam et al., 2022), hence we tested all monoclonal IgM for their efficacy in our in vitro complement activation assay (Fig.4 d). Most IgM did not mediate C3 deposition on AChR-expressing cells and even the most potent complement activators were merely as viable as the IgG control 1J7. The two patient-derived IgM, 5K16 and 1H7, generated such levels of complement activation, but only 1H7 comprised somatic hypermutations and both displayed a rather mediocre AChR-binding activity (Fig.4 c, d). None of the IgM with the greatest AChR-specific binding, such as 6G21 and 3O14 from the healthy donor pool or 3N17 from the MG-derived antibody panel, initiated the complement cascade. Even though 1M9 showed strong antigen-specific binding and contained the same heavy chain constant sequence as 5K16, it was incapable of inducing complement activation (Fig.4 d, Supplementary figure S.3). Further statistical analysis concluded that neither the total specific antibody binding nor the extent of somatic hypermutations demonstrated a significant indicator for complement activation (Fig.4 d, Fig.5 a). As a consequence of these unexpected results and in view of the clinical picture of MG showing only AChR-specific IgG antibodies, which are therefore considered to be the pathogenic antibody class, we decided to class switch the IgM to IgG and investigate complement activation again. To class switch the antibody while maintaining the epitope specificity of the original IgM, we kept the same light chain but fused the variable region of the mu heavy chain with the gamma constant region of an IgG_1. However, after cloning and expressing the class-switched IgG, most antibodies lost their binding activity completely, and only four IgG maintained the ability to bind specifically to AChR-expressing cells (Table 1,

Fig.4 e). The best results were produced by the class-switched 1H7, a hypermutated, patient-derived antibody that also mediated complement activation as IgM and exhibited average AChR-binding.

Despite the missing information about the subunit specificity, we started to test combinations of IgM for a synergistic effect on complement activation (Fig.4 f). Consistent with the previous results, single IgM activated complement to a low degree but none of the combinations provided a substantial enhancement that exceeded the addition of both individual results with higher antibody dilution. Conversely, no detrimental effect of competition from the IgM with weaker complement activation was detected for the selected combinations. Finally, we investigated the rat cross-reactivity of the IgM, since PTMG animal models are still the most reliable experimental approach to determine the pathogenicity of a given antibody. HEK cells were transfected with the orthologous rat AChR subunits, antibody binding was detected with fluorescently labeled secondary antibodies against human IgM and the results acquired via flow cytometry. Five IgM, four of which were patient-derived, recognized the rat AChR and none of these species cross-reactive antibodies contained somatic hypermutations that entailed amino acid replacements (Table 1). The tested IgM antibodies displayed heterogenous characteristics, which is reflected by the absence of significant correlations between pairs of variables, including the number of somatic hypermutations, complement activation, specific AChR-binding and rat AChR cross-reactivity (Fig.5 a).

Discussion

The application of the complement C5 inhibitor demonstrated a cause-and-effect linkage between in vivo pathogenicity of the antibody combination and complement activity as principal mechanism for the development of myasthenic symptoms. We found that the pathogenicity mediated by the rat anti-AChR antibody mAb35 was similarly dependent on complement activation, which is in direct contrast to past studies. It was reported that $F(ab)_2$ fragments of mAb35 still induce muscle weakness through antigenic modulation in a PTMG rat model, as antibody fragments without the Fc region lose the ability to activate the complement system but retain the capacity to cross-link receptors (Loutrari et al., 1992). Nevertheless, we were confronted with the question of how to reconcile the two observations, that (1) antibody combinations with synergistic subunit specificity but also (2) single antibodies, such as mAb35 or B12L promote myasthenic pathology through complement activation (Chamberlain-Banoub et al., 2006; Kordas et al., 2015; Makino et al., 2017).

Common features of single pathogenic antibodies are the α-subunit specificity and the IgG_1 subclass (van der Neut Kolfschoten et al., 2007; Makino et al., 2017; Rose et al., 2022; Pham et al., 2023). The potency of anti-α antibodies corresponded to the concept of the main immunogenic region, a short amino acid sequence of the extracellular α-subunit domain and to which a particular pathogenic significance has been attributed (Tzartos et al., 1982; Tzartos et al., 1988). This notion is widely represented in literature, yet not without challenge, since most antibodies recognize conformational epitopes on the AChR which makes precise mapping hardly feasible. Additionally, the main immunogenic region provides no mechanistic basis to explain an improved pathogenicity by antibody combinations. This phenomenon was observed in experimental autoimmune myasthenia gravis animal experiments in which disease symptoms were induced by immunization with a single AChR subunit and compared to a combination of α and β AChR-subunits (Lazaridis et al., 2017). By investigating monoclonal, patient-derived autoantibodies, we could show that combinations provide increased complement activation depending on different AChR-subunit specificities (Rose et al., 2022). These results were confirmed by a recent study from the group of Kevin O'Connor that reported a similar increase in effectiveness for antibody combinations and the significance of targeting distinct AChR-subunits (Pham et al., 2023).

The antibody density and the antigen array hypothesis incorporate a rational for an elevated potential of anti-α antibodies, either by doubling the number of bound antibodies which increases the local density or through the improved capacity to cross-link receptors and stabilize the spatial structure. The main objective of the three competing hypotheses, however, was to unravel the fundamental mechanism of the combination effect by assigning different priorities to parameters such as affinity, antibody class and antigen distribution, which influence complement activation. We found that the relative binding strength of individual anti-AChR antibodies lose their significance when used in combination, arguing that the underlying mechanism has an impact on affinity. Furthermore, the amplification of C3 complement depositions by adding a complement inhibiting IgG_4 is inconsistent with the density and hexamer hypothesis but well aligned with the antigen array model. The additional cross-linking of the AChR by an IgG_4 antibody improved complement activation and even out-competed decreasing antibody concentrations of the complement fixing IgG_1 it was paired with. However, the consistency of this observation needs to be reviewed, as 1J7 hardly benefited from the addition of an IgG_4. In this context, the affinity of the α-subunit targeting IgG_1 antibody might be important, as relative binding strength reflects the main difference between

1J7 and B12L.

The impact of a specific antigen arrangement on the cell membrane has been described, for example, in connection with the pathogenicity of neuromyelitis optica. Autoantibodies against the water-channel aquaporin-4 (AQP4) require the expression of a certain isotype, called M23-AQP4, which allows the formation of orthogonal arrays of particles (OPA) from individual tetrameric water-channels to induce complement-dependent cytotoxicity (Soltys et al., 2017). Even though the competing isoform M1-AQP4 forms similar homotetramers, their even distribution on the cell membrane prevents autoantibody-mediated complement activation. The aggregation of OAP was thought to enable multimeric IgG binding, stabilized by Fc-Fc interactions which ultimately form a hexameric structure for optimal C1q binding (Phuan et al., 2012). The notion of IgG hexamerization represents the predominant model for complement activation and is supported by multiple studies investigating IgG assembly on antigen-incorporated lipid bilayers or complement activation by engineered multimeric IgG constructs (Wang et al., 2016; Ugurlar et al, 2018; Strasser et al., 2019; Yanaka et al., 2019; Sopp et al., 2021). Under physiological conditions, the supremacy of hexameric IgM for complement activation compared to pentameric IgM or single IgG is well established and generated an intuitive connection with the model described by Diebolder et al. (2014) (Oskam et al., 2022). Monovalent binding of individual IgG is a crucial feature of this hexameric model, whereby the C-termini of the Fc regions form a central hub, while the Fab arms compose the rim (Diebolder et al., 2014). However, this structural arrangement is difficult to reconcile with the pathology of different diseases, including MG where receptor cross-linking is considered one of three main pathomechanisms (Gilhus et al., 2019; Iorio 2024). Super high resolution imaging analysis of the immune complex in neuromyelitis optica indicated that the geometry of AQP4 epitopes in congregated OAP might restrict the number of interacting IgG for C1q binding. Therefore, tetramers of bivalently bound IgG with favorable Fc modifications already led to a pathogenic degree of complement activation (Soltys et al., 2019). Rougé and colleagues (2020) employed electron microscopy approaches to investigate the immune complex of the integral membrane protein cluster of differentiation 20 (CD20) and rituximab, a monoclonal antibody used for the depletion of CD20-expressing B-cells. They elegantly showed that rituximab and CD20 form a closed ring structure consisting of three molecules each, which led to C1q binding and complement-dependent cytotoxicity. This trimer formation resulted from two identical but intricate epitopes at the CD20 protein, which require a specific binding angle to prevent steric interference and favor bivalent antibody binding between three CD20 molecules (Rougé et al., 2020). Both studies are supported by the research from Shaw et al.

(2019), who used DNA origami nanostructures on surface plasmon resonance chips to empirically measure the binding dynamics of bivalent IgG antibodies. Their study concluded, that unless the antigenic epitopes are separated by more than 16 nm or less than 3 nm, the binding modality will be dominated by bivalent configurations. In the example of six nearby antigens, three bivalent bound IgG antibodies were observed most frequently, whereas binding of six monovalent IgG was practically absent (Shaw et al., 2019).

In the present study we expressed AChR-specific IgM, derived from B cells of MG patients and healthy donors to investigate complement activation. According to the hexamer hypothesis the binding strength should reflect the main determinant for complement activation by IgM, as single molecules already provide the necessary structural requirements for C1q binding. However, most IgM did not trigger the complement system despite strong AChR-specific binding, accumulation of somatic hypermutations and in some cases a shared heavy chain constant region with complement fixing IgM. These results raised questions about the significance of the hexameric structure and the general mechanism that facilitates complement activation by IgM antibodies. The C1q binding site on the constant region of an antigen-free IgM has been reported to be inaccessible (Perkins et al., 1991; Taylor et al., 1994). Upon binding of the IgM Fab arms to an antigenic surface with an out-of-plane angle of at least 40° the steric hindrance gets resolved and C1q binding may commence (Czajkowsky et al., 2009; Chen et al., 2022). Therefore, the AChR-subunit specificity and in particular the epitope location might prevent complement activation by enabling IgM binding in a planar conformation. In comparison to IgG, other mechanisms appear to be decisive for IgM-mediated complement activation, e.g., a lack of affinity can be compensated by the given avidity, there are no different subclasses, but the distance to the cell surface and the spatial conformation of a single molecule are impactful parameters (Sharp et al., 2019; Chen et al., 2022).

One limitation of the current study is the missing knowledge about the subunit specificity of the IgM. This information will be crucial for testing the combinations of antibodies and evaluating the experimental results at hand. Irrespective of this constraint, the discovery of AChR-binding but complement deficient IgM provides an unexpected opportunity to validate the three proposed hypotheses. The antibody density and hexamer model predict no enhancement of complement activation by combining an α-subunit targeting IgG_1 with an IgM of different subunit specificity and no capacity for complement activation. Still, such IgM should facilitate receptor cross-linking, thereby stabilizing an extensive AChR platform which improves complement activation if the antigen array hypothesis holds true. According to the

results collected so far, the antigen array hypothesis is the most suitable model to explain the increased complement activation by antibody combinations in MG and it is conceivable that the proposed mechanism is relevant in other disease paradigms or for the design of therapeutic interventions.

References

Chamberlain-Banoub J, Neal JW, Mizuno M, Harris CL, Morgan BP. Complement membrane attack is required for endplate damage and clinical disease in passive experimental myasthenia gravis in Lewis rats. Clin Exp Immunol. 2006;146(2):278-286. doi:10.1111/j.1365-2249.2006.03198.x

Chen Q, Menon RP, Masino L, Tolar P, Rosenthal PB. Structural basis for Fc receptor recognition of immunoglobulin M. Nat Struct Mol Bio. 2022;30(7):1033-1039. doi.org/10.1038/s41467-022-34090-2

Callegari I, Schneider M, Berloffa G, et al. Potent neutralization by monoclonal human IgM against SARS-CoV-2 is impaired by class switch. EMBO Rep. 2022;23(7):e53956. doi:10.15252/embr.202153956

Crane JM, Tajima M, Verkman AS. Live-cell imaging of aquaporin-4 diffusion and interactions in orthogonal arrays of particles. Neuroscience. 2010;168(4):892-902. doi:10.1016/j.neuroscience.2009.08.034

Czajkowsky DM, Shao Z. The human IgM pentamer is a mushroom-shaped molecule with a flexural bias. Proc Natl Acad Sci U S A. 2009;106(35):14960-14965. doi:10.1073/pnas.0903805106

Dalakas MC, Alexopoulos H, Spaeth PJ. Complement in neurological disorders and emerging complement-targeted therapeutics. Nat Rev Neurol. 2020;16(11):601-617. doi:10.1038/s41582-020-0400-0

Diebolder CA, Beurskens FJ, de Jong RN, et al. Complement is activated by IgG hexamers assembled at the cell surface. Science. 2014;343(6176):1260-1263. doi:10.1126/science.1248943

Drachman DB, Angus CW, Adams RN, Michelson JD, Hoffman GJ. Myasthenic antibodies cross-link acetylcholine receptors to accelerate degradation. N Engl J Med. 1978;298(20):1116-1122. doi:10.1056/NEJM197805182982004

Gilhus NE, Tzartos S, Evoli A, Palace J, Burns TM, Verschuuren JJGM. Myasthenia gravis. Nat Rev Dis Primers. 2019 May 2;5(1):30. doi:10.1038/s41572-019-0079-y. PMID: 31048702.

Goldberg BS, Ackerman ME. Antibody-mediated complement activation in pathology and protection. Immunol Cell Biol. 2020;98(4):305-317. doi:10.1111/imcb.12324

Iorio R. Myasthenia gravis: the changing treatment landscape in the era of molecular therapies. Nat Rev Neurol. 2024;20(2):84-98. doi:10.1038/s41582-023-00916-w

Kordas G, Lagoumintzis G, Sideris S, Poulas K, Tzartos SJ. Direct proof of the in vivo pathogenic role of the AChR autoantibodies from myasthenia gravis patients. PLoS One. 2014;9(9):e108327. Published 2014 Sep 26. doi:10.1371/journal.pone.0108327

Kusner L.L., Kaminski H.J., Soltys J. Effect of complement and its regulation on myasthenia gravis pathogenesis. Expert Rev Clin Immunol. 2008 Jan;4(1):43-52. doi:10.1586/1744666X.4.1.43. PMID: 20477586.

Kusner LL, Losen M, Vincent A, et al. Guidelines for pre-clinical assessment of the acetylcholine receptor--specific passive transfer myasthenia gravis model-Recommendations for methods and experimental designs. Exp Neurol. 2015; 270:3-10. doi:10.1016/j.expneurol.2015.02.025

Lazaridis K, Baltatzidi V, Trakas N, Koutroumpi E, Karandreas N, Tzartos SJ. Characterization of a reproducible rat EAMG model induced with various human acetylcholine receptor domains. J Neuroimmunol. 2017;303:13-21. doi:10.1016/j.jneuroim.2016.12.011

Loutrari H, Kokla A, Tzartos SJ. Passive transfer of experimental myasthenia gravis via antigenic modulation of acetylcholine receptor. Eur J Immunol. 1992;22(9):2449-2452. doi:10.1002/eji.1830220939

Leite MI, Jacob S, Viegas S, et al. IgG1 antibodies to acetylcholine receptors in 'seronegative' myasthenia gravis. Brain. 2008;131(Pt 7):1940-1952. doi:10.1093/brain/awn092

Makino T, Nakamura R, Terakawa M, et al. Analysis of peripheral B cells and autoantibodies against the anti-nicotinic acetylcholine receptor derived from patients with myasthenia gravis using single-cell manipulation tools. PLoS One. 2017;12(10):e0185976. Published 2017 Oct 17. doi:10.1371/journal.pone.0185976

Masoudi-Nejad A, Tonomura K, Kawashima S, et al. EGassembler: online bioinformatics service for large-scale processing, clustering and assembling ESTs and genomic DNA fragments. Nucleic Acids Res. 2006;34(Web Server issue):W459-W462. doi:10.1093/nar/gkl066

Mastellos DC, Hajishengallis G, Lambris JD. A guide to complement biology, pathology and therapeutic opportunity. Nat Rev Immunol. 2024;24(2):118-141. doi:10.1038/s41577-023-00926-1

Morgan M, Anders S, Lawrence M, Aboyoun P, Pagès H, Gentleman R. ShortRead: a bioconductor package for input, quality assessment and exploration of high-throughput sequence data. Bioinformatics. 2009;25(19):2607-2608. doi:10.1093/bioinformatics/btp450

Oskam N, Ooijevaar-de Heer P, Derksen NIL, et al. At Critically Low Antigen Densities, IgM Hexamers Outcompete Both IgM Pentamers and IgG1 for Human Complement Deposition and Complement-Dependent Cytotoxicity. J Immunol. 2022;209(1):16-25. doi:10.4049/jimmunol.2101196

Perkins SJ, Nealis AS, Sutton BJ, Feinstein A. Solution structure of human and mouse immunoglobulin M by synchrotron X-ray scattering and molecular graphics modelling. A possible mechanism for complement activation. J Mol Biol. 1991;221(4):1345-1366. doi:10.1016/0022-2836(91)90937-2

Pham MC, Masi G, Patzina R, et al. Individual myasthenia gravis autoantibody clones can efficiently mediate multiple mechanisms of pathology. Acta Neuropathol. 2023;146(2):319-336. doi:10.1007/s00401-023-02603-y

Phuan PW, Ratelade J, Rossi A, Tradtrantip L, Verkman AS. Complement-dependent cytotoxicity in neuromyelitis optica requires aquaporin-4 protein assembly in orthogonal arrays. J Biol Chem. 2012;287(17):13829-13839. doi:10.1074/jbc.M112.344325

Rose N, Holdermann S, Callegari I, et al. Receptor clustering and pathogenic complement activation in myasthenia gravis depend on synergy between antibodies with multiple subunit specificities. Acta Neuropathol. 2022;144(5):1005-1025. doi:10.1007/s00401-022-02493-6

Rougé L, Chiang N, Steffek M, et al. Structure of CD20 in complex with the therapeutic monoclonal antibody rituximab. Science. 2020;367(6483):1224-1230. doi:10.1126/science.aaz9356

Sharp TH, Boyle AL, Diebolder CA, Kros A, Koster AJ, Gros P. Insights into IgM-mediated complement activation based on in situ structures of IgM-C1-C4b. Proc Natl Acad Sci U S A. 2019;116(24):11900-11905. doi:10.1073/pnas.1901841116

Shaw A, Hoffecker IT, Smyrlaki I, et al. Binding to nanopatterned antigens is dominated by the spatial tolerance of antibodies. Nat Nanotechnol. 2019;14(2):184-190. doi:10.1038/s41565-018-0336-3

Soltys JN, Meyer SA, Schumann H, Gibson EA, Restrepo D, Bennett JL. Determining the Spatial Relationship of Membrane-Bound Aquaporin-4 Autoantibodies by STED Nanoscopy. Biophys J. 2017;112(8):1692-1702. doi:10.1016/j.bpj.2017.03.012

Soltys J, Liu Y, Ritchie A, et al. Membrane assembly of aquaporin-4 autoantibodies regulates classical complement activation in neuromyelitis optica. J Clin Invest. 2019;129(5):2000-2013. Published 2019 Apr 8. doi:10.1172/JCI122942

Sopp JM, Peters SJ, Rowley TF, et al. On-target IgG hexamerisation driven by a C-terminal IgM tail-piece fusion variant confers augmented complement activation. Commun Biol. 2021;4(1):1031. Published 2021 Sep 2. doi:10.1038/s42003-021-02513-3

Strasser J, de Jong RN, Beurskens FJ, et al. Unraveling the Macromolecular Pathways of IgG Oligomerization and Complement Activation on Antigenic Surfaces. Nano Lett. 2019;19(7):4787-4796. doi:10.1021/acs.nanolett.9b02220

Taylor, B., Wright, J. F., Arya, S., Isenman, D. E., Shulman, M. J., & Painter, R. H. (1994). C1q binding properties of monomer and polymer forms of mouse IgM mu-chain variants. Pro544Gly and Pro434Ala. Journal of immunology (Baltimore, Md. : 1950), 153(11), 5303–5313.

Toyka, K. V., Brachman, D. B., Pestronk, A., & Kao, I. (1975). Myasthenia gravis: passive transfer from man to mouse. Science (New York, N.Y.), 190(4212), 397–399. https://doi.org/10.1126/science.1179220

Tzartos SJ, Seybold ME, Lindstrom JM. Specificities of antibodies to acetylcholine receptors in sera from myasthenia gravis patients measured by monoclonal antibodies. Proc Natl Acad Sci U S A. 1982;79(1):188-192. doi:10.1073/pnas.79.1.188

Tzartos SJ, Kokla A, Walgrave SL, Conti-Tronconi BM. Localization of the main immunogenic region of human muscle acetylcholine receptor to residues 67-76 of the alpha subunit. Proc Natl Acad Sci U S A. 1988;85(9):2899-2903. doi:10.1073/pnas.85.9.2899

Ugurlar D, Howes SC, de Kreuk BJ, et al. Structures of C1-IgG1 provide insights into how danger pattern recognition activates complement. Science. 2018;359(6377):794-797. doi:10.1126/science.aao4988

van der Neut Kolfschoten M, Schuurman J, Losen M, et al. Anti-inflammatory activity of human IgG4 antibodies by dynamic Fab arm exchange. Science. 2007;317(5844):1554-1557. doi:10.1126/science.1144603

Vincent, A., & Newsom-Davis, J. (1985). Acetylcholine receptor antibody as a diagnostic test for myasthenia gravis: results in 153 validated cases and 2967 diagnostic assays. Journal of neurology, neurosurgery, and psychiatry, 48(12), 1246–1252. https://doi.org/10.1136/jnnp.48.12.1246

Wang G, de Jong RN, van den Bremer ET, et al. Molecular Basis of Assembly and Activation of Complement Component C1 in Complex with Immunoglobulin G1 and Antigen. Mol Cell. 2016;63(1):135-145. doi:10.1016/j.molcel.2016.05.016

Yanaka S, Yogo R, Watanabe H, et al. On-Membrane Dynamic Interplay between Anti-GM1 IgG Antibodies and Complement Component C1q. Int J Mol Sci. 2019;21(1):147. Published 2019 Dec 24. doi:10.3390/ijms21010147

Zimmermann M, Rose N, Lindner JM, et al. Antigen Extraction and B Cell Activation Enable Identification of Rare Membrane Antigen Specific Human B Cells. Front Immunol. 2019;10:829. Published 2019 Apr 16. doi:10.3389/fimmu.2019.00829

Figure Legends

Fig.1: Impact of C5 complement inhibitor on pathogenicity in a PTMG rat model. The effect of the terminal complement pathway inhibition in animals injected with a combination of two patient-derived, AChR-specific, monoclonal antibodies was compared to the co-administration of an isotype control. A total of 24 female Lewis rats were injected with PBS, the combination of 2 mg/kg 1J7 and 2 mg/kg 6J2 IgG_1, or 3 mg/kg mAb35 and either with 20 mg/kg C5 complement inhibitor or 20 mg/kg isotype control (n=4 for each condition). **a** Depiction of clinical scores at 24 h after the injection, ranging between 0 – 3 (0 equals healthy and 4 equals death, as described in Rose et al. (2022)). The differences in health score were compared statistically using a Kruskal–Wallis test, followed by Dunn's multiple comparison (*p<0.0332). **b** Rotarod performance measured in a 12 h interval over the course of 24 h after injection and normalized to the baseline value. The time that an animal remained on the rotarod is presented as ratio to the baseline on the vertical axis and the time point of each measurement is shown on the horizontal axis. Each circle represents the mean of every animal tested per condition (n=4) and the bar depicts the standard error of mean. **c** Destruction of the NMJ dependent on the co-administration with the isotype control or complement inhibitor. Histology images of gastrocnemius muscle cryosections from rats whose health status and physical performance is depicted in a and b were sacrificed 24 h after injection and immunolabelled for SV2A (green), C3 complement component (magenta) and AChR content visualized via α-BTX labelling (red). The three images from top to bottom were acquired from cryosections of rats injected with PBS and C5 complement inhibitor, the combination of 1J7 and 6J2 IgG_1 with the isotype control and the combination of 1J7 and 6J2 IgG_1 with the C5 inhibitor. The scale bar shown in the bottom right image represents 10 µm. **d** Column scatter plot with bar to left depicting the relative abundance of AChR content at the NMJ according to the different injection regiments. Each dot represents a single NMJ measured for α-BTX fluorescence intensity and normalized to the co-localizing SV2A fluorescence intensity. The ratio is plotted along the x-axis and the values for all tested animals are grouped according to the label on the y-axis. Approximately 100 NMJs were analyzed per animal. The bar graph in the middle shows the mean values of the fluorescence signal ratio for each animal with an error bar for the standard deviation of the mean. The difference between each condition was compared using a One-Way ANOVA followed by a multiple comparison corrected according to Tukey (*p<0.0332, **p<0.0021, ***p<0.0002). The bar graph on the right displays C3 complement

deposition at the NMJ, measured by the fluorescence intensity of immunolabelled C3 with the mean summarized for each animal in a single dot. The error bar illustrates the standard deviation of the mean. The differences in complement activation analyzed by C3 deposition were statistically compared with a One-Way ANOVA and a multiple comparison corrected according to Tukey (*p<0.0332, **p<0.0021). **e** Representative confocal images of a gastrocnemius muscle cryosection from a rat injected with the combinations of antibodies and in addition the C5 complement inhibitor. The muscle cryosection was labelled with α-BTX (red) and immunolabelled for human IgG (cyan) and C3 (magenta) deposition at the NMJ.

Fig.2: Complement activation by anti-AChR specific, patient derived IgG with different antibody characteristics. **a** Heatmap adapted from Rose et al. (2022) comparing the C3 depositions measured in in vitro complement activation assays. Single antibodies and all possible combinations were assayed at 500 ng/ml in three independent experimental runs and the mean is displayed by each square. On the horizontal axis the subunit specificity is noted beneath the label of the tested antibody and the vertical axis includes the antibody subclasses. **b** Relative binding strength of monoclonal anti-AChR antibodies, calculated with the help of the depicted dose-response curve. A serial dilution of single antibodies was incubated with AChR-GFP transfected HEK cells and the geometric mean fluorescence intensity (GMFI) measured via flow cytometry. The ratio was calculated by dividing the GMFI of AChR-transfected cells by the immunofluorescence signal on non-transfected cells, depicted on the y-axis and the applied antibody concentration on the x-axis. A sigmoidal, four parameter logistic curve was fitted to the acquired dilution series for each antibody and the concentration for half maximal specific binding (EC50) calculated using GraphPad Prism. The according values are shown in the table. **c** Correlation between AChR-dependent complement activation, amino acid replacements and relative binding strength. The relationship of these three parameters was determined with the Spearman's rank correlation coefficients, indicated by the upper value in each square of the correlation matrix and the p values were calculated by a two-tailed permutation test, indicated by the lower number in each square (*p<0.0332). **d** Complement activation measured via C3 deposition on AChR-GFP expressing cells for two different concentrations of individual and combinations of monoclonal AChR-specific antibodies. The horizontal axis shows the total amount of antibody used, thus 1000 ng/ml of combination consists of 500 ng/ml of each single antibody. The vertical axis displays the GMFI ratio for complement C3 deposition.

Fig.3: Theoretical hypotheses explaining the enhanced complement activation by combinations of anti-AChR antibodies with differing subunit specificities. **a** Schematic depiction of the three competing hypotheses with different structural relationships between antibodies and AChR that influence C1q binding. The AChR is represented by pentamers, IgG by Y-shaped symbols, IgM by hexameric complexes of Y-shaped symbols and the differing subunit-specificities by alternative colors. The upper row illustrates the general concept of each hypothetical model for IgG combinations and the lower row for a combination of IgG and IgM. Note that the AChR contains two α subunits and only one each of the β, δ and ε, thus anti-α targeting antibodies can mediate a degree of complex formation, while antibodies against any other subunit only provides cross-linking between two AChR. **b** Table listing the different

predictions of the three hypotheses for complement activation depending on various experimental manipulations.

Fig.4: Characterization and complement activation of AChR-specific IgM derived from patients and healthy donors. **a** Live-cell flow cytometry assay of HEK cells expressing AChR-GFP incubated with supernatant harvested from IgM expressing cells. The first two IgM were derived from a healthy donor followed by three IgM from a MG patient. Declining dilutions of IgM were tested, starting with undiluted supernatant, 5 and 25 times diluted from top to bottom. The vertical axis depicts IgM binding detected with a secondary anti-human IgM antibody and the horizontal axis demonstrates AChR expression according to the fluorescence signal from the α-subunit which is fused with GFP. AChR-specific IgM display an elevated binding to the AChR-transfected cells on the far right of the gate, leading to an upward shift of the population. **b** Heatmap comparing the number of somatic hypermutations and resulting amino acid substitutions of the heavy and light chain variable region for each expressed IgM antibody. The mutational load of the different immunoglobulin variable regions was determined by aligning the gene sequences with their putative germline version using the IgBlast tool. The upper half of the displayed IgM ranging from 1M9 to 1H10 derived from healthy donors and the lower half from MG patients. **c** Bar graph summarizing the AChR-specific binding according to the GMFI ratio determined from live-cell flow cytometry assays using a 1:5 dilution of IgM supernatant. The GMFI, calculated as described before, is shown on the horizontal axis, red bars represent IgM from healthy donors and blue bars IgM from MG patients, PBS is included as negative control and 2M6, a patient-derived but commercially produced IgM as positive control. In both donor groups, the IgM are ordered from top to bottom according to the descending number of hypermutations. **d** Bar graph summarizing complement activation mediated by anti-AChR IgM in a live-cell in vitro assay using flow cytometric analysis of C3 deposition as readout. The GMFI ratio for C3 deposition is displayed on the horizontal axis and the general arrangement of the depicted data follows the structure used for Fig.4 c. **e** All AChR-specific IgM were class switched to IgG and tested for antigen-specific binding in the live-cell flow cytometry assay described in Fig.4 a. The bar graph shows the GMFI measured for three different concentrations of six different IgG including the only two patient and two healthy donor derived IgG that retained binding capacity after the class switch. PBS was employed as negative control and B12L as positive control. The horizontal axis displays the dilutions of the recombinant IgG antibodies and the vertical axis the GMFI values. **f** Complement activation measured by C3 deposition for three different concentrations of single and combinations of AChR-specific IgM. The horizontal axis of the bar graph displays the antibody dilutions and the vertical axis the GMFI ratios of C3 immunofluorescence calculated as described in Fig.2 b.

Fig.5: Relationship between C3 deposition, AChR-specific binding, heavy chain hypermutations and species cross-reactivity. The IgM were categorized in MG-derived (blue) and healthy volunteer (HV)-derived (red) and C3 deposition as a measure for complement activation was plotted against the GMFI for AChR-specific binding (as measured in Fig.4 c and d). The size of the circular symbols represents the number of somatic hypermutations detected in the heavy chain variable region (as reported in Fig.4 b). The heatmap to the right

of the graph displays the correlation between of all four measured parameters. The upper number in each cell of the heatmap is the Spearman's rank correlation coefficient and the lower number is the corresponding p-value calculated by a two-tailed permutation test. None of the correlations between the different pairs of variables was found to be significant.

Table 1: List of all IgM antibodies produced from cDNA of AChR-specific B cells isolated with the MACACS method. The antibodies were arranged according to the health status of the donor ("HV" = healthy volunteer, "MG" = myasthenic donor) and the number of hypermutations found in the heavy chain variable region. Characteristics, such as AChR-specific binding, complement activation and binding after class switch to IgG are displayed. IgM additionally labelled with the same symbol (✱/※) are clonally related with shared use of H and L chain V(D)J genes and corresponding hypermutations.

Table 2: List with characteristics of donors for PBMC isolation and antigen-specific B cell identification.

Table 3: List of primers used in this study to clone recombinant IgM antibodies from cDNA and for generation of class switch from IgM to IgG.

Supplementary figure

S.1: Flow cytometry analysis of anti-AChR antibody content in the blood of rats from the PTMG complement inhibitor experiment. Animals were injected with PBS or antibodies and either an isotype control or a C5 complement inhibitor. One animal treated with the rat anti-AChR monoclonal antibody mAb35 and the isotype control showed no behavioral phenotype, counter to the other three animals from the same cohort. Using AChR-GFP expressing HEK cells, the serum was tested for AChR-specific antibodies in a flow cytometric assay. The results from the animal with no clinical symptoms are shown in the lower left plot. **S.2**: Graphic depiction of antibody concentration according to ELISA results and approximated via four-parameter logistic (4PL) curve fitted to the measured values. The graph to the left displays the absorbance at 450 nm for different antibody dilutions tested by ELISA. The sigmoidal 4PL regression model in GraphPad was used to fit a curve to the measured values and by comparing the results of the different antibody dilutions to a standard curve of commercially produced IgM with known concentration the approximate concentration in the IgM antibody preparation was determined. **S.3**: Rooted phylogenetic tree with branch length representing the divergence of the DNA sequence from the different IgM mu constant regions. The sequences of the heavy chain constant regions were extracted from each IgM and subjected to MAFFT (Multiple Alignment using Fast Fourier Transform) multiple sequence alignment. The parameters used for the alignment are depicted in the box to the right and the algorithm as well as the computation was provided by the open-source online tool from the Kyoto University Bioinformatic Center (https://www.genome.jp/tools-bin/mafft). The difference between the constant regions is illustrated for selected examples in terms of single nucleotide mutations and ensuing amino acid changes.

Fig.1

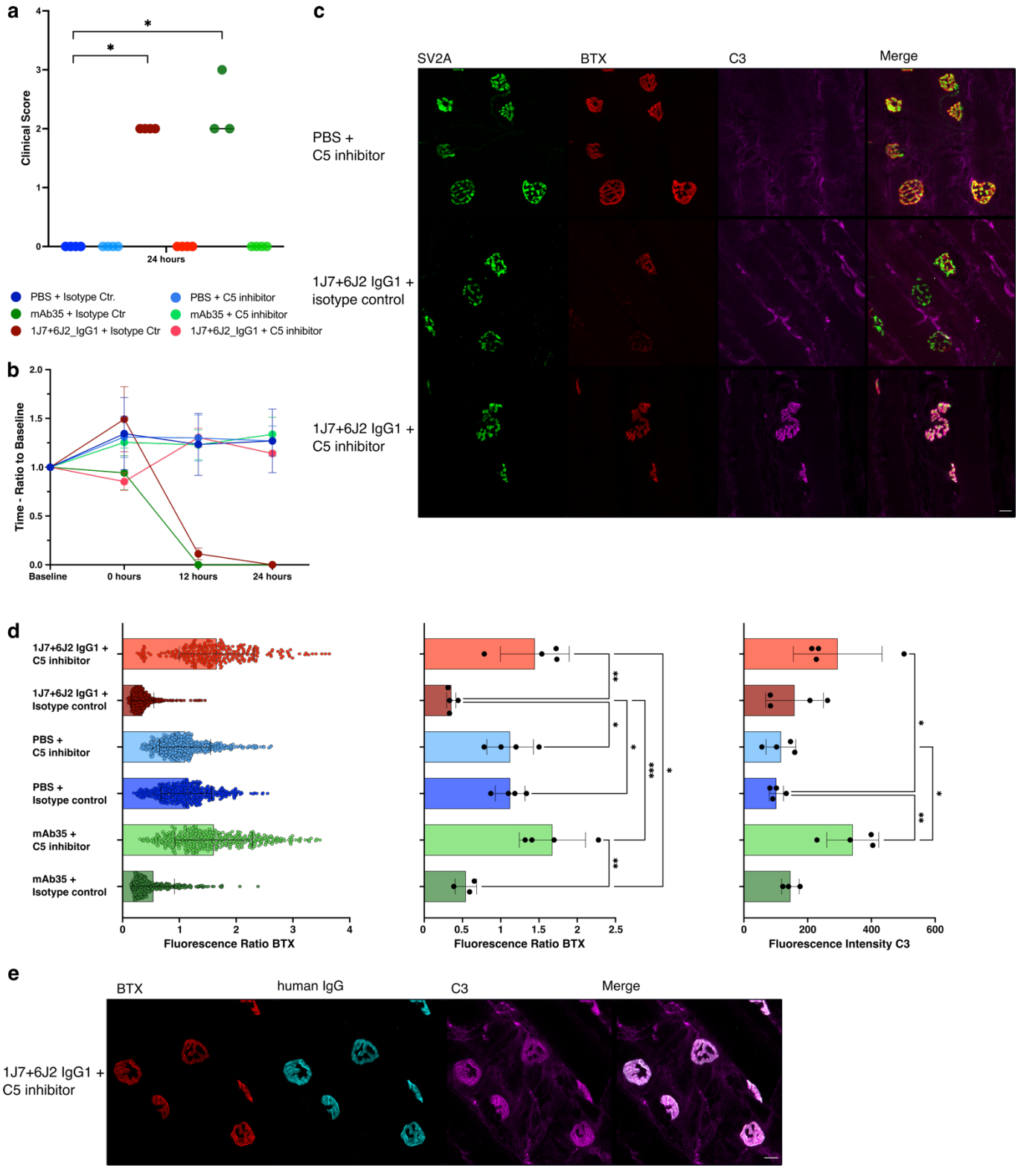
a
Clinical Score
24 hours
PBS + Isotype Ctr.
mAb35 + Isotype Ctr
1J7+6J2_IgG1 + Isotype Ctr
PBS + C5 inhibitor
mAb35 + C5 inhibitor
1J7+6J2_IgG1 + C5 inhibitor
b
Time - Ratio to Baseline
Baseline
0 hours
12 hours
24 hours
c
SV2A
BTX
C3
Merge
PBS + C5 inhibitor
1J7+6J2 IgG1 + isotype control
1J7+6J2 IgG1 + C5 inhibitor
d
1J7+6J2 IgG1 + C5 inhibitor
1J7+6J2 IgG1 + Isotype control
PBS + C5 inhibitor
PBS + Isotype control
mAb35 + C5 inhibitor
mAb35 + Isotype control
Fluorescence Ratio BTX
Fluorescence Ratio BTX
Fluorescence Intensity C3
e
BTX
human IgG
C3
Merge
1J7+6J2 IgG1 + C5 inhibitor

Fig.2

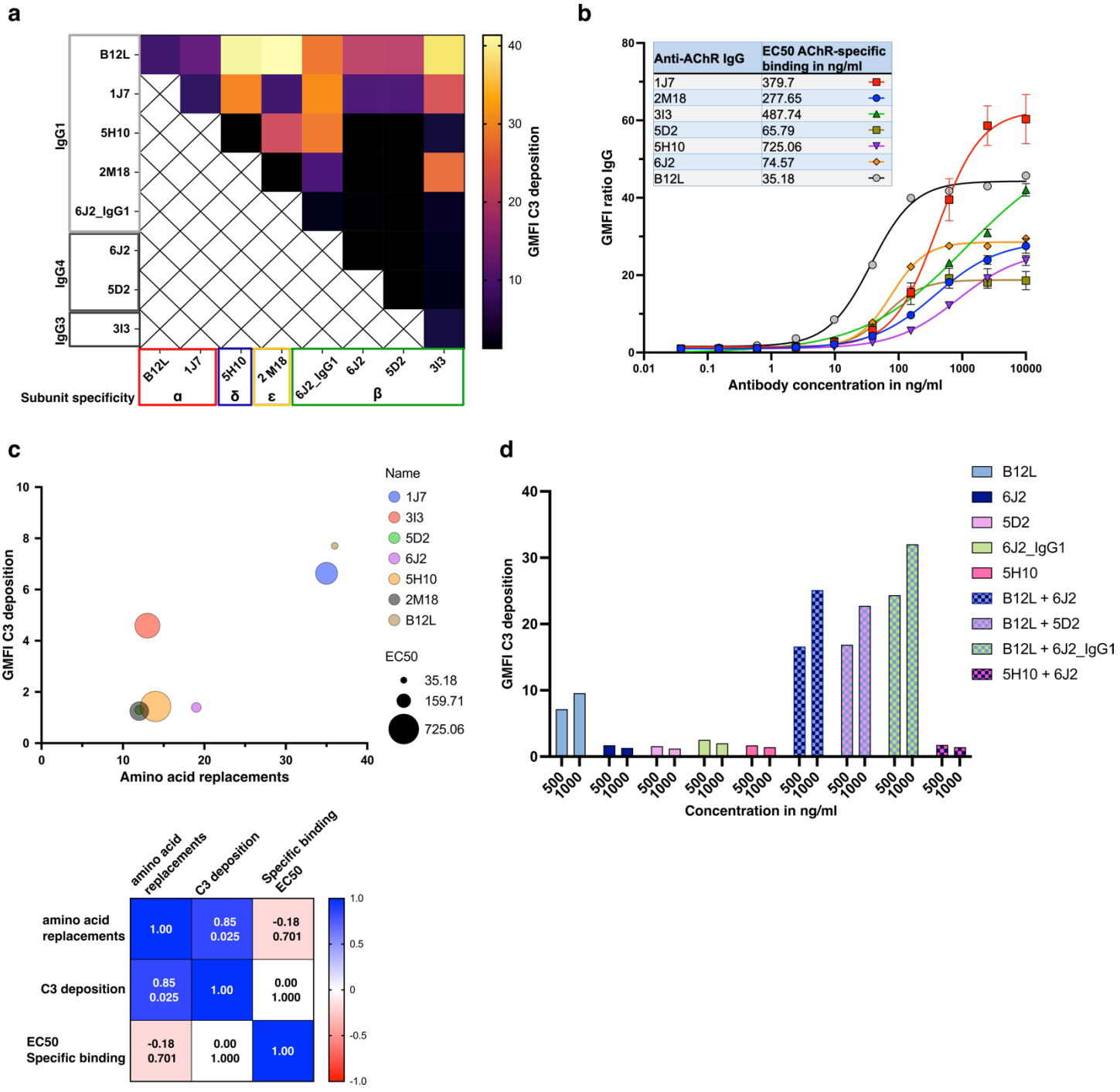
a
B12L
1J7
5H10
2M18
6J2_IgG1
6J2
5D2
3I3
IgG1
IgG4
IgG3
Subunit specificity
α
δ
ε
β
GMFI C3 deposition
b
Anti-AChR IgG
EC50 AChR-specific binding in ng/ml
1J7 379.7
2M18 277.65
3I3 487.74
5D2 65.79
5H10 725.06
6J2 74.57
B12L 35.18
GMFI ratio IgG
Antibody concentration in ng/ml
c
GMFI C3 deposition
Amino acid replacements
Name
1J7
3I3
5D2
6J2
5H10
2M18
B12L
EC50
35.18
159.71
725.06
amino acid replacements
C3 deposition
Specific binding EC50
1.00
0.85 0.025
-0.18 0.701
0.00 1.000
d
GMFI C3 deposition
Concentration in ng/ml
B12L
6J2
5D2
6J2_IgG1
5H10
B12L + 6J2
B12L + 5D2
B12L + 6J2_IgG1
5H10 + 6J2

Fig.3

a

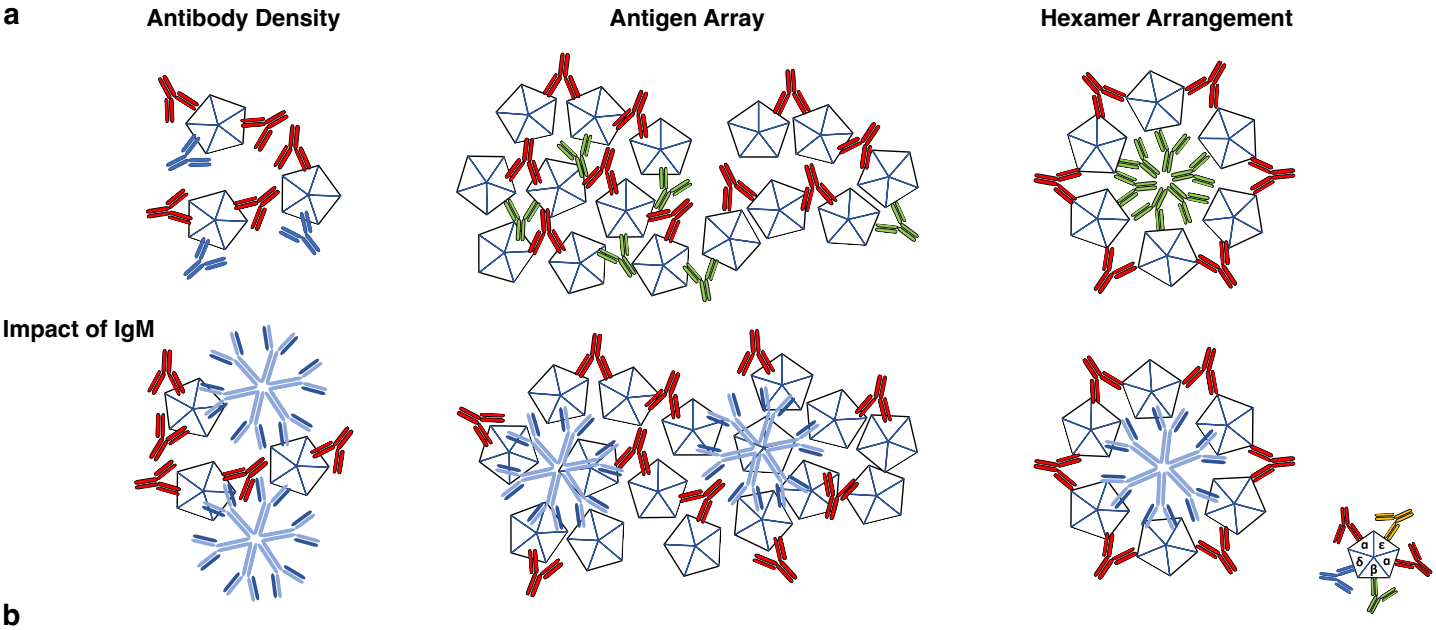

b

Exp.	Parameter investigated	H1: IgG Density	H2 Antigen Array	H3: IgG Hexamers
1	AChR/irrelevant bispecific antibodies	No impact, or reduction via lower avidity	Eliminates effect of combinations	Enhances complement activation
2	One antibody of the combination switched to IgG_4	IgG_4 has no additive effect	IgG_4 anti-β potentiates IgG_1 anti-α	Eliminates complement activation
3	ratio of IgG to AChR	Higher ratio increases complement up to ceiling	Inverted U shaped response	Higher ratio increases complement up to ceiling
4	Titration of antibody concentrations and ratio of anti-α to anti-β	Ceiling of anti-**α** + anti-**β** > ceiling of anti-**α**	Anti-**α** + anti-**β** > 2x anti-**α**	2x anti-**α** > anti-**α** + anti-**β**
5	Combination of multiple subunit specificities	The more the stronger the activation, max. with all 4 subunits (**α**+**β**+**δ**+**ε**) > 3 > 2 > 1	Effect subunit dependent: **α** + non-**α** > non-**α** + non-**α** >> **α** > non-**α**	Complement activation independent of additional subunit specificity
6	Combination of IgG with IgM	High local density, higher dose response, delayed and weak combination effect	Anti-**α** IgM max. potency in combination, strong synergy with IgG	IgM ideal formation, anti-**α** highest activation, no combination effect

Fig.4

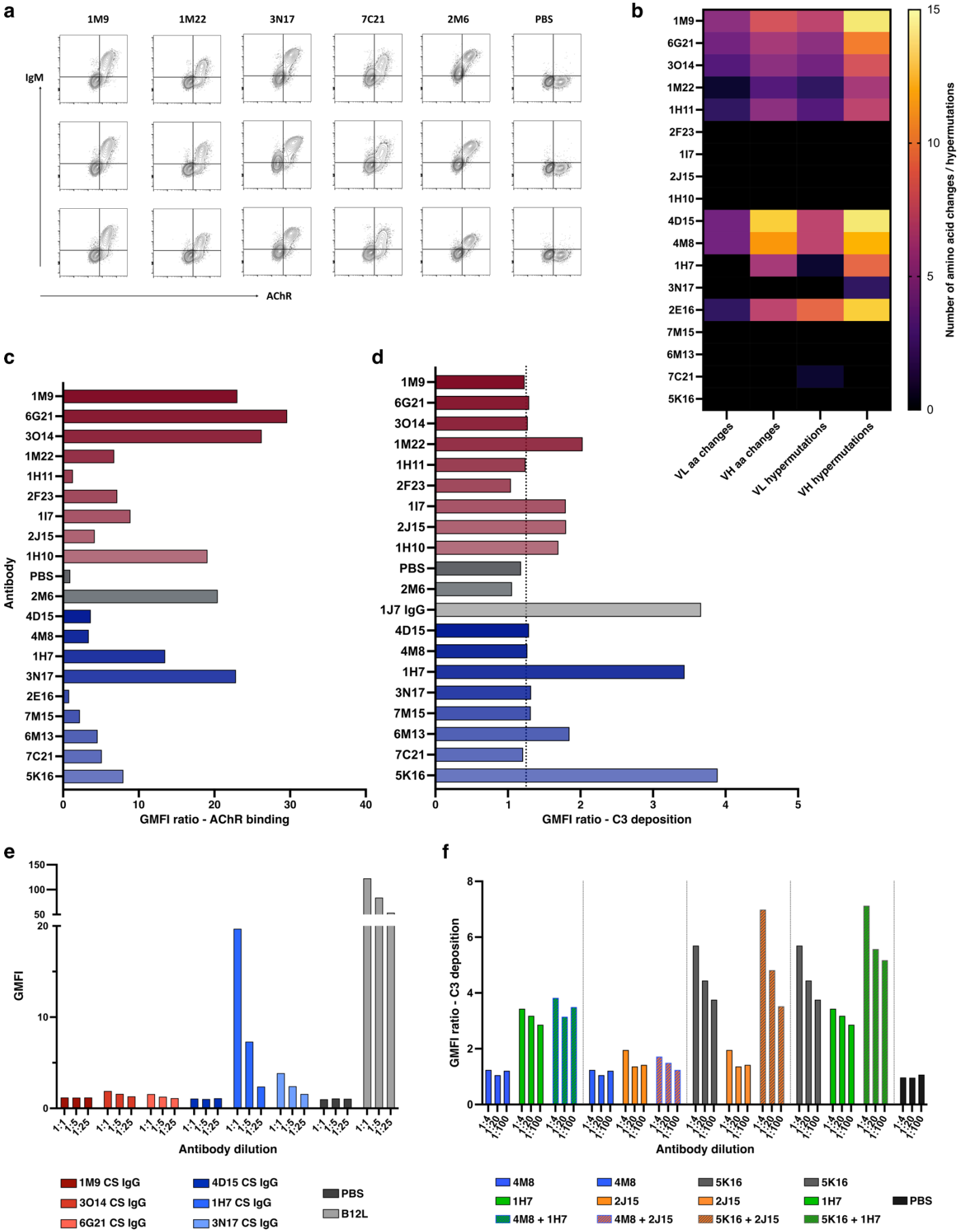
a
1M9
1M22
3N17
7C21
2M6
PBS
IgM
AChR
b
1M9
6G21
3O14
1M22
1H11
2F23
1I7
2J15
1H10
4D15
4M8
1H7
3N17
2E16
7M15
6M13
7C21
5K16
VL aa changes
VH aa changes
VL hypermutations
VH hypermutations
Number of amino acid changes / hypermutations
15
10
5
0
c
Antibody
GMFI ratio - AChR binding
0
10
20
30
40
d
1J7 IgG
GMFI ratio - C3 deposition
0
1
2
3
4
5
e
GMFI
150
100
50
20
10
0
Antibody dilution
1M9 CS IgG
3O14 CS IgG
6G21 CS IgG
4D15 CS IgG
1H7 CS IgG
3N17 CS IgG
PBS
B12L
f
GMFI ratio - C3 deposition
8
6
4
2
0
Antibody dilution
4M8
1H7
4M8 + 1H7
4M8
2J15
4M8 + 2J15
5K16
2J15
5K16 + 2J15
5K16
1H7
5K16 + 1H7
PBS

Fig.5

a

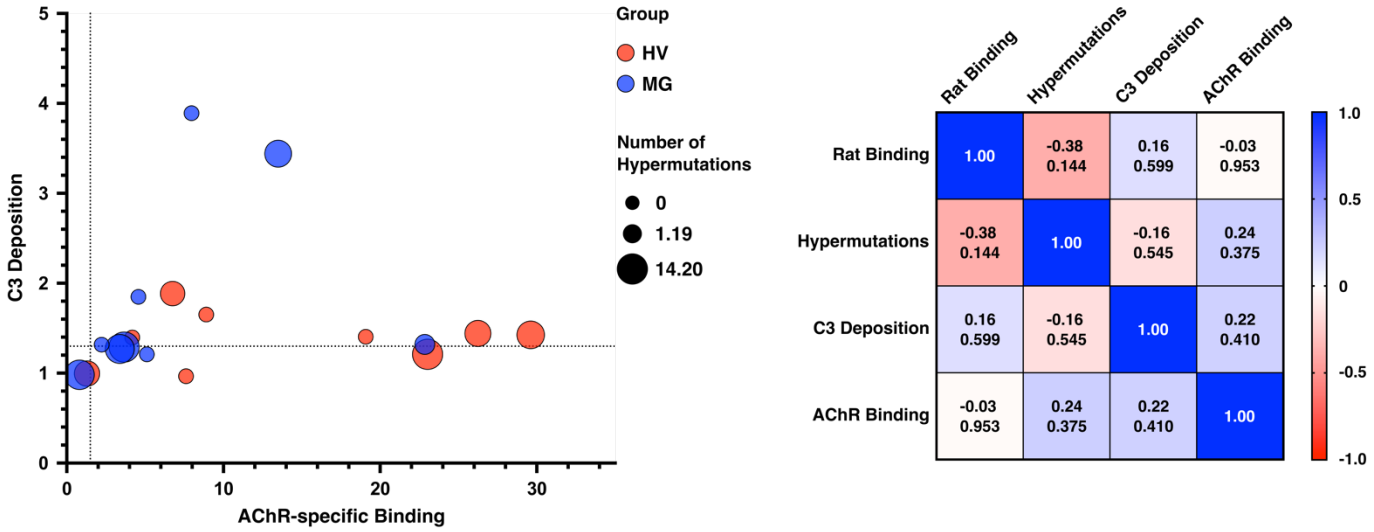

Antibody	Source	AChR - Binding	Heavy chain VDJ gene usage	Hypermut./ aa changes	Light chain VJ gene usage	Hypermut./ aa changes	Conc. in ng/ml	Complement activation (IgM)	Class switch IgG binding	Rat cross - reactivity
1M9	HV A1209 ※	Yes	3-23, 3-10, 4*02	14 / 8	K, 1-6, 1*01	7 / 5	2720	No	No	No
6G21	HV A1209 ※	Yes	3-23, 3-10, 4*02	10 / 6	K, 1-6, 1*01	5 / 4	2812	No	Weak	No
3O14	HV A1209 ※	Yes	3-23, 3-10, 4*02	8 / 5	K, 1-6, 1*01	4 / 3	3288	No	Weak	No
1M22	HV E2476	Yes	3-48, 3-3, 4*02	6 / 3	K, 1-16, 1*01	2 / 1	1094	Yes	No	No
1H11	HV E2476	No	4-34, 5-12, 4*02	7 / 5	L1, 3-21, 1*01	3/ 2	-	-	-	-
2F23	HV A1209	Yes	4-39, 3-10, 4*02	0 / 0	K, 4-1, 1*01	0 / 0	526	No	No	No
1I7	HV E2476	Yes	4-4, 2-2, 6*02	0 / 0	K, 3-11, 5*01	0 / 0	2734	Yes	No	Yes
2J15	HV A1209	Yes	3-21, 2-15, 6*02	0 / 0	K, 1-9, 1*01	0 / 0	2048	Yes	No	No
1H10	HV A1209	Yes	4-31, 2-21, 4*02	0 / 0	L2, 3-9, 2*01	0 / 0	1886	Yes	No	No
4D15	MG D2255 *	Yes	3-30, 3-10, 6*02	14 / 13	L1, 1-40, 1*01	7 / 4	1439	No	No	No
4M8	MG D2255 *	Yes	3-30, 3-10, 6*02	12 / 11	L1, 1-40, 1*01	7 / 4	1327	No	No	No
1H7	MG D2246	Yes	4-4, 6-13, 4*02	9 / 6	K, 4-1, 4*01	1 / 0	3081	Yes	Yes	No
3N17	MG D2246	Yes	3-23, 3-10, 5*02	2 / 0	K, 1-39, 2*02	0 / 0	804	No	Yes	Yes
2E16	MG D2246	No	4-34, 3-10, 4*02	13 / 7	K, 2-30, 1*01	9 / 2	-	-	-	-
7M15	MG D2255	Yes	5-51, 6-13, 6*02	0 / 0	K, 3D-15, 4*01	0 / 0	4324	No	No	No
6M13	MG D2255	Yes	3-21, 3-22, 5*02	0 / 0	L2, 1-40, 2*01	0 / 0	1678	Yes	No	Yes
7C21	MG D2432	Yes	3-21, 6-13, 6*02	0 / 0	K, 2-28, 4*01	1 / 0	4840	No	No	Yes
5K16	MG D2432	Yes	3-23, 4-17, 5*02	0 / 0	K, 3-15, 1*01	0 / 0	3189	Yes	No	Yes

Table 1

Participant	Sex	Age	Diagnosis	Besinger Score	RIA AChR antibody titer (nmol/l)
A1209	M	44	Healthy donor	-	-
E2476	F	63	Healthy donor	-	-
D2255	M	39	Generalized myasthenia graivs	6	366
D2246	M	35	Generalized myasthenia graivs	8	27.4
D2432	F	60	Poly autoimmunity	-	193.7

Table 2

Heavy chain forward

V gene	forward primer name	forward primer sequence
3-21	H_3-21_5UTR_LIC_for	ctacttccaatcatttgACTGAGCACCGAGGATTCAC
3-53	H_3-53_5UTR_LIC_for	ctacttccaatcatttgCCATGGAGTTTTGGCTGAGC
1-69	H_1-69_5UTR_LIC_for	ctacttccaatcatttgTCCTCCTCTAAAGAAGCCCCT
3-15	H_3-15_5UTR_LIC_for	ctacttccaatcatttgTCCCAAGTGTTTTCATTCAGTG
1-2	H_1-2_5UTR_LIC_for	ctacttccaatcatttgAATCCCCTGAGAGCTCCGTT
3-9	H_3-9_5UTR_LIC_for	ctacttccaatcatttgTGTTTCCATTCAGTGATCAGCA
3-66	H_3-66_5UTR_LIC_for	ctacttccaatcatttgCCATGGAGTTTGGGCTGAAC
3-7	H_3-7_5UTR_LIC_for	ctacttccaatcatttgCATGGAATTGGGGCTGAGC
5-51	H_5-51_5UTR_LIC_for	ctacttccaatcatttgCTGGGATCTCAGGGCTTCAT
4-30	H_4-30_5UTR_LIC_for	ctacttccaatcatttgACCTCCTGTGCAAGAACATG
3-74	H_3-74_5UTR_LIC_for	ctacttccaatcatttgTGCACACAGAGAACTCACCA
4-31	A1209_1H10_heavy_for_LIC	ctacttccaatcatttgACCTCCTGTGCAAGAACATG
3-23	A1209_1M9_heavy_for_LIC	ctacttccaatcatttgCTGGGATTTTCAGGTGTTTTCA
3-48	E2576_1M22_heavy_for_LIC	ctacttccaatcatttgATGGAGTTGGGGCTGTGC
4-39	A1209_2F23_heavy_for_LIC	ctacttccaatcatttgTGCAAGAAAATGAAGCACCTGT
3-23	D2246_3N17_heavy_for_LIC	ctacttccaatcatttgCTGGGATTTTCAGGTGTTTTCA
3-21	D2432_7C21_heavy_for_LIC	ctacttccaatcatttgACTGAGCACCGAGGATTCAC

Light Chain forward

V gene	forward primer	forward primer sequence
1-17	K_1-17_5UTR_LIC_for	atccctacttccaatcatttcttaagCGCAGAGTACGGGAGGAAT
1-5	K_1-5_5UTR_LIC_for	atccctacttccaatcatttcttaagGGAGTCAGACCCAGTCAGGA
1-39	K_1-39_5UTR_LIC_for	atccctacttccaatcatttcttaagTCTCAGTCAGGACACAGCAT
6-57	L_6-57_5UTR_LIC_for	atccctacttccaatcatttcttaagAGGGTGGTAGCTCAGGAAG
1-5	K_1-5_5UTR_LIC_for	atccctacttccaatcatttcttaagGGAGTCAGACCCAGTCAGGA
1-27	K_1-27_5UTR_LIC_for	atccctacttccaatcatttcttaagCTCTCAGTCAGGACACAGCA
1-9	K_1-9_5UTR_LIC_for	atccctacttccaatcatttcttaagTCAGGACACAGCATGGACAT
1-44	L_1-44_5UTR__LIC_for	atccctacttccaatcatttcttaagAGACAGGACTCAGGACAATCTC
3-10	L_3-10_5UTR_LIC_for	atccctacttccaatcatttcttaagAGAGCTCTGGGAATCTCACC
3-1	L_3-1_5UTR_LIC_for	atccctacttccaatcatttcttaagCATGGCATGGATCCCTCTCT
2-14	L_2-14_5UTR_LIC_for	atccctacttccaatcatttcttaagCGCTCTCAGGACATCTCCAC
3-21	L_3-21_5UTR_LIC_for	atccctacttccaatcatttcttaagGCCTAAGGAAGCAGCACTG
1-33	K_1-33_5UTR_LIC_for	atccctacttccaatcatttcttaagGAAAGGGGAGGAGTCAGTC
4-69	L_4-69_5UTR_LIC_for	atccctacttccaatcatttcttaagTGGGGAGTCTGCACCATG
2-23	L_2-23_5UTR_LIC_for	atccctacttccaatcatttcttaagCACAAGAGGCAGCGCTCT
3-9	A1209_1H10_light_for_LIC	atccctacttccaatcatttcttaagTCAGGAAGCAGCATCGGG
1-6	A1209_1M9_light_for_LIC	atccctacttccaatcatttcttaagAGTACGGGAGGAGTCAGACC
1-16	E2576_1M22_light_for_LIC	atccctacttccaatcatttcttaagAGTACGGGAGGAATCAGACC
4-1	A1209_2F23_light_for_LIC	atccctacttccaatcatttcttaagCAGGGGCAGCAAGATGGT
1-39	D2246_3N17_light_for_LIC	atccctacttccaatcatttcttaagTCTCAGTCAGGACACAGCAT
2-28	D2432_7C21_light_for_LIC	atccctacttccaatcatttcttaagCTCACAATGAGGCTCCCTGCT

Heavy chain reverse

reverse primer name	reverse primer sequence
Mu_heavy_rev_LIC	tttatccacttcatttgATGCAACATCTCACCCCGTT
heavychain_gamma_rev_1	TTTATCCACTTCATTTGATGCAACATCTCACCCCGTT
alpha_3pUTR_rev_LIC	tttatccacttcatttgAGCATGGAGTTTATTCAGGGGT

Light chain reverse

reverse primer name	reverse primer sequence
Kappa_light_rev_LIC	tttatccacttcatttcttaagGGGTGAGGTGAAAGATGAGCT
5K21_light_rev	tttatccacttcatttcttaagCTATGAACATTCTGTAGGGGCCACTGTCTT

Class switch primers

primer name	primer sequence
pVitro_CS3_out_tag_for	ctacttccaatcatttgTGAAAACCACCGCTAATTCAAAG
1M9_CS_h_var_IgG1_rev	gaagaccgatgggcccttggtggaggcTGAGGAGACGGTGACCAGG
gamma1_constant_for	gcctccACCAAGGGCCCATCGGTC
pVitro_CS3_out_tag_rev	tttatccacttcatttgGCATTCTAGTTGTGGTTTGTCC
heavy_var_IGHJ6.02_CS_rev	gaagaccgatgggcccttggtggaggcTGAGGAGACCGTGACCGTG

Table 3

Supplementary figure

S.1

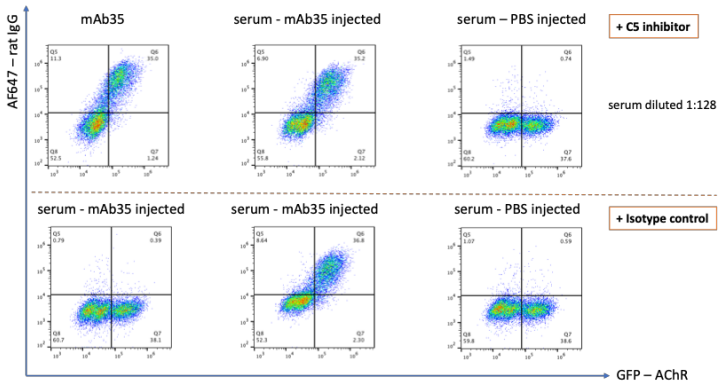

S.2

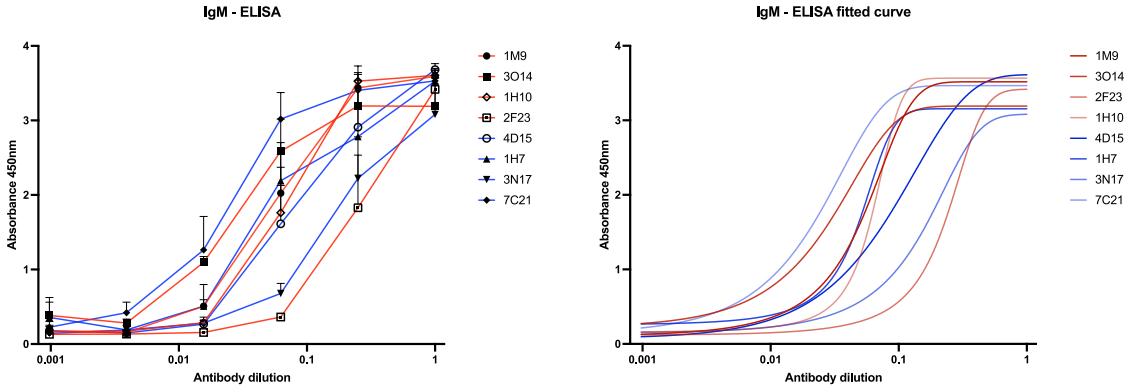

S.3

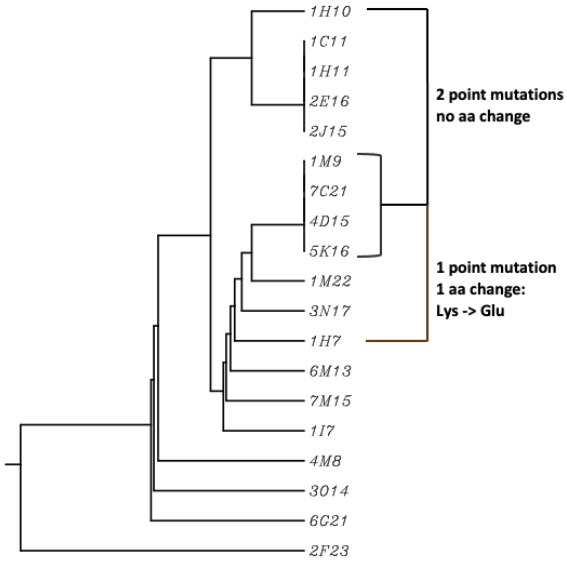

Multiple Sequence Alignment by MAFFT

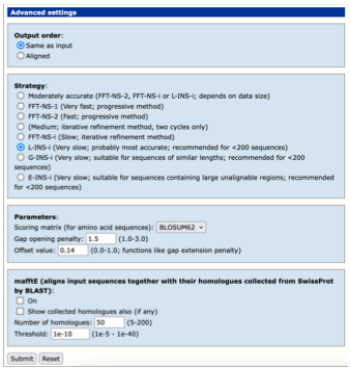

Source: https://www.genome.jp/tools-bin/mafft

4. Supplementary results

4.1 Adaptation of the MACACS protocol for the simultaneous isolation of B cells with different antigen specificities

Our initial efforts were focused on the identification and characterization of anti-AChR IgG antibodies, since only immunoglobulins of the IgG class are detected in MG patients and are therefore assumed to be the only pathologically relevant antibody. However, we detected somatically hypermutated, IgM AChR-specific (SHIgMA) B cells in patients and also in healthy donors which led us to the believe that these B cells could provide a physiological function. We hypothesized that following a pathological developmental switch, SHIgMA B cells would start producing disease-causing IgG autoantibodies and effectively represent the healthy precursor of the autoreactive anti-AChR B cells that induce MG. As part of this overarching hypothesis, we aspired to define the phenotype of the SHIgMA B cells to examine their response after the encounter of the cognate self-antigen and to compare the B cell phenotypes in different disease paradigms. The MACACS protocol proved to be a powerful suit of methods to isolate individual antigen-specific B cells, yet we realized that in the context of a phenotypic analysis some optimizations become necessary. The two main objectives were to increase the efficiency of the protocol and to develop an appropriate control that is applicable for future CITE-Seq (Cellular Indexing of Transcriptomes and Epitopes by Sequencing) phenotyping experiments. We found that after removing α-BTX as second marker for antigen-specific B cells and by restricting the gate for the GFP-positive cell population, the number of antibody-producing and antigen-specific B cells remained constant in comparison to previous MACACS protocols. The results from a previous MACACS experiment with a MG donor sample, called C2058 are summarized in a pie-chart as representative baseline (Supplementary Results Fig. 1d). Furthermore, we included antibody-coated polybead carboxylate microspheres to capture human immunoglobulin in the live-cell flow cytometry assay to screen single seeded B cell supernatants (Supplementary Results Fig. 1c, h). As a result, we were able to simultaneously test the supernatant of cultured B cells for antigen-specificity and antibody production which eliminated the additional analysis of the antibody content via ELISA. The final optimization of the workflow was achieved by streamlining the production of monoclonal antibodies from cDNA of isolated B cells, for which we adapted the well-established ligation independent cloning (LIC) system and generated a new expression plasmid for increased antibody production (Supplementary Results Fig. 1f). The LIC cloning vector contained two

pre-defined restriction sites with distinct sequences flanking the enzymatic restriction site. These unique sequences were mirrored at the 3' and 5' ends of the heavy and light chain sequence as complementary overlaps, allowing a site-specific insertion of the constructs and the expression of the whole antibody from a single plasmid (Supplementary Results Fig. 1f). We then employed the LIC system to clone AChR-specific IgM from cDNA of previously isolated B cells, which were introduced in chapter 3.2.

Phenotypic markers can be relative in nature and must therefore be defined in relation to reliable references. This prerequisite excluded the combination of different donors as source for B cells since we have to account for inter-individual differences. Additionally, the enrichment of AChR-specific B cells is achieved by antigenic stimulation which inevitably changes the expression profile of the surface receptors and the transcriptome. Therefore, we concluded, that the best reference is provided by B cell populations of the same donor, isolated in parallel but targeting an alternative antigen. The initial concept was to perform sequential membrane-antigen capture with the same B cell sample by reusing the non-adherent B cells from the first panning for a subsequent incubation on a separate monolayer of cells expressing a different membrane-antigen. As proof of concept, we applied this protocol using three membrane-expressed antigens, the AChR, the SARS-CoV-2 spike (spike) protein and the myelin oligodendrocyte glycoprotein (MOG) which is the target of antibodies in an inflammatory demyelinating disease of the central nervous system. The MOG transmembrane protein and the α-subunit of the AChR were fused with GFP while the spike protein was joined with mCherry and accordingly the final gate of the fluorescence activated single cell sorting had to be adjusted for this paradigm (Supplementary Results Fig. 1a). The PBMC sample for this experiment originated from a healthy donor of whom we successfully isolated spike-specific and SHIgMA B cells in previous MACACS iterations. An unwelcome side effect of the successive incubation with different feeder cells in different flasks was the resulting time discrepancy of 60 min between the first and the last B cell panning step. Nevertheless, a total number of 1254 B cells were sorted, which, according to the antigen specificity corresponded to 392 spike, 671 MOG and 191 AChR recognizing B cells (Supplementary Results Fig. 1b). Screening of the single seeded B cell supernatant yielded antibody production of all three tested isotypes: IgG, IgM and IgA, for each condition. No AChR-specific antibody producing B cells were detected, but 5 MOG-specific IgM and collectively 19 spike-specific antibodies, of which two were IgA and 18 IgG. Approximately 17.5% of all seeded B cells produced antibody, representing a lower efficiency compared to previous MACACS protocols with about 25%

(Supplementary Results Fig. 1b, d). However, the ratio of antigen-specific antibodies increased to 2.5% as opposed to 1.6% from the C2058 reference. That said, most of the antigen-specific B cells (80%) originated from the spike condition, reflecting the disease paradigm of a viral infection in which we expected a higher percentage of antigen-specific B cells in contrast to the autoimmune disease of donor C2058. All of the MOG IgM, 9 spike IgG and 1 spike IgA were picked for mRNA isolation, reverse transcription and Illumina sequencing. One MOG IgM did not maintain antigen-specific binding after production of the corresponding monoclonal antibody, yet cloning the antibody encoded by the marginally positive B cell called 1N15 concluded in a highly specific anti-MOG IgM antibody (Supplementary Results Fig. 1c, g). Analysis of the immunoglobulin sequences revealed varying numbers of hypermutations and amino acid changes in the spike antibodies but almost no aberration in the amino acid sequences of MOG-specific IgM (Supplementary Results Fig. 1e). Aside from a single mutation in a single MOG IgM, all the immunoglobulin sequences aligned with the reported germline sequence of their respective V, D and J gene.

So far, the need for a transient transfection with the AChR-GFP encoding plasmids prior to any live-cell assay was considered rather a bug than a feature. But in the context of the MACACS protocol and a TE671 cell line with stable expression of spike-mCherry the additional transfection with the AChR-plasmids allowed the potential for further optimization. After verifying a sufficient transfection efficiency while upholding specific binding of antibodies against the spike protein, we used double positive cells for simultaneous B cell antigen-capture of two different antigen targets. Thereby we removed the sequential B cell panning and guaranteed the identical treatment of all B cells subjected to the enrichment and sorting process of the MACACS method. We identified 665 mCherry- and 616 GFP-positive B cells from a PBMC sample of a MG patient, with double-positive cells being included in the GFP-positive population. Single supernatant screening of AChR-GFP positive and double positive (616 single wells in total) B cells showed antibody production in more than 30% of all tested single seeded B cell wells. Additionally, we detected AChR- and spike-specific antibodies of the IgM and IgG class in the combined B cell population (Supplementary Results Fig. 1h). With approximately 1.6% of B cells producing antibodies against one of the two membrane-expressed targets, the results resembled the earlier described C2058 reference. Further analysis of the individual antigen-specific B cells is still ongoing, including the recombinant production of the antibodies, the functional characterization as well as the comparison of the B cell transcriptomes following the Illumina sequencing.

Supplementary Results Fig. 1: Optimization of the MACACS protocol to simultaneously identify B cells with different antigen-specificities from a single PBMC sample. **a** Gating scheme for fluorescence activated cell sorting (FACS) of B cells that captured either AChR-GFP, spike-mCherry or MOG-GFP. Following the initial enrichment of antigen-specific B cells, fluorescent antibody for the activation marker CD69 was used to select the population of CD69 high, CTV-, AChR-GFP+/spike-mCherry+/MOG-GFP+ B cells via FACS. B cells with corresponding phenotypes were collected in separate tubes, single cell seeded and cultured with CD40L-expressing TE cells and IL21 for 9 days. **b** Screening of the supernatant via live-cell flow cytometry assay. HEK cells expressing either AChR-GFP, spike-mCherry or MOG-GFP were used to examine antigen-specific binding and coated polybead carboxylate microspheres were included to assess the general antibody content of the supernatant. The y-axis displays either human IgG or IgM as noted in the caption, the horizontal axis of the upper row represents AChR-GFP expression, the middle row MOG-GFP expression and in the bottom row spike-mCherry expression. The population found to the far left of each flow cytometry gating scheme represents the polybeads, which indicate general antibody production. An upward shift of a cell population into the upper right quadrant illustrates antigen-specific binding. **c** Analysis of single cell supernatant screening summarized in different pie charts. The total number of tested wells is depicted below each diagram, “negative wells” represents the number of wells with no antibody production, the different antibody classes combined with the suffix “Beads” signifies unspecific antibody production of a specific isotype and the addition of “Cells” denotes antigen-specific antibody production. The table to the right of each pie chart displays the accurate number of positive wells for each condition. **d** Results of a previous MACACS protocol without adjustments to the method, using the MG patient PBMC sample C2058. The values of the pie chart and its table to the right were collected from the screening of the single cell supernatants. The AChR-specific antibody binding was tested with a live-cell flow cytometry assay as described in 1b, but the general antibody production by single seeded B cells was measured via ELISA. **e** Sequence analysis of spike and MOG-specific antibodies, showing somatic hypermutations and corresponding amino acid substitutions for each heavy (VH) and light (VL) chain. The heatmap displays the number of changes determined from the sequence alignment of the antibody variable region with its putative germline sequence of the rearranged V(D)J gene segments using the IgBlast tool from NCBI. **f** Expression vector and principle cloning procedure for ligation independent cloning. The vector contains two cloning sites for different restriction enzymes and specific flanking sequences, which are mirrored on the PCR primers and used as a tag. Digestion of the vector and the PCR products from the

antibody heavy and light chain generates overlaps that enable the bacterial repair mechanisms to fuse the different components. **g** Live-cell flow cytometry results of recombinant, monoclonal IgM antibodies against the MOG protein. The cDNA of the MOG-specific B cells whose supernatant screening results are depicted in 1b was synthesized and used for antibody production by LIC. The expression vector containing both the heavy and the light chain was transiently transfected into adherent HEK cells and the supernatant tested for antibody binding with live cells expressing MOG-GFP in a flow cytometry assay (as presented in 1b). **h** Double sort of B cells from a single PBMC sample. TE671 cells expressing two different membrane-antigens fused with fluorescent proteins were used to simultaneously identify B cells against two different antigens. The adjusted FACS gating and the summary of the single well supernatant screening displayed in the pie chart to the right follows the conception of 1a and c. Below, the readout of a flow cytometry assay with the double positive TE671 cells is depicted. The first row displays the AChR-GFP expression and the lower row the spike-mCherry expression on the horizontal axis, while the y-axis displays human IgG and IgM binding. The caption above each column either describes the antibody used as control condition or the antibody isotype detected in a single well. In addition to the AChR-GFP and spike-mCherry double positive cell line, anti-human IgG/IgM/IgA coated polybeads were used for the detection of general antibody content.

Supplementary Results Fig. 1

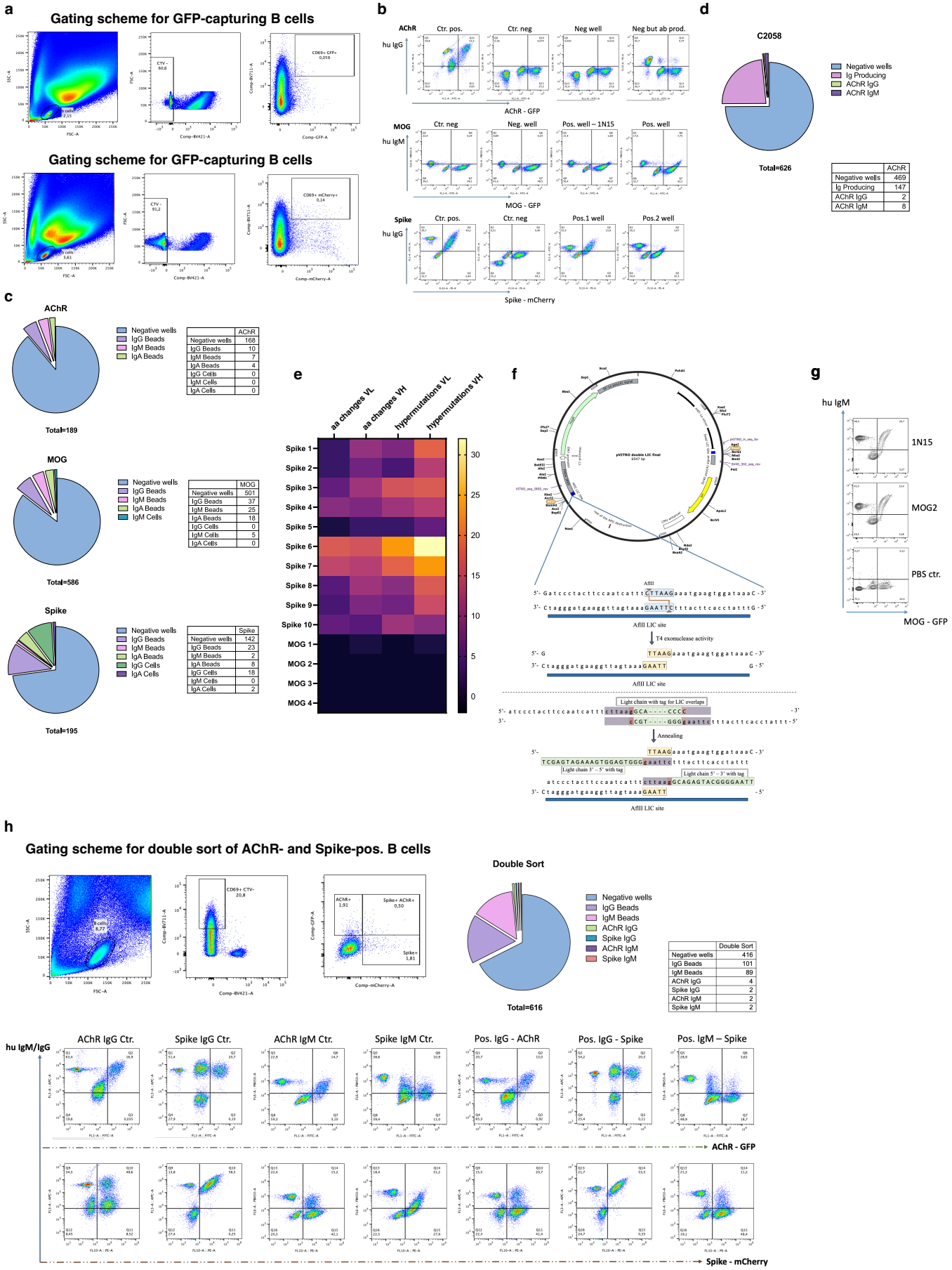

5. Discussion

Autoimmune diseases can develop due to the breakdown of tolerance mechanisms at different steps throughout B cell development. Antibody-mediated autoimmune disease such as rheumatoid arthritis or systemic lupus erythematosus are associated with defects in central tolerance checkpoints resulting in increased numbers of poly- and autoreactive B cells that enter into the periphery. However, the acquisition of a disease-inducing phenotype is dependent on dysregulated germinal center reactions as autoantibodies typically display signs of antigen-driven selection by means of accumulated somatic hypermutations and class switch to IgG (51, 177, 178). Further evidence for a central role of misguided affinity maturation was provided by detailed examination of somatic hypermutations and their effect on autoreactivity of antibodies. Reverse mutation of autoantibodies from SLE patients has revealed that the acquisition of somatic hypermutations leads to a gradual increase in reactivity to self-antigens (51, 179). Studies of neurological diseases have reported de novo autoreactivity against AQP4 and LGI1 following dysregulated germinal center reactions, indicated by a similar observation of autoantibodies that lose their binding capacity to the self-antigen when reverted back to the germline sequence (96,107).

The pathogenesis of MG presents similar patterns of defective central and peripheral tolerance checkpoints with patients exhibiting AChR-specific, hypermutated IgG antibodies that mediate pathogenicity (137, 180, 181). Therefore, MG is considered a T cell dependent, B cell mediated autoimmune disease with essential contribution of dysregulated germinal centers and affinity maturation (80, 180).

Our discovery of unmutated, assumably naïve transitional IgM B cells with reactivity to a given self-antigen was expected and in agreement with other studies investigating autoreactive B cell populations (12, 20, 182). However, the isolation of somatically hypermutated, AChR-specific IgM B cells in MG patients and especially healthy donors was unprecedented. According to the BCR properties, the cell population corresponded most closely to regular memory B cells, meaning that a repeated stimulation with the cognate antigen would result in the production of AChR-specific IgM antibodies. Yet, anti-AChR antibodies of the IgM class have not been detected in healthy or diseased individuals and since class switch recombination takes place prior to the acquisition of somatic hypermutations, these B cells had already experienced affinity maturation (80, 112, 183). Based on this contradiction, we developed the pathological phenotypic switch hypothesis, which postulated that hypermutated, AChR-specific B cells provide an immunoregulatory function and only upon a pathogenic switch start secreting

soluble autoantibodies. The accumulation of somatic hypermutations and high affinity of the BCR for a self-antigen would constitute a normal process, but the expression of the encoded IgM or at least an artificially class-switched IgG should induce myasthenic symptoms. However, the experiments presented in this study demonstrated that almost every AChR-specific IgM lost their binding capacity when secreted as IgG. Not even high numbers of somatic hypermutations or strong specific AChR-binding as IgM displayed predictive criteria for the efficacy as class-switched IgG. The functional characterization of the IgM revealed that hypermutations are also not correlating with the pathogenic potential of an antibody, as measured by their in vitro capacity to activate the complement system. The heterogenous mix of IgM B cells suggested that some might still represent a pathogenic precursor with a germline IgM specific for the AChR but in need of additional affinity maturation to realize its true pathogenic potential. While somatically hypermutated, AChR-specific IgM B cells present a regulatory phenotype with low pathogenic potential but efficient AChR binding, which might facilitate potent antigen presentation. Tolerogenic functions of B cells have been reported, for example the support of the central T cell tolerance in the thymus or the interaction with autoreactive T cells, which induced the development of regulatory T cells (184, 185, 186). But whether the peptides presented by B cells and used for interaction with T cells are exclusively endogenous proteins or also derived from external antigen capture has not been resolved yet. Additionally, B cells can serve an immunoregulatory function in an antigen-specific context by suppressing effector T cells through IL-10 expression, CD40-CD40L interactions and MHC class II expression (187, 188).

In the framework of this study, we established fundamental methods and obtained initial results about the functional properties of this extraordinary B cell population. But further research efforts are required to obtain a better understanding of these autoreactive, somatically hypermutated B cells and potentially apply this knowledge for therapeutic purposes.

6. Conclusion and outlook

In the first part of the study, we characterized six MG patient derived, hypermutated IgG antibodies that were isolated with the membrane-antigen capture activated cell sorting method. The antibodies targeted different subunits of the AChR and individually none induced myasthenic symptoms according to the three tested pathomechanisms that drive the MG pathology. In contrast, a combination of antibodies with synergistic subunit specificities

provided enhanced complement activation in vitro and mediated pathogenicity in a PTMG rat model, resulting likewise from the activation of the complement system. We subsequently investigated the underlying mechanism that amplified complement activation by comparing three hypotheses that predicted different outcomes due to antigen arrangement and individual antibody properties. Based on the experimental data to date, the antigen array hypothesis provided the best-fitting model to explain the combination effect. From research with AChR-specific, somatically hypermutated IgM antibodies derived from MG patients and healthy donors we concluded that a hexameric model of antigen arrangement is not mandatory for disease-inducing complement activation. Still, additional experiments with IgM antibodies of known subunit specificity but without the capacity to initiate the complement system are required to validate the antigen array hypothesis. Moreover, testing a bi-specific antibody as a means of falsifying this hypothesis would be an interesting line of enquiry. Blocking the assembly of a beneficial antibody conformation to inhibit complement activity combined with a Fc constant region that mediates immunosuppressive effector functions could delineate a new therapeutic avenue.

The simultaneous examination of AChR-specific IgM antibodies challenged the concept of somatically hypermutated B cells as pathogenic precursors, yet upheld the notion of physiological functions performed by this B cell population found in both healthy and diseased donors. The recognition of a self-antigen and the occurrence of somatic hypermutations in IgM B cells can no longer automatically be attributed to dysregulated germinal center reactions that lead to detrimental autoantibody production. Therefore, phenotyping and functionally analysing these AChR-specific B cells will be necessary to elucidate the real purpose of the somatically hypermutated, autoreactive IgM B cells. Comparing this memory-like B cell population between different disease paradigms, e.g., autoimmunity and viral infection with the established membrane-antigen capture activated cell sorting assay for multiple antigens will provide valuable information about unique markers and the physiological response of hypermutated IgM B cells to their cognate antigen. The accurate characterization of a potentially immunoregulatory B cell phenotype would expand our knowledge about B cell biology and could help explain the limitations of generalized B cell depleting therapies.

7. References

1. Janeway's immunobiology / Kenneth Murphy, Casey Weaver ; with contributions by Allan Mowat, Leslie Berg, David Chaplin ; with acknowledgment to Charles A. Janeway Jr., Paul Travers, Mark Walport. 9th edition; New York, NY : Garland Science/Taylor & Francis Group, LLC, [2017], ISBN: 9780815345053

2. Cellular and molecular immunology / Abul K. Abbas, Andrew H. Lichtman, Shiv Pillai. 7.th edition; Philadelphia, PA : Saunders/Elsevier, c2010., ISBN: 9781437715286

3. Kurosaki T, Kometani K, Ise W. Memory B cells. Nat Rev Immunol. 2015;15(3):149-159. doi:10.1038/nri3802

4. Nutt SL, Hodgkin PD, Tarlinton DM, Corcoran LM. The generation of antibody-secreting plasma cells. Nat Rev Immunol. 2015;15(3):160-171. doi:10.1038/nri3795

5. Lu LL, Suscovich TJ, Fortune SM, Alter G. Beyond binding: antibody effector functions in infectious diseases. Nat Rev Immunol. 2018;18(1):46-61. doi:10.1038/nri.2017.106

6. Akkaya M, Kwak K, Pierce SK. B cell memory: building two walls of protection against pathogens. Nat Rev Immunol. 2020;20(4):229-238. doi:10.1038/s41577-019-0244-2

7. Schroeder HW, Imboden JB & Torres RM (2019) Antigen Receptor Genes, Gene Products, and Coreceptors. In Clinical Immunology pp 55-77.e1. Elsevier

8. Lee DSW, Rojas OL, Gommerman JL. B cell depletion therapies in autoimmune disease: advances and mechanistic insights. Nat Rev Drug Discov. 2021;20(3):179-199. doi:10.1038/s41573-020-00092-2

9. Doyon-Laliberté K, Aranguren M, Poudrier J, Roger M. Marginal Zone B-Cell Populations and Their Regulatory Potential in the Context of HIV and Other Chronic Inflammatory Conditions. Int J Mol Sci. 2022;23(6):3372. Published 2022 Mar 21. doi:10.3390/ijms23063372

10. Bleul CC, Fuhlbrigge RC, Casasnovas JM, Aiuti A, Springer TA. A highly efficacious lymphocyte chemoattractant, stromal cell-derived factor 1 (SDF-1). J Exp Med. 1996;184(3):1101-1109. doi:10.1084/jem.184.3.1101

11. Sun B, Ramberger M, O'Connor KC, Bashford-Rogers RJM, Irani SR. The B cell immunobiology that underlies CNS autoantibody-mediated diseases. Nat Rev Neurol. 2020;16(9):481-492. doi:10.1038/s41582-020-0381-z

12. Nemazee D. Mechanisms of central tolerance for B cells. Nat Rev Immunol. 2017;17(5):281-294. doi:10.1038/nri.2017.19

13. Romanow WJ, Langerak AW, Goebel P, et al. E2A and EBF act in synergy with the V(D)J recombinase to generate a diverse immunoglobulin repertoire in nonlymphoid cells. Mol Cell. 2000;5(2):343-353. doi:10.1016/s1097-2765(00)80429-3

14. Lin YC, Jhunjhunwala S, Benner C, et al. A global network of transcription factors, involving E2A, EBF1 and Foxo1, that orchestrates B cell fate. Nat Immunol. 2010;11(7):635-643. doi:10.1038/ni.1891

15. Matsuda F, Honjo T. Organization of the human immunoglobulin heavy-chain locus. Adv Immunol. 1996;62:1-29. doi:10.1016/s0065-2776(08)60426-5

16. Agrawal A, Schatz DG. RAG1 and RAG2 form a stable postcleavage synaptic complex with DNA containing signal ends in V(D)J recombination. Cell. 1997;89(1):43-53. doi:10.1016/s0092-8674(00)80181-6

17. Weigert M, Perry R, Kelley D, Hunkapiller T, Schilling J, Hood L. The joining of V and J gene segments creates antibody diversity. Nature. 1980;283(5746):497-499. doi:10.1038/283497a0

18. Hsu LY, Liang HE, Johnson K, Kang C, Schlissel MS. Pax5 activates immunoglobulin heavy chain V to DJ rearrangement in transgenic thymocytes. J Exp Med. 2004;199(6):825-830. doi:10.1084/jem.20032249

19. Hardy RR, Carmack CE, Shinton SA, Kemp JD, Hayakawa K. Resolution and characterization of pro-B and pre-pro-B cell stages in normal mouse bone marrow. J Exp Med. 1991;173(5):1213-1225. doi:10.1084/jem.173.5.1213

20. Keenan RA, De Riva A, Corleis B, et al. Censoring of autoreactive B cell development by the pre-B cell receptor. Science. 2008;321(5889):696-699. doi:10.1126/science.1157533

21. Ehlich A, Schaal S, Gu H, Kitamura D, Müller W, Rajewsky K. Immunoglobulin heavy and light chain genes rearrange independently at early stages of B cell development. Cell. 1993;72(5):695-704. doi:10.1016/0092-8674(93)90398-a

22. Kitamura D, Rajewsky K. Targeted disruption of mu chain membrane exon causes loss of heavy-chain allelic exclusion. Nature. 1992;356(6365):154-156. doi:10.1038/356154a0

23. Neuberger MS, Caskey HM, Pettersson S, Williams GT, Surani MA. Isotype exclusion and transgene down-regulation in immunoglobulin-lambda transgenic mice. Nature. 1989;338(6213):350-352. doi:10.1038/338350a0

24. Kraus M, Pao LI, Reichlin A, et al. Interference with immunoglobulin (Ig)alpha immunoreceptor tyrosine-based activation motif (ITAM) phosphorylation modulates or blocks B cell development, depending on the availability of an Igbeta cytoplasmic tail. J Exp Med. 2001;194(4):455-469. doi:10.1084/jem.194.4.455

25. Nussenzweig MC, Shaw AC, Sinn E, et al. Allelic exclusion in transgenic mice that express the membrane form of immunoglobulin mu. Science. 1987;236(4803):816-819. doi:10.1126/science.3107126

26. Gay D, Saunders T, Camper S, Weigert M. Receptor editing: an approach by autoreactive B cells to escape tolerance. J Exp Med. 1993;177(4):999-1008. doi:10.1084/jem.177.4.999

27. Halverson R, Torres RM, Pelanda R. Receptor editing is the main mechanism of B cell tolerance toward membrane antigens. Nat Immunol. 2004;5(6):645-650. doi:10.1038/ni1076

28. Fang W, Weintraub BC, Dunlap B, et al. Self-reactive B lymphocytes overexpressing Bcl-xL escape negative selection and are tolerized by clonal anergy and receptor editing. Immunity. 1998;9(1):35-45. doi:10.1016/s1074-7613(00)80586-5

29. Wardemann H, Yurasov S, Schaefer A, Young JW, Meffre E, Nussenzweig MC. Predominant autoantibody production by early human B cell precursors. Science. 2003;301(5638):1374-1377. doi:10.1126/science.1086907

30. Russell DM, Dembić Z, Morahan G, Miller JF, Bürki K, Nemazee D. Peripheral deletion of self-reactive B cells. Nature. 1991;354(6351):308-311. doi:10.1038/354308a0

31. Cyster JG. B cell follicles and antigen encounters of the third kind. Nat Immunol. 2010;11(11):989-996. doi:10.1038/ni.1946

32. Bajénoff M, Egen JG, Koo LY, et al. Stromal cell networks regulate lymphocyte entry, migration, and territoriality in lymph nodes. Immunity. 2006;25(6):989-1001. doi:10.1016/j.immuni.2006.10.011

33. Cinamon G, Zachariah MA, Lam OM, Foss FW Jr, Cyster JG. Follicular shuttling of marginal zone B cells facilitates antigen transport. Nat Immunol. 2008;9(1):54-62. doi:10.1038/ni1542

34. Thien M, Phan TG, Gardam S, et al. Excess BAFF rescues self-reactive B cells from peripheral deletion and allows them to enter forbidden follicular and marginal zone niches. Immunity. 2004;20(6):785-798. doi:10.1016/j.immuni.2004.05.010

35. Lechner M, Engleitner T, Babushku T, et al. Notch2-mediated plasticity between marginal zone and follicular B cells. Nat Commun. 2021;12(1):1111. Published 2021 Feb 17. doi:10.1038/s41467-021-21359-1

36. Mackay F, Schneider P. Cracking the BAFF code. Nat Rev Immunol. 2009;9(7):491-502. doi:10.1038/nri2572

37. Schweighoffer E, Vanes L, Nys J, et al. The BAFF receptor transduces survival signals by co-opting the B cell receptor signaling pathway. Immunity. 2013;38(3):475-488. doi:10.1016/j.immuni.2012.11.015

38. Cariappa A, Tang M, Parng C, et al. The follicular versus marginal zone B lymphocyte cell fate decision is regulated by Aiolos, Btk, and CD21. Immunity. 2001;14(5):603-615. doi:10.1016/s1074-7613(01)00135-2

39. Schiemann B, Gommerman JL, Vora K, et al. An essential role for BAFF in the normal development of B cells through a BCMA-independent pathway. Science. 2001;293(5537):2111-2114. doi:10.1126/science.1061964

40. Weller S, Braun MC, Tan BK, et al. Human blood IgM "memory" B cells are circulating splenic marginal zone B cells harboring a prediversified immunoglobulin repertoire. Blood. 2004;104(12):3647-3654. doi:10.1182/blood-2004-01-0346

41. He B, Santamaria R, Xu W, et al. The transmembrane activator TACI triggers immunoglobulin class switching by activating B cells through the adaptor MyD88. Nat Immunol. 2010;11(9):836-845. doi:10.1038/ni.1914

42. Hendricks J, Bos NA, Kroese FGM. Heterogeneity of Memory Marginal Zone B Cells. Crit Rev Immunol. 2018;38(2):145-158. doi:10.1615/CritRevImmunol.2018024985

43. Yuseff MI, Pierobon P, Reversat A, Lennon-Duménil AM. How B cells capture, process and present antigens: a crucial role for cell polarity. Nat Rev Immunol. 2013;13(7):475-486. doi:10.1038/nri3469

44. Lankar D, Vincent-Schneider H, Briken V, Yokozeki T, Raposo G, Bonnerot C. Dynamics of major histocompatibility complex class II compartments during B cell receptor-mediated cell activation. J Exp Med. 2002;195(4):461-472. doi:10.1084/jem.20011543

45. Reif K, Ekland EH, Ohl L, et al. Balanced responsiveness to chemoattractants from adjacent zones determines B-cell position. Nature. 2002;416(6876):94-99. doi:10.1038/416094a

46. Schaerli P, Willimann K, Lang AB, Lipp M, Loetscher P, Moser B. CXC chemokine receptor 5 expression defines follicular homing T cells with B cell helper function. J Exp Med. 2000;192(11):1553-1562. doi:10.1084/jem.192.11.1553

47. Kim CH, Rott LS, Clark-Lewis I, Campbell DJ, Wu L, Butcher EC. Subspecialization of CXCR5+ T cells: B helper activity is focused in a germinal center-localized subset of CXCR5+ T cells. J Exp Med. 2001;193(12):1373-1381. doi:10.1084/jem.193.12.1373

48. Jumper MD, Splawski JB, Lipsky PE, Meek K. Ligation of CD40 induces sterile transcripts of multiple Ig H chain isotypes in human B cells. J Immunol. 1994;152(2):438-445.

49. Donjerković D, Scott DW. Activation-induced cell death in B lymphocytes. Cell Res. 2000;10(3):179-192. doi:10.1038/sj.cr.7290047

50. Muramatsu M, Kinoshita K, Fagarasan S, Yamada S, Shinkai Y, Honjo T. Class switch recombination and hypermutation require activation-induced cytidine deaminase (AID), a potential RNA editing enzyme. Cell. 2000;102(5):553-563. doi:10.1016/s0092-8674(00)00078-7

51. Vinuesa CG, Sanz I, Cook MC. Dysregulation of germinal centres in autoimmune disease. Nat Rev Immunol. 2009;9(12):845-857. doi:10.1038/nri2637

52. William J, Euler C, Christensen S, Shlomchik MJ. Evolution of autoantibody responses via somatic hypermutation outside of germinal centers. Science. 2002;297(5589):2066-2070. doi:10.1126/science.1073924

53. Shapiro-Shelef M, Calame K. Regulation of plasma-cell development. Nat Rev Immunol. 2005;5(3):230-242. doi:10.1038/nri1572

54. Porter RR. Structural studies of immunoglobulins. Science. 1973;180(4087):713-716. doi:10.1126/science.180.4087.713

55. Ramsland PA, Farrugia W. Crystal structures of human antibodies: a detailed and unfinished tapestry of immunoglobulin gene products. J Mol Recognit. 2002;15(5):248-259. doi:10.1002/jmr.585

56. Edmundson AB, Shan L, Fan Zc, Guddat LW, Hanson BL, Andersen KN. Crystallographic Analysis of Antigen-Antibody Complexes: End-on Insertion of Ligands in Antibodies-CDR3 Loops as Arbiters. Methods. 1996;9(3):542-558. doi:10.1006/meth.1996.0062

57. Wilson IA, Stanfield RL. Antibody-antigen interactions: new structures and new conformational changes. Curr Opin Struct Biol. 1994;4(6):857-867. doi:10.1016/0959-440x(94)90267-4

58. Hozumi N, Tonegawa S. Evidence for somatic rearrangement of immunoglobulin genes coding for variable and constant regions. Proc Natl Acad Sci U S A. 1976;73(10):3628-3632. doi:10.1073/pnas.73.10.3628

59. Seidman JG, Leder P. The arrangement and rearrangement of antibody genes. Nature. 1978;276(5690):790-795. doi:10.1038/276790a0

60. Di Noia JM, Neuberger MS. Molecular mechanisms of antibody somatic hypermutation. Annu Rev Biochem. 2007;76:1-22. doi:10.1146/annurev.biochem.76.061705.090740

61. Shinkura R, Tian M, Smith M, Chua K, Fujiwara Y, Alt FW. The influence of transcriptional orientation on endogenous switch region function. Nat Immunol. 2003;4(5):435-441. doi:10.1038/ni918

62. Chaudhuri J, Alt FW. Class-switch recombination: interplay of transcription, DNA deamination and DNA repair. Nat Rev Immunol. 2004;4(7):541-552. doi:10.1038/nri1395

63. Czajkowsky DM, Shao Z. The human IgM pentamer is a mushroom-shaped molecule with a flexural bias. Proc Natl Acad Sci U S A. 2009;106(35):14960-14965. doi:10.1073/pnas.0903805106

64. Vidarsson G, Dekkers G, Rispens T. IgG subclasses and allotypes: from structure to effector functions. Front Immunol. 2014;5:520. Published 2014 Oct 20. doi:10.3389/fimmu.2014.00520

65. Redpath S, Michaelsen TE, Sandlie I, Clark MR. The influence of the hinge region length in binding of human IgG to human Fcgamma receptors. Hum Immunol. 1998;59(11):720-727. doi:10.1016/s0198-8859(98)00075-5

66. Krapp S, Mimura Y, Jefferis R, Huber R, Sondermann P. Structural analysis of human IgG-Fc glycoforms reveals a correlation between glycosylation and structural integrity. J Mol Biol. 2003;325(5):979-989. doi:10.1016/s0022-2836(02)01250-0

67. Sakae Y, Satoh T, Yagi H, et al. Conformational effects of N-glycan core fucosylation of immunoglobulin G Fc region on its interaction with Fcγ receptor IIIa. Sci Rep. 2017;7(1):13780. Published 2017 Oct 23. doi:10.1038/s41598-017-13845-8

68. Nimmerjahn F, Ravetch JV. Fcgamma receptors as regulators of immune responses. Nat Rev Immunol. 2008;8(1):34-47. doi:10.1038/nri2206

69. Sondermann P, Kaiser J, Jacob U. Molecular basis for immune complex recognition: a comparison of Fc-receptor structures. J Mol Biol. 2001;309(3):737-749. doi:10.1006/jmbi.2001.4670

70. Pincetic A, Bournazos S, DiLillo DJ, et al. Type I and type II Fc receptors regulate innate and adaptive immunity. Nat Immunol. 2014;15(8):707-716. doi:10.1038/ni.2939

71. Selvaraj P, Carpén O, Hibbs ML, Springer TA. Natural killer cell and granulocyte Fc gamma receptor III (CD16) differ in membrane anchor and signal transduction. J Immunol. 1989;143(10):3283-3288.

72. Bournazos S, Gupta A, Ravetch JV. The role of IgG Fc receptors in antibody-dependent enhancement. Nat Rev Immunol. 2020;20(10):633-643. doi:10.1038/s41577-020-00410-0

73. Muta T, Kurosaki T, Misulovin Z, Sanchez M, Nussenzweig MC, Ravetch JV. A 13-amino-acid motif in the cytoplasmic domain of Fc gamma RIIB modulates B-cell receptor signalling. Nature. 1994;368(6466):70-73. doi:10.1038/368070a0

74. Bournazos S, Klein F, Pietzsch J, Seaman MS, Nussenzweig MC, Ravetch JV. Broadly neutralizing anti-HIV-1 antibodies require Fc effector functions for in vivo activity. Cell. 2014;158(6):1243-1253. doi:10.1016/j.cell.2014.08.023

75. Dalakas MC, Alexopoulos H, Spaeth PJ. Complement in neurological disorders and emerging complement-targeted therapeutics. Nat Rev Neurol. 2020;16(11):601-617. doi:10.1038/s41582-020-0400-0

76. Mastellos DC, Hajishengallis G, Lambris JD. A guide to complement biology, pathology and therapeutic opportunity. Nat Rev Immunol. 2024;24(2):118-141. doi:10.1038/s41577-023-00926-1

77. Arvieux J, Yssel H, Colomb MG. Antigen-bound C3b and C4b enhance antigen-presenting cell function in activation of human T-cell clones. Immunology. 1988;65(2):229-235.

78. Dempsey PW, Allison ME, Akkaraju S, Goodnow CC, Fearon DT. C3d of complement as a molecular adjuvant: bridging innate and acquired immunity. Science. 1996;271(5247):348-350. doi:10.1126/science.271.5247.348

79. Croix DA, Ahearn JM, Rosengard AM, et al. Antibody response to a T-dependent antigen requires B cell expression of complement receptors. J Exp Med. 1996;183(4):1857-1864. doi:10.1084/jem.183.4.1857

80. Iorio R. Myasthenia gravis: the changing treatment landscape in the era of molecular therapies. Nat Rev Neurol. 2024;20(2):84-98. doi:10.1038/s41582-023-00916-w

81. Mortensen SA, Sander B, Jensen RK, et al. Models of the complement C1 complex. Proc Natl Acad Sci U S A. 2018;115(17):E3866. doi:10.1073/pnas.1803577115

82. Sharp TH, Boyle AL, Diebolder CA, Kros A, Koster AJ, Gros P. Insights into IgM-mediated complement activation based on in situ structures of IgM-C1-C4b. Proc Natl Acad Sci U S A. 2019;116(24):11900-11905. doi:10.1073/pnas.1901841116

83. Rawal N, Pangburn MK. Structure/function of C5 convertases of complement. Int Immunopharmacol. 2001;1(3):415-422. doi:10.1016/s1567-5769(00)00039-4

84. Zwarthoff SA, Berends ETM, Mol S, et al. Functional Characterization of Alternative and Classical Pathway C3/C5 Convertase Activity and Inhibition Using Purified Models. Front Immunol. 2018;9:1691. Published 2018 Jul 23. doi:10.3389/fimmu.2018.01691

85. Parsons ES, Stanley GJ, Pyne ALB, et al. Single-molecule kinetics of pore assembly by the membrane attack complex. Nat Commun. 2019;10(1):2066. Published 2019 May 6. doi:10.1038/s41467-019-10058-7

86. Chen ZA, Pellarin R, Fischer L, et al. Structure of Complement C3(H2O) Revealed By Quantitative Cross-Linking/Mass Spectrometry And Modeling. Mol Cell Proteomics. 2016;15(8):2730-2743. doi:10.1074/mcp.M115.056473

87. Lindorfer MA, Hahn CS, Foley PL, Taylor RP. Heteropolymer-mediated clearance of immune complexes via erythrocyte CR1: mechanisms and applications. Immunol Rev. 2001;183:10-24. doi:10.1034/j.1600-065x.2001.1830102.x

88. Erdei A, Kovács KG, Nagy-Baló Z, et al. New aspects in the regulation of human B cell functions by complement receptors CR1, CR2, CR3 and CR4. Immunol Lett. 2021;237:42-57. doi:10.1016/j.imlet.2021.06.006

89. Tuveson DA, Ahearn JM, Matsumoto AK, Fearon DT. Molecular interactions of complement receptors on B lymphocytes: a CR1/CR2 complex distinct from the CR2/CD19 complex. J Exp Med. 1991;173(5):1083-1089. doi:10.1084/jem.173.5.1083

90. Spiller OB, Criado-García O, Rodríguez De Córdoba S, Morgan BP. Cytokine-mediated up-regulation of CD55 and CD59 protects human hepatoma cells from complement attack. Clin Exp Immunol. 2000;121(2):234-241. doi:10.1046/j.1365-2249.2000.01305.x

91. Sim RB, Day AJ, Moffatt BE, Fontaine M. Complement factor I and cofactors in control of complement system convertase enzymes. Methods Enzymol. 1993;223:13-35. doi:10.1016/0076-6879(93)23035-l

92. Krych-Goldberg M, Atkinson JP. Structure-function relationships of complement receptor type 1. Immunol Rev. 2001;180:112-122. doi:10.1034/j.1600-065x.2001.1800110.x

93. Davidson A, Diamond B. Autoimmune diseases. N Engl J Med. 2001;345(5):340-350. doi:10.1056/NEJM200108023450506

94. Burnett DL, Langley DB, Schofield P, et al. Germinal center antibody mutation trajectories are determined by rapid self/foreign discrimination. Science. 2018;360(6385):223-226. doi:10.1126/science.aao3859

95. Galvin JE, Hemric ME, Ward K, Cunningham MW. Cytotoxic mAb from rheumatic carditis recognizes heart valves and laminin. J Clin Invest. 2000;106(2):217-224. doi:10.1172/JCI7132

96. Prüss H. Autoantibodies in neurological disease. Nat Rev Immunol. 2021;21(12):798-813. doi:10.1038/s41577-021-00543-w

97. Monneaux F, Muller S. Epitope spreading in systemic lupus erythematosus: identification of triggering peptide sequences. Arthritis Rheum. 2002;46(6):1430-1438. doi:10.1002/art.10263

98. Cappione A 3rd, Anolik JH, Pugh-Bernard A, et al. Germinal center exclusion of autoreactive B cells is defective in human systemic lupus erythematosus. J Clin Invest. 2005;115(11):3205-3216. doi:10.1172/JCI24179

99. Allen CD, Okada T, Tang HL, Cyster JG. Imaging of germinal center selection events during affinity maturation. Science. 2007;315(5811):528-531. doi:10.1126/science.1136736

100. Gitlin AD, Shulman Z, Nussenzweig MC. Clonal selection in the germinal centre by regulated proliferation and hypermutation. Nature. 2014;509(7502):637-640. doi:10.1038/nature13300

101. Allen CD, Ansel KM, Low C, et al. Germinal center dark and light zone organization is mediated by CXCR4 and CXCR5. Nat Immunol. 2004;5(9):943-952. doi:10.1038/ni1100

102. Smith KG, Light A, O'Reilly LA, Ang SM, Strasser A, Tarlinton D. bcl-2 transgene expression inhibits apoptosis in the germinal center and reveals differences in the selection of memory B cells and bone marrow antibody-forming cells. J Exp Med. 2000;191(3):475-484. doi:10.1084/jem.191.3.475

103. Linterman MA, Rigby RJ, Wong RK, et al. Follicular helper T cells are required for systemic autoimmunity. J Exp Med. 2009;206(3):561-576. doi:10.1084/jem.20081886

104. Watanabe-Fukunaga R, Brannan CI, Copeland NG, Jenkins NA, Nagata S. Lymphoproliferation disorder in mice explained by defects in Fas antigen that mediates apoptosis. Nature. 1992;356(6367):314-317. doi:10.1038/356314a0

105. Hsu HC, Yang P, Wang J, et al. Interleukin 17-producing T helper cells and interleukin 17 orchestrate autoreactive germinal center development in autoimmune BXD2 mice. Nat Immunol. 2008;9(2):166-175. doi:10.1038/ni1552

106. Kornau HC, Kreye J, Stumpf A, et al. Human Cerebrospinal Fluid Monoclonal LGI1 Autoantibodies Increase Neuronal Excitability. Ann Neurol. 2020;87(3):405-418. doi:10.1002/ana.25666

107. Cotzomi E, Stathopoulos P, Lee CS, et al. Early B cell tolerance defects in neuromyelitis optica favour anti-AQP4 autoantibody production. Brain. 2019;142(6):1598-1615. doi:10.1093/brain/awz106

108. Baumann I, Kolowos W, Voll RE, et al. Impaired uptake of apoptotic cells into tingible body macrophages in germinal centers of patients with systemic lupus erythematosus. Arthritis Rheum. 2002;46(1):191-201. doi:10.1002/1529-0131(200201)46:1<191::AID-ART10027>3.0.CO;2-K

109. Mietzner B, Tsuiji M, Scheid J, et al. Autoreactive IgG memory antibodies in patients with systemic lupus erythematosus arise from nonreactive and polyreactive precursors. Proc Natl Acad Sci U S A. 2008;105(28):9727-9732. doi:10.1073/pnas.0803644105

110. Carter LM, Isenberg DA, Ehrenstein MR. Elevated serum BAFF levels are associated with rising anti-double-stranded DNA antibody levels and disease flare following B cell depletion therapy in systemic lupus erythematosus. Arthritis Rheum. 2013;65(10):2672-2679. doi:10.1002/art.38074

111. Edwards JC, Szczepanski L, Szechinski J, et al. Efficacy of B-cell-targeted therapy with rituximab in patients with rheumatoid arthritis. N Engl J Med. 2004;350(25):2572-2581. doi:10.1056/NEJMoa032534

112. Gilhus NE, Tzartos S, Evoli A, Palace J, Burns TM, Verschuuren JJGM. Myasthenia gravis. Nat Rev Dis Primers. 2019;5(1):30. Published 2019 May 2. doi:10.1038/s41572-019-0079-y

113. Tzartos SJ, Sophianos D, Efthimiadis A. Role of the main immunogenic region of acetylcholine receptor in myasthenia gravis. An Fab monoclonal antibody protects against antigenic modulation by human sera. J Immunol. 1985;134(4):2343-2349.

114. Heldal AT, Owe JF, Gilhus NE, Romi F. Seropositive myasthenia gravis: a nationwide epidemiologic study. Neurology. 2009;73(2):150-151. doi:10.1212/WNL.0b013e3181ad53c2

115. Carr AS, Cardwell CR, McCarron PO, McConville J. A systematic review of population based epidemiological studies in Myasthenia Gravis. BMC Neurol. 2010;10:46. Published 2010 Jun 18. doi:10.1186/1471-2377-10-46

116. Gilhus NE, Verschuuren JJ. Myasthenia gravis: subgroup classification and therapeutic strategies. Lancet Neurol. 2015;14(10):1023-1036. doi:10.1016/S1474-4422(15)00145-3

117. Gilhus NE, Skeie GO, Romi F, Lazaridis K, Zisimopoulou P, Tzartos S. Myasthenia gravis - autoantibody characteristics and their implications for therapy. Nat Rev Neurol. 2016;12(5):259-268. doi:10.1038/nrneurol.2016.44

118. Gregersen PK, Kosoy R, Lee AT, et al. Risk for myasthenia gravis maps to a (151) Pro→Ala change in TNIP1 and to human leukocyte antigen-B*08. Ann Neurol. 2012;72(6):927-935. doi:10.1002/ana.23691

119. Marx A, Pfister F, Schalke B, Saruhan-Direskeneli G, Melms A, Ströbel P. The different roles of the thymus in the pathogenesis of the various myasthenia gravis subtypes. Autoimmun Rev. 2013;12(9):875-884. doi:10.1016/j.autrev.2013.03.007

120. Stålberg E, Sanders DB, Kouyoumdjian JA. Pitfalls and errors in measuring jitter. Clin Neurophysiol. 2017;128(11):2233-2241. doi:10.1016/j.clinph.2017.09.001

121. Claytor B, Cho SM, Li Y. Myasthenic crisis. Muscle Nerve. 2023;68(1):8-19. doi:10.1002/mus.27832

122. Lazaridis K, Tzartos SJ. Myasthenia Gravis: Autoantibody Specificities and Their Role in MG Management. Front Neurol. 2020;11:596981. Published 2020 Nov 30. doi:10.3389/fneur.2020.596981

123. Zisimopoulou P, Evangelakou P, Tzartos J, et al. A comprehensive analysis of the epidemiology and clinical characteristics of anti-LRP4 in myasthenia gravis. J Autoimmun. 2014;52:139-145. doi:10.1016/j.jaut.2013.12.004

124. Higuchi O, Hamuro J, Motomura M, Yamanashi Y. Autoantibodies to low-density lipoprotein receptor-related protein 4 in myasthenia gravis. Ann Neurol. 2011;69(2):418-422. doi:10.1002/ana.22312

125. Heinemann S, Bevan S, Kullberg R, Lindstrom J, Rice J. Modulation of acetylcholine receptor by antibody against the receptor. Proc Natl Acad Sci U S A. 1977;74(7):3090-3094. doi:10.1073/pnas.74.7.3090

126. Engel AG, Tsujihata M, Lindstrom JM, Lennon VA. The motor end plate in myasthenia gravis and in experimental autoimmune myasthenia gravis. A quantitative ultrastructural study. Ann N Y Acad Sci. 1976;274:60-79. doi:10.1111/j.1749-6632.1976.tb47676.x

127. Engel AG, Sakakibara H, Sahashi K, Lindstrom JM, Lambert EH, Lennon VA. Passively transferred experimental autoimmune myasthenia gravis. Sequential and quantitative study of the motor end-plate fine structure and ultrastructural localization of immune complexes (IgG and C3), and of the acetylcholine receptor. Neurology. 1979;29(2):179-188. doi:10.1212/wnl.29.2.179

128. Sine SM. End-plate acetylcholine receptor: structure, mechanism, pharmacology, and disease. Physiol Rev. 2012;92(3):1189-1234. doi:10.1152/physrev.00015.2011

129. Unwin N. Nicotinic acetylcholine receptor and the structural basis of neuromuscular transmission: insights from Torpedo postsynaptic membranes. Q Rev Biophys. 2013;46(4):283-322. doi:10.1017/S0033583513000061

130. Karlin A. Emerging structure of the nicotinic acetylcholine receptors. Nat Rev Neurosci. 2002;3(2):102-114. doi:10.1038/nrn731

131. Rødgaard A, Nielsen FC, Djurup R, Somnier F, Gammeltoft S. Acetylcholine receptor antibody in myasthenia gravis: predominance of IgG subclasses 1 and 3. Clin Exp Immunol. 1987;67(1):82-88.

132. Lefvert AK, Holm G, Pirskanen R. Autoantiidiotypic antibodies in myasthenia gravis. Ann N Y Acad Sci. 1987;505:133-154. doi:10.1111/j.1749-6632.1987.tb51288.x

133. Lefvert AK, Cuénoud S, Fulpius BW. Binding properties and subclass distribution of anti-acetylcholine receptor antibodies in myasthenia gravis. J Neuroimmunol. 1981;1(1):125-135. doi:10.1016/0165-5728(81)90015-1

134. Barrett DJ, Ayoub EM. IgG2 subclass restriction of antibody to pneumococcal polysaccharides. Clin Exp Immunol. 1986;63(1):127-134.

135. Luo J, Taylor P, Losen M, de Baets MH, Shelton GD, Lindstrom J. Main immunogenic region structure promotes binding of conformation-dependent myasthenia gravis autoantibodies, nicotinic acetylcholine receptor conformation maturation, and agonist sensitivity. J Neurosci. 2009;29(44):13898-13908. doi:10.1523/JNEUROSCI.2833-09.2009

136. Ching KH, Burbelo PD, Kimball RM, Clawson LL, Corse AM, Iadarola MJ. Recombinant expression of the AChR-alpha1 subunit for the detection of conformation-dependent epitopes in Myasthenia Gravis. Neuromuscul Disord. 2011;21(3):204-213. doi:10.1016/j.nmd.2010.12.003

137. Pham MC, Masi G, Patzina R, et al. Individual myasthenia gravis autoantibody clones can efficiently mediate multiple mechanisms of pathology. Acta Neuropathol. 2023;146(2):319-336. doi:10.1007/s00401-023-02603-y

138. Tzartos SJ, Sophianos D, Efthimiadis A. Role of the main immunogenic region of acetylcholine receptor in myasthenia gravis. An Fab monoclonal antibody protects against antigenic modulation by human sera. J Immunol. 1985;134(4):2343-2349.

139. Tzartos SJ, Barkas T, Cung MT, et al. Anatomy of the antigenic structure of a large membrane autoantigen, the muscle-type nicotinic acetylcholine receptor. Immunol Rev. 1998;163:89-120. doi:10.1111/j.1600-065x.1998.tb01190.x

140. Hara H, Hayashi K, Ohta K, Itoh N, Nishitani H, Ohta M. Detection and characterization of blocking-type anti-acetylcholine receptor antibodies in sera from patients with myasthenia gravis. Clin Chem. 1993;39(10):2053-2057.

141. Sanderson NSR. Complement and myasthenia gravis. Mol Immunol. 2022;151:11-18. doi:10.1016/j.molimm.2022.08.018

142. Cetin H, Webster R, Liu WW, et al. Myasthenia gravis AChR antibodies inhibit function of rapsyn-clustered AChRs. J Neurol Neurosurg Psychiatry. 2020;91(5):526-532. doi:10.1136/jnnp-2019-322640

143. Engel AG, Sahashi K, Fumagalli G. The immunopathology of acquired myasthenia gravis. Ann N Y Acad Sci. 1981;377:158-174. doi:10.1111/j.1749-6632.1981.tb33730.x

144. Christadoss P. C5 gene influences the development of murine myasthenia gravis. J Immunol. 1988;140(8):2589-2592.

145. Tüzün E, Scott BG, Goluszko E, Higgs S, Christadoss P. Genetic evidence for involvement of classical complement pathway in induction of experimental autoimmune myasthenia gravis. J Immunol. 2003;171(7):3847-3854. doi:10.4049/jimmunol.171.7.3847

146. Tüzün E, Li J, Saini SS, Yang H, Christadoss P. Pros and cons of treating murine myasthenia gravis with anti-C1q antibody. J Neuroimmunol. 2007;182(1-2):167-176. doi:10.1016/j.jneuroim.2006.10.014

147. Zhou Y, Gong B, Lin F, Rother RP, Medof ME, Kaminski HJ. Anti-C5 antibody treatment ameliorates weakness in experimentally acquired myasthenia gravis. J Immunol. 2007;179(12):8562-8567. doi:10.4049/jimmunol.179.12.8562

148. Martinez-Pena Y Valenzuela I, Akaaboune M. The Metabolic Stability of the Nicotinic Acetylcholine Receptor at the Neuromuscular Junction. Cells. 2021;10(2):358. Published 2021 Feb 9. doi:10.3390/cells10020358

149. Drachman DB, Angus CW, Adams RN, Michelson JD, Hoffman GJ. Myasthenic antibodies cross-link acetylcholine receptors to accelerate degradation. N Engl J Med. 1978;298(20):1116-1122. doi:10.1056/NEJM197805182982004

150. Sophianos D, Tzartos SJ. Fab fragments of monoclonal antibodies protect the human acetylcholine receptor against antigenic modulation caused by myasthenic sera. J Autoimmun. 1989;2(6):777-789. doi:10.1016/0896-8411(89)90004-8

151. Conti-Tronconi B, Tzartos S, Lindstrom J. Monoclonal antibodies as probes of acetylcholine receptor structure. 2. Binding to native receptor. Biochemistry. 1981;20(8):2181-2191. doi:10.1021/bi00511a017

152. Tzartos SJ, Starzinski-Powitz A. Decrease in acetylcholine-receptor content of human myotube cultures mediated by monoclonal antibodies to alpha, beta and gamma subunits. FEBS Lett. 1986;196(1):91-95. doi:10.1016/0014-5793(86)80220-4

153. Drachman DB, Adams RN, Josifek LF, Self SG. Functional activities of autoantibodies to acetylcholine receptors and the clinical severity of myasthenia gravis. N Engl J Med. 1982;307(13):769-775. doi:10.1056/NEJM198209233071301

154. Messéant J, Dobbertin A, Girard E, et al. MuSK frizzled-like domain is critical for mammalian neuromuscular junction formation and maintenance. J Neurosci. 2015;35(12):4926-4941. doi:10.1523/JNEUROSCI.3381-14.2015

155. DeChiara TM, Bowen DC, Valenzuela DM, et al. The receptor tyrosine kinase MuSK is required for neuromuscular junction formation in vivo. Cell. 1996;85(4):501-512. doi:10.1016/s0092-8674(00)81251-9

156. Gautam M, Noakes PG, Mudd J, et al. Failure of postsynaptic specialization to develop at neuromuscular junctions of rapsyn-deficient mice. Nature. 1995;377(6546):232-236. doi:10.1038/377232a0

157. Evoli, A. and Iorio, R. (2015), Characteristics of myasthenia gravis with antibodies to muscle-specific kinase and low-density lipoprotein-related receptor protein 4. Clin Exp Neuroimmunol, 6: 40-48. https://doi.org/10.1111/cen3.12173

158. van der Neut Kolfschoten M, Schuurman J, Losen M, et al. Anti-inflammatory activity of human IgG4 antibodies by dynamic Fab arm exchange. Science. 2007;317(5844):1554-1557. doi:10.1126/science.1144603

159. Huijbers MG, Vergoossen DL, Fillié-Grijpma YE, et al. MuSK myasthenia gravis monoclonal antibodies: Valency dictates pathogenicity. Neurol Neuroimmunol Neuroinflamm. 2019;6(3):e547. Published 2019 Feb 21. doi:10.1212/NXI.0000000000000547

160. Verschuuren JJ, Huijbers MG, Plomp JJ, et al. Pathophysiology of myasthenia gravis with antibodies to the acetylcholine receptor, muscle-specific kinase and low-density lipoprotein receptor-related protein 4. Autoimmun Rev. 2013;12(9):918-923. doi:10.1016/j.autrev.2013.03.001

161. Hong Y, Zisimopoulou P, Trakas N, et al. Multiple antibody detection in 'seronegative' myasthenia gravis patients. Eur J Neurol. 2017;24(6):844-850. doi:10.1111/ene.13300

162. Mantegazza R, Bonanno S, Camera G, Antozzi C. Current and emerging therapies for the treatment of myasthenia gravis. Neuropsychiatr Dis Treat. 2011;7:151-160. doi:10.2147/NDT.S8915

163. Iorio R, Damato V, Alboini PE, Evoli A. Efficacy and safety of rituximab for myasthenia gravis: a systematic review and meta-analysis. J Neurol. 2015;262(5):1115-1119. doi:10.1007/s00415-014-7532-3

164. Dos Santos A, Noury JB, Genestet S, et al. Efficacy and safety of rituximab in myasthenia gravis: a French multicentre real-life study. Eur J Neurol. 2020;27(11):2277-2285. doi:10.1111/ene.14391

165. Hehir MK, Hobson-Webb LD, Benatar M, et al. Rituximab as treatment for anti-MuSK myasthenia gravis: Multicenter blinded prospective review. Neurology. 2017;89(10):1069-1077. doi:10.1212/WNL.0000000000004341

166. Hillmen P, Young NS, Schubert J, et al. The complement inhibitor eculizumab in paroxysmal nocturnal hemoglobinuria. N Engl J Med. 2006;355(12):1233-1243. doi:10.1056/NEJMoa061648

167. Howard JF Jr, Utsugisawa K, Benatar M, et al. Safety and efficacy of eculizumab in anti-acetylcholine receptor antibody-positive refractory generalised myasthenia gravis (REGAIN): a phase 3, randomised, double-blind, placebo-controlled, multicentre study. Lancet Neurol. 2017;16(12):976-986. doi:10.1016/S1474-4422(17)30369-1

168. Nelke C, Schroeter CB, Stascheit F, et al. Eculizumab versus rituximab in generalised myasthenia gravis. J Neurol Neurosurg Psychiatry. 2022;93(5):548-554. doi:10.1136/jnnp-2021-328665

169. Howard JF Jr, Bresch S, Genge A, et al. Safety and efficacy of zilucoplan in patients with generalised myasthenia gravis (RAISE): a randomised, double-blind, placebo-controlled, phase 3 study. Lancet Neurol. 2023;22(5):395-406. doi:10.1016/S1474-4422(23)00080-7

170. Vu T, Meisel A, Mantegazza R, et al. Summary of Research: Terminal Complement Inhibitor Ravulizumab in Generalized Myasthenia Gravis. Neurol Ther. 2023;12(5):1435-1438. doi:10.1007/s40120-023-00514-4

171. Vu T, Ortiz S, Katsuno M, et al. Ravulizumab pharmacokinetics and pharmacodynamics in patients with generalized myasthenia gravis. J Neurol. 2023;270(6):3129-3137. doi:10.1007/s00415-023-11617-1

172. Tang GQ, Tang Y, Dhamnaskar K, et al. Zilucoplan, a macrocyclic peptide inhibitor of human complement component 5, uses a dual mode of action to prevent terminal complement pathway activation. Front Immunol. 2023;14:1213920. Published 2023 Aug 9. doi:10.3389/fimmu.2023.1213920

173. Pyzik M, Kozicky LK, Gandhi AK, Blumberg RS. The therapeutic age of the neonatal Fc receptor. Nat Rev Immunol. 2023;23(7):415-432. doi:10.1038/s41577-022-00821-1

174. Bril V, Drużdż A, Grosskreutz J, et al. Safety and efficacy of rozanolixizumab in patients with generalised myasthenia gravis (MycarinG): a randomised, double-blind, placebo-controlled, adaptive phase 3 study. Lancet Neurol. 2023;22(5):383-394. doi:10.1016/S1474-4422(23)00077-7

175. Kordas G, Lagoumintzis G, Sideris S, Poulas K, Tzartos SJ. Direct proof of the in vivo pathogenic role of the AChR autoantibodies from myasthenia gravis patients. PLoS One. 2014;9(9):e108327. Published 2014 Sep 26. doi:10.1371/journal.pone.0108327

176. Tzartos SJ, Seybold ME, Lindstrom JM. Specificities of antibodies to acetylcholine receptors in sera from myasthenia gravis patients measured by monoclonal antibodies. Proc Natl Acad Sci U S A. 1982;79(1):188-192. doi:10.1073/pnas.79.1.188

177. Shlomchik MJ, Marshak-Rothstein A, Wolfowicz CB, Rothstein TL, Weigert MG. The role of clonal selection and somatic mutation in autoimmunity. Nature. 1987;328(6133):805-811. doi:10.1038/328805a0

178. Yurasov S, Wardemann H, Hammersen J, et al. Defective B cell tolerance checkpoints in systemic lupus erythematosus. J Exp Med. 2005;201(5):703-711. doi:10.1084/jem.20042251

179. Wellmann U, Letz M, Herrmann M, Angermüller S, Kalden JR, Winkler TH. The evolution of human anti-double-stranded DNA autoantibodies. Proc Natl Acad Sci U S A. 2005;102(26):9258-9263. doi:10.1073/pnas.0500132102

180. Lee JY, Stathopoulos P, Gupta S, et al. Compromised fidelity of B-cell tolerance checkpoints in AChR and MuSK myasthenia gravis. Ann Clin Transl Neurol. 2016;3(6):443-454. Published 2016 Apr 27. doi:10.1002/acn3.311

181. Rose N, Holdermann S, Callegari I, et al. Receptor clustering and pathogenic complement activation in myasthenia gravis depend on synergy between antibodies with multiple subunit specificities. Acta Neuropathol. 2022;144(5):1005-1025. doi:10.1007/s00401-022-02493-6

182. Goodnow CC, Crosbie J, Jorgensen H, Brink RA, Basten A. Induction of self-tolerance in mature peripheral B lymphocytes. Nature. 1989;342(6248):385-391. doi:10.1038/342385a0

183. Roco JA, Mesin L, Binder SC, et al. Class-Switch Recombination Occurs Infrequently in Germinal Centers. Immunity. 2019;51(2):337-350.e7. doi:10.1016/j.immuni.2019.07.001

184. Klein L, Kyewski B, Allen PM, Hogquist KA. Positive and negative selection of the T cell repertoire: what thymocytes see (and don't see). Nat Rev Immunol. 2014;14(6):377-391. doi:10.1038/nri3667

185. Frommer F, Waisman A. B cells participate in thymic negative selection of murine auto-reactive CD4+ T cells. PLoS One. 2010;5(10):e15372. Published 2010 Oct 20. doi:10.1371/journal.pone.0015372

186. Perera J, Meng L, Meng F, Huang H. Autoreactive thymic B cells are efficient antigen-presenting cells of cognate self-antigens for T cell negative selection. Proc Natl Acad Sci U S A. 2013;110(42):17011-17016. doi:10.1073/pnas.1313001110

187. Yoshizaki A, Miyagaki T, DiLillo DJ, et al. Regulatory B cells control T-cell autoimmunity through IL-21-dependent cognate interactions. Nature. 2012;491(7423):264-268. doi:10.1038/nature11501

188. Catalán D, Mansilla MA, Ferrier A, et al. Immunosuppressive Mechanisms of Regulatory B Cells. Front Immunol. 2021;12:611795. Published 2021 Apr 29. doi:10.3389/fimmu.2021.611795

8. Acknowledgements

I want to thank Tobias Derfuss who took me in as a PhD student and gave me the opportunity to work in his lab. It was an immense pleasure to be part of the research group and to this day I consider it one of my best professional decisions to join the Clinical Neuroimmunology lab at the DBM. I not only grew as a researcher, by learning different methods, formulating hypotheses and conceptualizing difficult problems, but learned something about every aspect of the life as a scientist. I'm deeply grateful for all these valuable experiences, the confidence placed in me and the guidance I received.

I'm similarly grateful to Nicholas Sanderson, who is an amazing sensei with an admirable approach to scientific questions. It was hugely reassuring to have such a great source of knowledge and expertise sitting right next to me and he never failed to encourage curiosity and asking the hard question. Also, it was a true bliss to discuss scientific topics and to spent time outside the lab discussing anything but scientific topics.

But of course, working and sometimes living in the lab wouldn't have been anywhere as pleasurable as it was without all the members of the Derfuss lab. Especially Ilaria, Hye-In and Mika, who made essential contributions to my research results by showing me methods, giving advice and providing reliable support at any time. I'm immensely grateful for to friendship and the time we spent together. Furthermore, I would like to thank new, former and returning members of the lab, including Elif, Edo, Noemi, Hong, and Sebastian for all of their hard work and the wonderful atmosphere they helped create.

My sincere thanks goes to Markus Rüegg and Bettina Schreiner for agreeing to participate as members of the PhD committee and supervising me throughout the whole journey of my doctorate. I'm very thankful for the discussions and the insightful comments on experimental approaches and the general outline of the project.

Next, I would like to thank the in-house facilities, namely the DBM Microscopy Core Facility and the DBM Flow Cytometry Core Facility for their dedicated work and help. The same is true for all the nurses and doctors of the neurological clinic and policlinic who helped us recruit patients and enabled the collection of samples in the first place. A special thanks to Paolo, who is probably the most diligent collaborator I have ever had the pleasure of working with. I extend my deepest gratitude to all patients who have kindly donated blood for research purposes, hopefully our work makes a difference and enhances our understanding of the disease.

Many thanks to Dan and his team at Alexion for generously sharing their resources. I have always looked forward to our meetings and deeply valued the input and fruitful discussions we have had over the years.

Finally, I want to thank my family, friends and amazing partner Isabel for their constant support and love. I'm eternally grateful for their presence in my life and the profound impact they had on me as a person and on my professional success.